Technische Universität München

Wissenschaftszentrum Weihenstephan

für Ernährung, Landnutzung und Umwelt

Lehrstuhl für Bodenkunde

Spatial heterogeneity of phosphorus concentration and speciation at the micro and profile scale in German forest soils

Florian Werner

Vollständiger Abdruck der von der Fakultät Wissenschaftszentrum Weihenstephan für Ernährung, Landnutzung und Umwelt der Technischen Universität München zur Erlangung des akademischen Grades eines

Doktors der Naturwissenschaften (Dr. rer. nat.)

genehmigten Dissertation.

Vorsitzende:	Prof. Dr. Anja Rammig
Prüfer der Dissertation:	1. apl. Prof. Dr. Jörg Prietzel
	2. Prof. Dr. Dr. h.c. Ingrid Kögel-Knabner
	3. Prof. Dr. Sandra Spielvogel

Die Dissertation wurde am 18.05.2017 bei der Technischen Universität München eingereicht und durch die Fakultät Wissenschaftszentrum Weihenstephan für Ernährung, Landnutzung und Umwelt am 21.07.2017 angenommen.

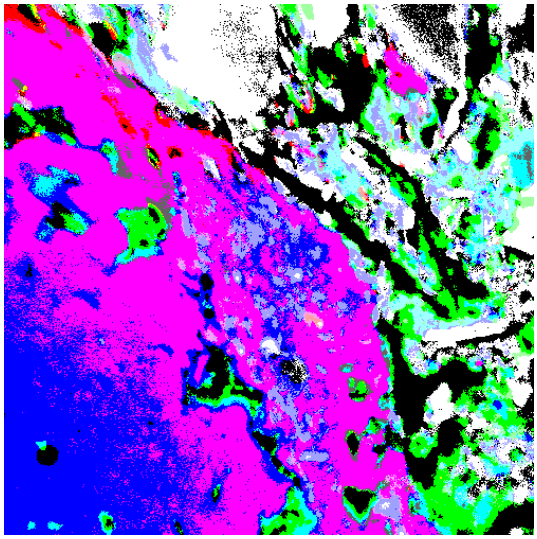

"It's not what you look at that matters, it's what you see."

Henry David Thoreau

Zusammenfassung

Phosphor ist ein lebensnotwendiges Element. Die biologische Verfügbarkeit von Phosphor in Böden limitiert die Produktivität vieler terrestrischer Ökosysteme. Diese Bioverfügbarkeit hängt nicht nur vom Gesamtgehalt des Bodenphosphors, sondern auch von dessen chemischer Bindungsform, der „Phosphor-Speziierung“ ab. Je nach Ausgangsmaterial, Bodentiefe und Grad der Bodenentwicklung enthalten Böden eine Vielzahl unterschiedlicher Phosphorbindungsformen, darunter organische, okkludierte, adsorbierte, ausgefällte und lithogene Formen. Des Weiteren wird die Bioverfügbarkeit von Phosphor durch die räumliche Heterogenität dieses Elements und seiner unterschiedlichen Bindungsformen beeinflusst. Daher erfordert die Untersuchung der Verfügbarkeit von Phosphor für beispielsweise Mikroorganismen oder Waldökosysteme unterschiedliche Skalen der Betrachtung. Die räumliche Heterogenität von Elementverteilungen auf der Mikroskala in Bodenfeststoffen hat wegen ihres Einflusses auf Bodenfunktionen und Bodenfruchtbarkeit deshalb jüngst gesteigerte Aufmerksamkeit in der Bodenkunde erhalten. Dennoch ist über die mikroskalige Verteilung von Phosphor und Phosphorbindungsformen in Bodenaggregaten wenig bekannt. Auch die horizontale Verteilung von Phosphor im Bodenprofil, sowie die räumliche Variabilität der vorliegenden Bindungsformen sind weitgehend unerforscht.

Um die Phosphorverteilung und -bindungsform in Böden auf der Mikro- und der Profilebene zu untersuchen, sind sowohl häufig genutzte Bodenfraktionierungen als auch innovative, fortschrittliche instrumentelle Technologien erforderlich. Fraktionierungen sind relativ günstig und einfach in der Anwendung, wohingegen fortschrittliche Technologien oft kostspielig sind und einen großen Aufwand bei der Datenerhebung und -analyse darstellen. Diese Dissertation behandelt (i) die räumlichen Muster unterschiedlicher Phosphorfraktionen und bedeutender Phosphorbindungspartner (wie z. B. organische Bodensubstanz und pedogene Aluminium- und Eisenminerale) auf der Profilebene und (ii) die mikroskalige Verteilung von unterschiedlichen Phosphorbindungsformen in Bodenaggregaten. Die untersuchten *Cambisole* (nach deutscher Klassifikation, etwa Braunerden) haben sich aus silikatischem Ausgangsmaterial gebildet, waren größtenteils mit haubaren Rotbuche-Wäldern bepflanzt und

wiesen unterschiedliche Grade der Versauerung auf. Ziel war, die räumlichen und pedogenetischen Veränderungen der standortspezifischen mikro- und profilskaligen Verteilung von Phosphor zu beschreiben, um die Mechanismen für diese Veränderungen aufzudecken und neue Erkenntnisse über Phosphorzugänglichkeit und -verfügbarkeit in Böden zu präsentieren.

Die Gesamtkonzentrationen von Phosphor und weiteren Elementen wurden durch Aufschluss mit Flusssäure bzw. Perchlorsäure und Messung mittels optischer Emissionsspektrometrie mit induktiv gekoppeltem Plasma (ICP-OES) ermittelt. Gleichermaßen wurden im ICP-OES die Eisen-, Aluminium- und Phosphorkonzentrationen von Produkten der chemischen Aufspaltung mittels Dithionit-Citrat-Bicarbonat- bzw. Ammonium-Oxalat-Lösungen gemessen. Die Gesamtkonzentration organisch gebundenen Phosphors wurde durch Glühverlust bestimmt. Durch Nutzung photometrischer Methoden wurde außerdem der Anteil des anorganisch gebundenen Phosphors in den Ammonium-Oxalat-Extrakten gemessen. Wie erwartet, ergaben meine Untersuchungen, dass die profilskalige Verteilung des Gesamtphosphors dem Verteilungsmuster von organischem Phosphor am meisten ähnelt. Beide zeigten an allen Standorten abnehmende Gehalte vom Ober- zum Unterboden. Anorganisch gebundener Phosphor wurde hauptsächlich in Apatit und in silikatischen Primärsilikaten nachgewiesen. Mit zunehmender Bodenversauerung nahm der prozentuale Anteil an anorganischem Phosphor im Bezug auf die Gesamtphosphorkonzentration ab. Organische Bodensubstanz, pedogene Aluminium- und Eisenminerale sowie Eisen-/Aluminiumoxid-Mischphasen wurden an allen Standorten als Hauptbindungspartner von organisch gebundenem Phosphor identifiziert. Mit zunehmender Bodentiefe nahmen die Korrelationen vieler Phosphorfraktionen mit organischer Bodensubstanz ab, wohingegen jene mit pedogenen Aluminium- und Eisenmineralen zunahmen. In mäßig entwickelten Böden zeigte sich dieses Korrelationsmuster im Oberboden durch die Mobilisierung von pedogenen Aluminiummineralen, in späteren Stadien der Pedogenese auch durch die Mobilisierung von pedogenen Eisenmineralen.

Eine direkte Phosphorspeziierung kann durch Fraktionierungen wegen der umfassenden chemischen Veränderungen durch die genutzten Fraktionierungsmittel jedoch nicht erreicht

werden. Mittels Synchrotron-basierter Röntgenabsorptionsspektroskopie im Nahkantenbereich (XANES- bzw. NEXAFS-Spektroskopie) der Phosphor-K-Kante ist eine direkte Phosphorsspeziierung jedoch realisierbar. Bei dieser Methode wird ein unbekanntes Probenspektrum als Linearkombination aus bekannten Standardspektren modelliert. Die Qualität der Phosphorspeziierungsergebnisse wird jedoch kontrovers diskutiert, teilweise, weil geringe Veränderungen der angewendeten Modellierprozedur zu deutlichen Veränderungen in diesen Ergebnissen führen können. Da bei diesem Vorgehen bisher keine allgemein genutzte Vorschrift bestand, entwickelte ich ein Standardprotokoll, um Speziierungsergebnisse von Bodenphosphor reproduzierbar zu erzeugen. Dafür nutzte ich ternäre Mischungen unterschiedlicher Konzentrationen von Apatit, Aluminiumphosphat, Eisenphosphat und Inositolhexakisphosphat, da Phosphor im Boden größtenteils an Kalzium, Aluminium, Eisen oder organische Bodensubstanz gebunden ist. Die Modellierprozedur mittels Linearkombination wurde vornehmlich durch eine angepasste Basislinienkorrektur und Kantenstufennormalisierung verbessert. Auch wenn durch die Nutzung des neu entwickelten Standardprotokolls die Phosphorspeziierung mittels XANES-Spektroskopie optimiert werden konnte, wurden zum Beispiel geringe Konzentrationen einer Spezies oft nicht korrekt detektiert. Gemäß guter wissenschaftlicher Praxis sollten Speziierungsergebnisse deshalb weiterhin mit anderen Methoden nachgeprüft und Phosphoranteile kleiner als 5% des Gesamtphosphors aus den Modellierergebnissen ausgeschlossen werden.

Die überarbeitete Modellierprozedur erlaubte des Weiteren die punktuelle Untersuchung der mikroskaligen Speziierung von Bodenphosphor in silikatischen Bodenaggregaten. Diese Phosphorspeziierung wurde ergänzt durch die mikroskalige Flächenuntersuchung mittels Röntgenabsorptionsfloureszenz (XRF) und nanoskaliger Sekundärionen-Massenspektrometrie (NanoSIMS). Diese Thesis zeigt deshalb auch, wie die mikroskalige Heterogenität von Bodenphosphor mit der Heterogenität von einerseits organischer Bodensubstanz, pedogenen Aluminium- und Eisenmineralen und Tonmineralen und andererseits Faktoren der Bodenbildung (Ausgangsmaterial, Pedogenese) in Beziehung stehen. Ich belegte, dass mikroskalige Heterogenität von Bodenphosphor großteils durch Bodensubstrat und Bodentiefe bestimmt wird. Abschließend bewertete ich den Einfluss der Podsolierungsintensität in Waldböden

der gemäßigten Breiten auf die räumliche Heterogenität, Zugänglichkeit, und letztlich Verfügbarkeit von Phosphor, die sich in der mikro- und profilskaligen Bodenvariabilität der untersuchten Böden offenbarte. Die in dieser Dissertation dargelegten Ergebnisse unterstützen das Konzept unterschiedlicher Ökosystemernähungsstrategien auf den jeweiligen Flächen: zu Beginn der Bodenentwicklung vornehmlich Aufnahme von anorganisch gebundenem Phosphor aus verwittertem Ausgangsmaterial hin zu Minimierung des Verlusts organisch gebundenen Phosphors durch effizientes Phosphorrecycling in stark entwickelten Böden.

Abstract

Phosphorus (P) is a crucial element for life, and soil P bioavailability limits the productivity of many terrestrial ecosystems. This bioavailability depends not only on the total soil P content, but also on the soil P binding form, the "soil P speciation". Depending on parent material, soil depth, and stage of pedogenesis, soils contain various different P binding forms of organic, occluded, adsorbed, precipitated, and lithogenic P forms. Furthermore, the P bioavailability is influenced by the spatial heterogeneity of total P and different P species. Thus, different observational scales are required when studying P availability for example for microorganisms or forest ecosystems. Recently, micro scale spatial heterogeneity of element distributions has received increased attention in soil science due to its influence on soil functions and soil fertility. However, little is known about the distribution of total P and different P binding forms in soil aggregates at the micro scale. Additionally, only scarce information exists on the profile scale horizontal distribution of P and the spatial variability of the P binding forms.

Studying the soil P distribution and binding form on the micro and profile scale requires using traditional bulk soil fractionations, as well as ground-breaking advanced instrumental techniques. Soil fractionation techniques are widely implemented and rather affordable, whereas advanced technologies are often costly and constitute large efforts in data acquisition and data analysis. This thesis presents novel information on (i) the spatial patterns of different P fractions, and of major P binding partners (e.g. soil organic matter, pedogenic aluminium and iron minerals) at the profile scale, and (ii) the distribution of different P binding forms in soil aggregates at the micro scale. The investigated *Cambisols* have formed from siliceous parent material, were mainly stocked with mature European Beech (*Fagus sylvatica*) forests, and exhibited different grades of acidification. I aimed at describing the site-specific spatial and pedogenetic changes of the micro and profile scale P distributions to reveal the mechanisms for these changes and to introduce new insights on P accessibility and availability in soils.

The total concentrations of P and other elements (e.g. Fe, Al) were assessed using in-

ductively coupled plasma optical emission spectrometry (ICP-OES) after total digestion with hydrofluoric acid / perchloric acid. Additionally, the concentrations of Fe, Al, and P were analysed by ICP-OES after digestion with dithionite-citrate-bicarbonate and acidic NH_4 oxalate solutions. The total organic P concentration was quantified by ignition loss. Using photometric methods, the acidic NH_4 oxalate solutions were further subdivided into organic and ortho-P. As expected, my results showed that the profile scale distribution of total P was generally best matched by the distribution pattern of organic P, both showing decreasing contents from the top- to the subsoil at all sites. Inorganic P was mainly bound in apatite and in primary silicate minerals. The share of inorganic P decreased with increasing soil acidification. Soil organic matter, pedogenic aluminium and iron minerals, as well as mixed phases of these compounds were identified as main binding partners of organic P at all sites. With increasing soil depth, correlations of various P fractions with soil organic matter decreased, whereas those with pedogenic aluminium and iron minerals increased. This pattern originated due to the topsoil mobilisation of pedogenic aluminium minerals in moderately developed soils, and also of pedogenic iron minerals during later stages of pedogenesis.

A direct P speciation is not achievable using soil fractionation techniques due to the reactant-induced changes of the soil. Using synchrotron-based X-ray absorption near edge structure (XANES or NEXAFS) spectroscopy at the K-edge of phosphorus, direct P speciation can be obtained by fitting an unknown sample spectrum as linear combination of standard compound spectra. However, the quality of the P speciation results are debated controversially, partly because minor modifications of the applied deconvolution procedure can lead to considerable changes in these results. I developed a protocol for reproducible spectrum deconvolution of soil P speciation results to standardise the data analysis using this advanced spectroscopic technique. Ternary mixtures of apatite, iron phosphate, aluminium phosphate, and inositol hexakisphosphate in different concentrations were produced, as soil P is mostly bound to calcium, aluminium, iron, or soil organic matter. The linear combination fitting procedure was mainly improved on the basis of the observation that appropriate baseline correction and edge-step normalisation are crucial for correct fit-

ting results. Even though P speciation was optimised using my newly-established standard protocol for P XANES spectroscopy, for example, small amounts of a species were not detected adequately or falsely claimed. Thus, P speciation results should still be double-checked with other methods, and P portions smaller than 5% of total P should be excluded from the fitting results.

Additionally, the new fitting procedure allowed for assessing the micro scale soil P speciation of P hot spots in siliceous soil aggregates. This selective assessment was supplemented by elemental mapping using X-ray fluorescence (XRF) and nano scale secondary ion mass spectrometry (NanoSIMS). Thus, this thesis also reveals how the micro scale soil P heterogeneity is related to the heterogeneity of soil organic matter, pedogenic aluminium/iron minerals, and clay minerals, as well as to soil forming factors (parent material, pedogenesis). The results of this study showed that micro scale heterogeneity of soil P is largely determined by soil substrate and depth. I concluded, that assessing the micro and profile scale soil variability enables investigating the influence of podsolisation intensity in temperate forest soils on the spatial P heterogeneity, accessibility, and ultimately P availability. The results presented in this thesis support the concept of different ecosystem P nutrition strategies at each of the investigated sites: ranging from acquiring inorganic P from weathered parent material in early stages of pedogenesis to minimising loss of organic P by efficient recycling in highly developed soils.

Contents

List of Figures

List of Tables

List of Abbreviations

Al	aluminium
C	carbon
Ca	calcium
DCB	dithionite-citrate-bicarbonate
DOP	dissolved organic phosphorus
E_0	edge energy
ESRF	European Synchrotron Radiation Facility
Fe	iron
$HF/HClO_4$	hydrofluoric acid/perchloric acid
Hydap	hydroxyapatite
ICP-OES	inductively coupled plasma optical emission spectrometry
IHP	inositol hexakisphosphate
LCF	linear combination fitting
NanoSIMS	nano scale secondary ion mass spectrometry
NMR	nuclear magnetic resonance
OX	acidic NH_4 oxalate
oxi-hydroxides	oxides and hydroxides
P	phosphorus
SEM	scanning electron microscope
SLRI	Synchrotron Light Research Institute
SOM	soil organic matter
XANES	X-ray absorption near edge structure
XRF	X-ray fluorescence

1 Introduction

Phosphorus (P) is one of the macro-nutrients for life. When P is poorly available in soils, this nutrient often limits growth in many terrestrial ecosystems, and P may even become a limiting nutrient for humanity[1]. The bioavailability of soil P changes during soil development, in this process altering soil P stocks and binding forms[2;3;4;5;6]. In 1976, a model was introduced to describe changes of soil P forms and contents during soil succession by Walker & Syers[2]. The authors stated that lithogenic apatite, the primary P source in soils, is mobilised during the first 20.000 years of pedogenesis[2]. While total P resources gradually decrease with time, the relative shares of organically- and soil mineral-bound P increase with time[7]. Ongoing soil development then leads to a "steady state" in which P losses from the system equal gains, however, leaving only scarce resources for plants and microbes to nourish on.

Bioavailable soil P amounts increase in early stages of soil succession due to release of bioavailable P forms, such as newly dissolved ortho-phosphate and labile organic P[8]. With increasing organic P stocks, plant and microbial communities contribute successively more to the P in the soil[7;9;10;11]. Phosphorus supply is optimal in an intermediate stage of soil development when P binding forms are highly diverse[2]. After this phase, total soil P stocks and particularly stocks of bioavailable P decrease[9]. This is due to P leaching, P translocation during soil erosion, and P sequestration into biomass[12]. Bioavailable P forms are slowly, but continuously, transformed into unavailable P forms[13], such as stable organic P and occluded P in pedogenic aluminium (Al) and iron (Fe) oxides and hydroxides (oxi-hydroxides)[3].

This dissertation project is a sub-project of the priority programme SPP 1685 which is funded by the German Research Foundation (DFG). At various institutes in Germany and Switzerland research is performed on the processes, interactions, and feedbacks that control forest ecosystem P nutrition[14]. Five central study sites were selected, sharing three major commonalities: (i) sites stocked with mature (mainly) *Fagus sylvatica* stands with an age of about 120 years, (ii) soils formed from siliceous parent material, (iii) availability of long-term

data sets on nutrient fluxes (obtained by federal institutes). A basic site description can be found online at https://www.ecosystem-nutrition.uni-freiburg.de/standorte. The sites differed in soil and in beech leaf P contents, characterising a P availability gradient[15]. The online description shows that the soils on all sites were pronouncedly acidified. However, only the soil formed from glacial sandy material exhibited marked podsolisation, whereas the less developed soils often showed numerous hardly weathered rock fragments.

The initiators of the priority programme hypothesised that at sites which are rich in mineral-bound P, i.e. in early stages of soil development, forest ecosystems nourish on P mainly by P acquisition from soil minerals (referred to as "P-acquiring system"). In contrast, at later stages of pedogenesis, P recycling is supposed to be increasingly important for ecosystem P nutrition. Here, small cycling loops optimise plant-internal P re-allocation and enzymatic mobilisation of organic P from shoot and root litter (referred to as "P-recycling systems"). This sub-project, based at the Chair of Soil Science of the Technical University of Munich, focussed on the functional links between strategies of P nutrition and speciation and allocation of P in soils.

2 State of the art and objectives

2.1 Spatial heterogeneity of soil P

The SPP 1685 research programme focuses on how temperate forests on soils formed from siliceous parent material are sufficiently supplied with P[14]. Even though almost all soils in central Europe are geologically young, European forests often suffer from low or insufficient P supply[16;17]. Phosphorus availability is expected to become increasingly important, because limiting P resources may limit net primary production of plants and ecosystems[1;18]. Plant-available P is reduced by soil acidifaction and nitrogen eutrophication, which has been increasingly intensified in many regions of Central Europe by anthropogenic deposits in the last century[19]. Additionally, forest growth is limited in many ecosystems[9;20] by strong P sorption, e.g. onto clay minerals[21], Al and Fe oxi-hydroxides[22], or in humic-mineral com-

plexes[23], by P fixation in short-range order Al or Fe phosphates[24], as well as by retarded mineralisation of organic P[5].

Organic P is to a large extent present in soils as inositol hexakisphosphate (IHP), and inorganic P in soils is mostly associated with calcium (Ca), Al, or Fe[22]. A considerable share of the organic and inorganic P existing in soils is not in bioavailable form[25]. To investigate the bioavailability of P in soils and sediments, it is necessary to assess the binding form of P, also referred to as "P speciation"[26]. Moreover, the small scale (µm to cm) distribution of soil microorganisms, soil pH, Ca, Fe, and Al, as well as of soil P can be a crucial factor governing root P uptake[27;28]. In former and many recent studies, soil P distributions were assessed mainly by depth gradients[29], missing to address the horizontal variation of P in soil profiles. However, heterogenous horizontal spatial P patterns have been determined as important factors that control P availability for plants[30;31], or recently for an alpine treeline[32]. Thus, it remains unclear how vertical and horizontal small scale spatial distribution patterns of P and important P binding compounds affect plant P acquisition and supply. Geostatistics is a powerful tool to elucidate these patterns, because it enables the production of high resolution maps of P and important P binding variables.

Apart from profile scale distribution patterns, micro scale soil heterogeneity has received increased attention in soil studies[33;34]. For example, micro scale coatings on mineral surfaces of soil aggregates have been linked to microbial metabolites in a spatially-resolved element speciation study[35]. Once micro scale spatial heterogeneity of soils is represented mechanistically, micro scale structures and processes will help to soundly explain macroscopic soil properties that have been examined for decades[36]. As an example, soil micro sites have recently been addressed as independent, but interconnected micro-reactors of unique chemical composition[34], which more so emphasises the need for micro scale, spatially-resolved element speciation studies when studying soil aggregates.

It becomes apparent, that a robust assessment of P availability in ecosystems requires investigating not only bulk P speciation in soil compartments, but also spatial and chemical P heterogeneity at the micro scale. However, at the moment scant information is available on the spatial heterogeneity of physical and chemical soil properties of P in soils with

different stages of soil development both at the micro, and the profile scale. Thus, soil P availability assessments must account for spatial distribution patterns of P species and contents in soils, as assessed by wet-chemical fractionation of soil, mapping techniques, such as infrared and Raman spectroscopy[37], and/or by advanced spectroscopic/-metric techniques of P assessment[38].

2.2 Spatial soil P assessment techniques

Available P is difficult to quantify and rather regarded as a concept[6]. Phosphorus in the soil solution during the growing season ($\approx$ available P) is supported by P desorption, dissolution, and mineralisation[39]. Fractionation techniques have proven useful to answer questions about P bioavailability, e.g. as reported in a study about long-term acidification effects in spodic forest soils in Maine, USA[40]. The Hedley sequential fractionation method[39;41] is the most common. In this technique, P is removed sequentially first in labile, then in more stable forms. The procedure is time-consuming, but affordable, and it thus allows a widely-used assessment of P availability in soils[42]. However, the P fractions are operationally-defined, and consequently, a direct P speciation in soils is still not accomplishable by the Hedley sequential fractionation method. Other quantifying fractionation methods use e.g. acidic NH_4 oxalate[43] (OX) or dithionite-citrate-bicarbonate[44] (DCB) solution to dissolve Al and Fe phosphate (surface) precipitates and minerals, as well as P adsorbed to pedogenic Al and Fe minerals[45].

Indirect soil P speciation techniques are characterised by two disadvantages: i) Phosphorus binding forms can change during fractionation due to interactions with the reagents and therefore lead to biased P speciation results[26;46], ii) it is impossible to unambiguously assign the operationally-defined P fractions to distinct P species[45;47]. To overcome these disadvantages, studies[48;49] have tried to combine the advantages of sequential P fractionation in soils with those of advanced P speciation methods, as e.g. solution ^{31}P nuclear magnetic resonance (NMR) spectroscopy[50], synchrotron-based X-ray absorption near edge structure (XANES) spectroscopy at the K-edge[51] and $L_{2,3}$-edge[52] of P, and/or investigation after

field flow fractionation[53]. In conclusion, fractionation techniques are indispensable when studying P speciation, but only a combination of indirect and direct methods allows for a comprehensive soil P speciation[49].

Synchrotron-based XANES spectroscopy at the P *K*-edge has been used to study P speciation in soils for over 20 years[54]. Different P species vary in different XANES spectral features, e.g. white-line intensity and position, edge energy (E_0), pre-edge and post-edge structures[55]. These differences can be and have already been used to "fingerprint" distinct P species in P-bearing mineral standard compounds[55]. However, XANES spectroscopy also allows for quantification of standard specimens in samples of unknown P composition. These unknown sample spectra are regarded as a linear combination of known standard spectra, which are fitted as proportions to sum an unknown spectrum with least-squares deviation[56]. To obtain a measure of important standards for fitting, principal component analysis[57] was used. Partial least-squares regression[58] was made use of successfully as fitting procedure. It should already be apparent that unknown sample spectra can not be treated as a black box, because pre-selection of standards and fitting uncertainties determine the quantification essentially. Consequently, the validity of the quantities of different P species as determined by linear combination fitting (LCF) on P XANES spectra is still debated controversially[59]. Nonetheless, LCF on P XANES spectra has been applied for investigations of P speciation in poultry litter[60;61], manure[62;63], sequential extracts of fen peat soils[64] and organic substances[65], soils[58;66;67;68] and sediments[69;70], organic soil surface layers[71], and soil colloids[59;72]. Three of the five SPP 1685 sites were investigated in a recent study using *K*-edge XANES spectroscopy[73], concentrating on a methodological discussion of P speciation, and on the relationship of the P species with parent material in soil horizons.

At present, it is unclear how accurately LCF can represent P speciation in environmental samples, because the standard spectra selection simplifies complex environmental systems like soils and sediments. To overcome these uncertainties, studies were conducted on P sorption onto Al and Fe oxide minerals[74;75], and on binary mineral standard mixtures[76]. The latter authors compared the results from LCF on P *K*-edge XANES spectra obtained from

various defined binary mixtures of three standard reference compounds (variscite, phosphosiderite, and hydroxyapatite). They reproduced the mixture spectra with a relative error of 0.8−17%, being particularly accurate in mixtures with large proportion of hydroxyapatite[76]. However, apart from Ca, Al, and Fe phosphates, soil organic matter (SOM) is an additional major contributor to soil P[5;77]. Additionally, minor modifications in the correction and normalisation procedure have not been recognised to be leading to considerable changes in the P speciation results by LCF until recently. Thus, standardised procedures to ensure unequivocal and accurate results of P speciation by LCF on P *K*-edge XANES spectra are required, because synchrotron-based XANES spectroscopy is increasingly used for P speciation in environmental samples.

Combining advanced techniques allows for even more powerful analysis. For example, P mapping and P speciation can be assessed to characterise the spatial and chemical P heterogeneity at the micro scale, and ultimately P accessibility and availability in soil systems[78]. At the moment, only scarce data exist on spatial soil P micro distribution patterns[79] due to the lack of affordable, but highly versatile analytical techniques, instruments, and standardised data analysis[80]. Only few advanced techniques of P speciation meet these demands, because the structure of soil aggregates is often destroyed, as e.g. in solution ^{31}P NMR spectroscopy[81]. Nano scale Secondary Ion Mass spectrometry (NanoSIMS) allows preserving the structural integrity of a sample, while mapping high-resolution element distributions[82]. In-situ assessments of P distribution at the micro scale can also be mapped by spatially-resolved synchrotron-based X-Ray fluorescence (μ-XRF), due to recent improvements in instrumentation[79]. However, the use of both techniques are impeded by individual technique limitations, such as the comparibly large beam penetration depth for μ-XRF[83], and matrix effects for NanoSIMS[82]. Thus, mapping techniques should be complemented by direct P speciation, as e.g. by μ-XANES spectroscopy to overcome these individual technique limitations and to effectively study micro environments in soils and sediments[78].

2.3 Research aim and objectives

The overall research aim of this study is to reveal how micro and profile scale spatial and chemical heterogeneity of soil P determines P accessibility and availability in soils formed from siliceous parent material. To achieve this aim, the following objectives were constituted:

- How is P spatially distributed at the profile scale, both horizontally and vertically, as investigated by grid sampling and geostatistical methods?
- What P binding forms, as distinguished by wet-chemical fractionation techniques, characterise different stages of pedogenesis at the profile scale?
- How are different P fractions related to other important soil compounds (e.g. SOM, Al and Fe oxi-hydroxides) in different soil depths at the profile scale?
- How can the LCF procedure of P *K*-edge XANES spectra be standardised after appropriate spectrum deconvolution?
- What is the quality of a standardised LCF protocol, obtained with dilute ternary mixtures of the four major P compounds present in soils?
- How is P distributed as related to the distribution of major soil compounds at the micro scale, as mapped by NanoSIMS and µ-XRF in undisturbed aggregates of different horizons from two forest soils, with low and high P content, respectively?
- What major P binding forms can be detected at selected micro sites, as investigated by µ-XANES spectroscopy?

3 Materials and Methods

3.1 Study sites and soil sampling

Soil samples were obtained from four of the five sites of the priority programme SPP 1685 of the German Research Foundation (DFG). All sites are located in Germany and are stocked

with mature, about 120 year old stands of predominantly European beech (*Fagus sylvatica*). The site Bad Brückenau (BBR), Gauss-Krüger-coordinates: 3566195 E, 5579975 N, is located near Fulda, the Black forest site Conventwald (CON), Gauss-Krüger-coordinates: 3422803 E, 5321010 N near Freiburg. The third site is situated in the Bavarian forest near Mitterfels (MIT), Gauss-Krüger-coordinates: 4564502 E, 5426906, and the most northern site near Lüß (LUE), Gauss-Krüger-coordinates: 3585473 E, 5857057 N. The soils differ in parent material and soil type (Table 1).

Table 1: Basic soil characterisation of the four study sites Bad Brückenau (BBR), Conventwald (CON), Mitterfels (MIT), and Lüß (LUE).

	BBR	**CON**	**MIT**	**LUE**
parent material	Basalt	Paragneiss	Paragneiss	Pleistocene glacifluvial sands
soil type[84]	Dystric Skeletic Cambisol (Hyperhumic, Loamic)	Hyperdystric Skeletic Folic Cambisol (Hyperhumic, Loamic)	Hyperdystric Chromic Folic Cambisol (Humic, Loamic, Nechic)	Hyperdystric Folic Cambisol (Arenic, Loamic, Nechic, Protospodic)

At each site, a soil profile was excavated at a representative pure beech location. Samples were obtained from the mineral soil in a 70 x 100 cm rectangle (Fig. 1) at every 10 cm intersection with a steel tube (⌀ 2 cm, sampling depth 3 cm). Depending on profile depth and stone content, 56, 63, 71, and 68 (BBR, CON, MIT, and LUE) samples were taken. Within this grid, up to five smaller gridded nests (up to 6 samples with a distance of 3 cm, taken with the same steel tube) were included to improve geostatistical models[85]. Soil samples were dried at 60° C for 48 h and subsequently sieved ($<$ 2 mm).

3.2 Chemical fractionation

Finely ground subsamples were digested with hydrofluoric acid / perchloric acid ($HF/HClO_4$) to analyse the contents of total P (P_{TOT}), Ca (Ca_{TOT}), Al (Al_{TOT}), and Fe (Fe_{TOT}) by inductively coupled plasma optical emission spectrometry (ICP-OES, Vista-PRO Simulta-

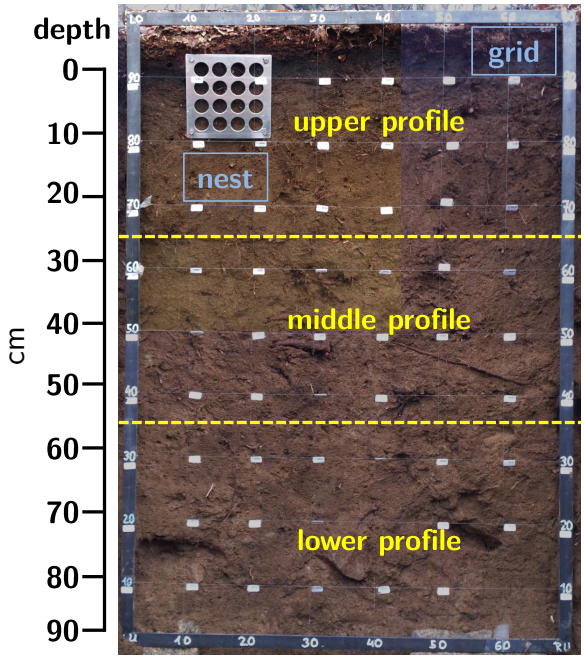

Figure 1: Sampling grid with nest for smaller gridded sampling and scheme of soil region compartmentation. The profile is from the site Mitterfels.

neous ICP-OES, Varian Inc., Palo Alto, CA, USA). To ensure complete digestion of silicate minerals and prevent underestimation of total P, this digestion was favoured over the *aqua regia* digestion[86]. Total carbon (C) and nitrogen contents were analysed with an Elementar VarioEL CN analyser (Elementar GmbH, Hanau, Germany). Because all soils were acidic and carbonate-free, total C content is exclusively total organic C (C_{ORG}). Content of organic P (P_{ORG}) was quantified by ignition loss[87], and the content of inorganic P (P_{INORG}) was calculated by subtracting P_{ORG} from P_{TOT}. The content of P in poorly-crystalline and crystalline Al and Fe pedogenic minerals was analysed by extraction with OX[43] and DCB[44;88] solution, respectively. In addition, OX extracts were analysed for orthophosphate P by colorimetry using the ascorbic acid method[89;90]. A more detailed description which compounds are dissolved and which content of Al, Fe and P is detectable, is given in Table 2.

The content of Fe in crystalline pedogenic minerals (Fe_{CR}) was calculated by subtracting Fe_{OX} from Fe_{DCB}. The respective amounts of OX-extractable P (P_{OX}), i.e. P bound by Fe_{OX} and Al_{OX}, and DCB-extractable P (P_{DCB}) were quantified concomitantly. By subtracting

Table 2: Compounds detectable by the chemical fractionation techniques used in this study.

	acidic NH_4 oxalate	**dithionite-citrate-bicarbonate**	**$HF/HClO_4$**
	P bound to/as		
detection of	1) organically-complexed Al and Fe, 2) Fe in poorly crystalline pedogenic minerals, as well as Al in $Al(OH)_3$, interlayer Al hydroxy polymers, imogolite, and allophane, 3) amorphous $AlPO_4$ and $FePO_4$, most crystalline $AlPO_4$ and some crystalline $FePO_4$	1), 2), and 3), however fewer crystalline $AlPO_4$ and 4) Fe in crystalline pedogenic minerals, as well as Al in crystalline and amorphous Fe minerals	complete digestion
colorimetry[90]	yes	no	no

P_{OX} from P_{DCB}, the content of P bound by crystalline pedogenic Fe minerals and by Al in crystalline and amorphous Fe minerals (P_{CR}) was calculated. Contents of Fe, Al, and P in primary silicate minerals (Fe_{MI}, Al_{MI}, P_{MI}) were calculated by subtracting Fe_{DCB}, Al_{DCB} and P_{DCB} from Fe_{TOT}, Al_{TOT} and P_{TOT}, respectively. The difference between P_{OX} and $P_{OX.INORG}$ was assigned to as organic P in OX-extractable Al and Fe ($P_{OX.ORG}$).

3.3 Bulk XANES spectroscopy

Phosphorus *K*-edge XANES spectra of unknown composition were fitted as linear combinations of standard compound spectra to yield a quantitative measure of the containing P species. For micro site soil samples, 17 P-bearing standard compounds, which represent the most important P species in temperate forest soils were used. In the ternary mixtures, four P standards, each representing a major soil P species, were used to test the quality of the standardised LCF procedure (indicated by *).

3.3.1 Standards and standard mixtures

Standard compounds. The 17 P-bearing standard compounds were: 1) crystalline and 2) amorphous* $Fe^{III}PO_4$, 3) crystalline* and 4) amorphous $AlPO_4$, 5) phytic acid sodium salt hydrate* (IHP; $C_6H_{18}(PO_4)_6 \times xNa + yH_2O$), 6) hydroxyapatite* (Hydap, $Ca_5(PO_4)_3(OH)$), 7) $MgHPO_4$, 8) orthophosphate and 9) IHP retained by boehmite (representing P adsorbed to Al oxi-hydroxides), 10) orthophosphate and 11) IHP retained by ferrihydrite (representing P adsorbed to Fe oxi-hydroxides), 12) orthophosphate and 13) IHP retained by Al-saturated montmorillonite (representing P adsorbed to clay minerals), 14) orthophosphate and 15) IHP retained by Al-saturated soil organic matter (representing P adsorbed to SOM via Al bridge cations), 16) P retained by precipitated Ca_3-IHP (representing Ca-bound IHP), and 17) IHP adsorbed to $CaCO_3$[91].
Compounds were either purchased from Sigma-Aldrich (St. Louis, MO, USA) or synthesised in the laboratory, as described in recent publications[45;91]. The compounds were tested for purity by X-ray diffraction analysis. To avoid self-absorption using XANES spectroscopy and to use P standard concentrations close to natural soil P abundances, the standards were diluted (if needed) with fine-ground, high-purity quartz (Merck KGaA, Darmstadt, Germany) to a concentration of 2 mg P g^{-1}. This diluent was favoured over the often-used boron nitride[56] to more adequately mimic soil matrices. The diluted standards were finely ground and homogenised with agate milling stones (Planetary ball mill Pulverisette 5, Fritsch GmbH, Idar-Oberstein, Germany) or agate mortar and pestle. The milling stones were flushed with deionised water, subjected to ultrasound, and reused with pure quartz after every grinding step. Mortar and pestle were flushed with ethanol and acetone after every grinding step to avoid cross contamination.

Mixtures of standards. Sixteen ternary mixtures of $AlPO_4$, $FePO_4$, Hydap, and IHP standards were produced by weighing defined different amounts of the standard compounds in various combinations to 1 g of sample. The mixtures were homogenised manually with agate mortar and pestle. They represent concentration distributions of three equal P proportions (e.g., P in $AlPO_4$, P in $FePO_4$, P in Hydap, and no P in IHP; mixing ratio 1:1:1:0)

as well as P proportion distributions in which one P species proportion is doubled compared to the remaining two species (e.g., 2:1:1:0). This approach was chosen to validate the general accuracy and the concentration disparities in particular.

3.3.2 Spectral data acquisition

The bulk XANES spectra were acquired at beamline 8 of the Synchrotron Light Research Institute (SLRI) in Nakhon Ratchasima, Thailand[92]. The storage ring had an energy of 1.2 GeV and a stored current of 150 mA. The X-ray photon energy was scanned by an InSb(111) double-crystal monochromator with an energy resolution of $\delta E / E = 3 \times 10^{-4}$ (i.e., ~0.6 eV at the P *K*-edge). The monochromator at beamline 8 was calibrated with pure elemental P (2145.5 eV) every 12 h. There was no indication of movement of E_0 throughout the entire beamtime. Fine-ground sample or standard powder was spread as thin, homogeneous film on P-free Kapton tape (Lanmar Inc., Northbrook, IL, USA). All spectra were recorded in fluorescence mode with a 13-element germanium detector. The sample-holding tape was mounted onto a sample holder, which was placed in a 45° angle from the incident monochromatic beam (beam size 10 mm × 1 mm) to increase fluorescence yield. The sample compartment was constantly purged with helium gas to minimise X-ray absorption by air surrounding the sample.

After calibration, spectra were measured in energy ranges from 2045.5 eV to 2495.5 eV with a 2 s dwell time per energy step. These ranges were selected to collect data in longer ranges (>200 eV)[56]. Energy steps were chosen as follows: From 2045.5 eV to 2105.5 eV and from 2245.5 eV to 2495.5 eV: energy step of 5 eV; from 2105.5 eV to 2135.5 eV and from 2195.5 eV to 2245.5 eV: energy step of 1 eV; from 2135.5 eV to 2195.5 eV: energy step of 0.25 eV. A minimum of four spectra for the standards and mixtures, and two spectra for the samples was acquired.

3.4 Micro-scale assessments

Micro-scale P distribution and speciation was assessed in four undisturbed aggregates of different horizons from the LUE and BBR soils (parent material with low and high P content, respectively). Samples were taken from the mineral topsoil (directly below the organic layer) and the subsoil (30 cm depth). The LUE soil showed at the sampled topsoil spot a total P bulk concentration of 0.22 mg g^{-1} and at the sampled subsoil spot a concentration of 0.06 mg g^{-1}. The BBR topsoil showed a total P bulk concentration of 3.12 mg g^{-1}, and the BBR subsoil 1.99 mg g^{-1}.

3.4.1 Sample preparation

For each site and depth, three dried, intact soil aggregates (~1 - 2 mm^3) were embedded in an epoxy resin (Araldite 502 Kit, Electron Microscopy Sciences, Hatfield, PA, USA). The embedded aggregates were then cured at 60° C for 24 hours, and subsequently thin-sectioned, polished and coated with gold by physical vapor deposition[93]. One aggregate per site was randomly selected for scanning electron microscopy (Jeol JSM 5900LV, Eching, Germany) imaging to locate regions of interest for the subsequent imaging techniques.

3.4.2 Element mapping using NanoSIMS

The NanoSIMS measurements were conducted with a Cameca NanoSIMS 50L instrument (Cameca, Gennevilliers Cedex, France) at Technical University of Munich, Germany. A Cs^+ source with a primary ion energy of 16 keV was used to produce secondary ions of the sample surface. The focused beam (lateral resolution about 100 nm) scanned over areas of 40 × 40 μm^2 while the mass signals of the secondary ions $^{12}C^-$, $^{16}O^-$, $^{12}C^{14}N^-$, $^{28}Si^-$, $^{27}Al^{16}O^-$, $^{31}P^{16}O_2^-$, and $^{56}Fe^{16}O^-$ were collected. In the latter three ions, ionisation is stronger than that of the individual Al, P, or Fe ions. The ion images were acquired using a 10 ms per pixel dwell time in an area of 512 × 512 pxs^2. On each aggregate 5 – 7 measurements were conducted.

3.4.3 Element mapping using µ-XRF

Due to time restrictions, at less, but at the same locations as the NanoSIMS measurements, µ-XRF was performed for measuring at the synchrotrons. Synchrotron-based µ-XRF measurements were conducted at the TwinMic Beamline of the ELETTRA synchrotron (storage ring energy 2.0 GeV) in Trieste, Italy, and at Beamline ID21 of the European Synchrotron Radiation Facility (ESRF, storage ring energy: 6.03 GeV) in Grenoble, France. The TwinMic Beamline was operated in low energy X-Ray Fluorescence (LEXRF) mode and was equipped with a 600 lines per mm Au plane-grating monochromator. The fluorescence detector consisted of 8 silicon drift detectors[94]. The samples were installed in a vertical plane, orthogonally to the incident photon beam. The data were acquired at 2.19 keV to optimise the P emission signal. The LEXRF dwell time varied between 1 and 7 s as a function of the samples, and the maps were acquired by raster scanning with a 1 µm step size and a minimum size of 40 $\times$ 40 pxs^2 (= 40 $\times$ 40 µm^2).

The ID21 Beamline[95] of ESRF was equipped with a double crystal Si(111) monochromator (resolution: 0.4 eV). The samples were tilted by 28° with respect to the incident beam and the fluorescence signal was collected by a silicon drift detector, placed at a 49° angle with respect to sample surface. After selection of the area of interest, raster maps were recorded using a focused beam at 2.165 keV to intensify P *K*-edge emission, with a dwell time of 150 ms and a step size of 0.5 µm. The elemental distributions were obtained by deconvoluting the µ-XRF spectra after incoming flux and detector deadtime correction, on maps of a minimum size of 80 $\times$ 80 pxs^2 (40 $\times$ 40 µm^2) with the PyMCA software[96].

3.4.4 P speciation using µ-XANES spectroscopy

Micro scale XANES measurements were conducted at Beamline ID21 of ESRF to support the elemental raster images by direct P speciation results from LCF with all 17 P reference spectra. Phosphorus *K*-edge µ-XANES spectra were collected with a 0.2 eV step size, a dwell time of 0.1 s, and in an energy range from 2130 to 2200 eV. For each P micro site (minute sites of increased P content), 10 – 40 spectra were recorded and merged.

Spectra were calibrated in energy by comparing apatite spectra taken at SLRI and ESRF: a correction value of δE = -1.15 eV was applied.

3.5 Data analysis

Data were generally analysed with the software package R, version 3.3.2[97]. One new R package was published on *CRAN* as result of this study (package *LCF*).

3.5.1 Wet-chemical fractionation data

Geostatistical Analysis. Bayesian Kriging was performed using geoR package, version 1.7-5.2[98]. This approach was preferred over ordinary or universal kriging because covariance parameters do not have to be considered known and to allow parameter uncertainty in the prediction[99]. However, the default Bayesian approach of treating the parameters as random variables often resulted in poor posterior distribution estimates due to small numbers of support points. In these cases, we calculated covariance parameters from empirical variograms to define the prior parameters. First, data were analysed for a depth trend. This was performed by testing the data values and the y-coordinates for correlation using the Kendall rank correlation coefficient and a scatter plot with a linear regression model. As second step, the data were checked for normal distribution using the Shapiro-Wilk test. When the assumption of normal distribution was rejected, the Cressie[100] variogram estimator was used to build robust variograms. In all other cases the classical method of moment estimator was applied. All variograms were computed using the geoR-Package (ordinary kriging) and the gstat-Package (universal kriging), version 1.1-3[101]. Each variogram was calculated for the maximum distance between all samples, half of the maximum distance and one third of the maximum distance. For each distance, variograms were computed for six to thirteen bins in each variogram. For map computation, the variogram parameters with the lowest root mean squared errors were set as prior parameter for Bayesian Kriging. Afterwards, Bayesian Kriging was performed using a 1 cm prediction grid.

Numerical Analysis. To characterise and compare the magnitudes of spatial variation of the investigated soil properties among the three profiles, coefficients of variation (CV) were calculated for the variables C_{ORG}, Ca_{TOT}, Fe_{MI}, Fe_{CR}, Fe_{OX}, Al_{MI}, Al_{DCB}, Al_{OX}, P_{TOT}, P_{ORG}, P_{MI}, P_{INORG}, P_{CR}, P_{OX}, $P_{OX.ORG}$, and $P_{OX.INORG}$. Additionally, in order to specifically address the horizontal and vertical variation of the variables, a vertical and a horizontal CV were calculated (CV_{ver} and CV_{hor}). These were the medians of the coefficients for every column and row, respectively, if the profile is imagined as a table consisting of rows (i.e. left to right part of the profile) and columns (depth increments). The proportion of horizontal CV by vertical CV ($CV_{hor/ver}$) served as a measure of variability in profile width and depth; i.e. values below 1 expressed a greater variation in vertical than in horizontal direction of the profile, and vice versa. Correlation patterns among the studied variables were analysed using the Spearman rank coefficient ρ. An upper profile region was defined by all sample points starting from the mineral soil surface to those of 25 cm depth (Fig. 1). The middle profile region included points less than 25 cm depth down to 55 cm depth, and the lower profile region contained points from less than 55 cm depth and reached until 70 cm (CON), 80 cm (LUE), or 90 cm (MIT) of depth. Additionally, factor analysis was performed on all variables of a given soil profile using psych package, version 1.6.9[102] to infer explanatory constructs from the observed variables. The Optimal Coordinate method was used to select the number of factors. For rotation varimax and as factoring method principal axis factoring was determined. Factor scores were identified using Thurstone regression.

3.5.2 XANES spectroscopy data

Spectrum Deconvolution. Initial spectrum deconvolution was performed with the program ATHENA of the software package DEMETER[103] (version 0.9.25). At first, E_0 of all raw spectra was calibrated to the zero crossing of the second derivative of the absorption. Replicate spectra of a given sample were then examined visibly for glitches, drifts, noise, and general quality before merging them. The data was further processed using the software R[97]. The exported spectra were initially baseline-corrected from –80 to –20 eV (linear regression) and normalised and flattened to an absorption (edge-step) of 1 from

+140 to +340 eV (linear regression) with respect to E_0. These values reproduced a longer spectrum (up to +850 eV) of IHP in the best way to make sure that our spectra were not biased by small normalisation ranges. Because in the past no standard protocol existed for the deconvolution of P *K*-edge XANES spectra, we concluded that the starting values for baseline correction and edge-step normalisation could be set personally.

Spectra with Smaller Energy Ranges. We also fitted our data with baseline correction and edge-step normalisation energy values closer to E_0 to test the applicability of our standard protocol for P *K*-edge XANES spectra acquired in a smaller energy range. These ranges (e.g., between 2140 and 2200 eV) have mostly been used for LCF in earlier studies[62;104], partly to avoid the superposition of P XANES spectra by the sulphur *K*-edge (+326.5 eV, with respect to the P *K*-edge) in soils and sediments. In this approach initial baseline correction of all spectra in the mixture study was performed from –40 to –10 eV and edge-step normalisation from +35 to +65 eV with respect to E_0. These values were chosen from corrected and normalised standard spectra that represented best the spectra of the respective standard compound obtained with the larger energy ranges described above. Due to even smaller energy energy ranges in the μ-XANES spectroscopy study, the reference spectra were initially baseline corrected from -36 to -15 eV and normalised from +37 to +57 eV with respect to E_0 of the respective spectra.

Linear combination fitting. Linear combination fitting, using quadratic programming, was conducted from -14 eV to +46 eV (with respect to E0) with the function *solve.QP* of package *quadprog* (Version 1.5-5). In the mixture study, all four standards were used to create the fit. We allowed the baseline and normalisation parameters of the samples to be modified, on the basis of the observation that minor modifications of these parameters can lead to considerable changes in the P speciation results. Computerised combination of all possible baseline correction and edge-step normalisation parameters using R code resulted in over 65000 baseline-corrected and edge-step-normalised sample spectra. Among these spectra, the lower energy level used for baseline correction varied between –80 and –40 eV

(2.5 eV step), and the upper energy level varied between –30 and –10 eV (2.5 eV step) with respect to E_0. The lower energy level used for edge-step normalisation varied between +120 and +170 eV (2.5 eV step), and the upper level varied between +290 and +340 eV (2.5 eV step) with respect to E_0. All spectra were automatically fitted, using the initially baseline-corrected and edge-step-normalised standard spectra as predictor compounds. The best fit was chosen, as seen by the lowest R-factor (χ^2 divided by the sum of the squared sample data; same as in ATHENA). For the smaller energy ranges, parameters of the samples were allowed to vary between –48 and –28 eV (baseline parameter at the lower energy level) and between –18 and –8 eV (baseline parameter at the upper energy level) with respect to E_0, both with a 1 eV step. The edge-step normalisation parameter at the lower energy level varied between +29 and +39 eV (0.5 eV step); the edge-step normalisation parameter at the upper energy level varied between +60 and +70 eV (1 eV step) with respect to E_0. All other data processing was performed as already described before for the deconvolution of XANES spectra with the larger energy ranges.

As for the µ-XANES spectroscopy, the first baseline correction parameter was allowed to vary from -28 to -18 eV (step: 1 eV) and the second from -16 to -8 eV (step: 0.5 eV) with respect to the edge-step. The first normalisation parameter was allowed to vary between +29 and +39 eV (step: 0.5 eV) and the second between +42 and +48 eV (step: 1 eV) with respect to the edge-step. The actual LCF was performed from -14 to 46 eV with respect to E_0 of a sample spectrum. Phosphorus speciation shares below 5% of total P were excluded and LCF was repeated without the respective standards. Only fits with R-factors smaller than 0.005 were included because fits with R-factors greater than this value were obviously unreliable.

3.5.3 Micro scale distribution patterns

First, we performed k-means cluster analysis[80] on every ion/element count rate of all NanoSIMS and XRF measured ions/elements to determine regions with similar element identity. The count rates of every pixel were assigned to one of five cluster centres, respectively. The three largest cluster centre values were combined to result images where each pixel

is either assigned as "area rich in", or as a negligible count value. For the NanoSIMS images, ions of the elements and element pairs of P, Fe, Al, CN and Si were selected. The latter four ions and their combinations were then assigned to soil compound classes: i) Fe/Al oxi-hydroxides (Al, Fe, Fe+Al), ii) Fe/Al oxi-hydroxides + SOM (Al+CN, Fe+CN, Fe+Al+CN, Fe+CN+Si), iii) clay minerals (Al+Si, Fe+Al+Si), iv) clay minerals + SOM (Al+CN+Si, Fe+Al+CN+Si), v) quartz (Si), vi) SOM (CN, CN+Si), and vii) unspecified (i.e. mainly resin). The total number of pixels, respective total area, of these compounds and the compound-rich areas that were co-located with P were counted. Dividing the P-rich area that is co-located with a specific compound by the total P-rich area resulted in a proportional measure for P binding. Dividing the compound-rich area that is co-located with P by the total compound-rich area resulted in a proportional measure for compound-specific P allocation. Both measures are displayed as percentage of total P/compound-rich area, respectively.

Micro scale XRF maps were processed alike, but the elements for co-localisation differed due to different instrument conditions. The ELETTRA instrument also allowed all stated P binding categories, however, CN was replaced by N only. The attribution to the seven categories persisted as stated. The ESRF instrument unfortunately did not provide information on N, but on the L_2-edge of Fe (719.9 eV). During compound classification, this element was treated similarly as the other Fe edge. The compound classes, to which element combinations were assigned to, were therefore limited to only those that did not include SOM (i, iii, v, and vii). This procedure and the heterogeneity of P and soil compounds resulted in different proportions of P and soil compounds depending on the instrument used.

4 Results and Discussion

This section focusses on a general discussion and only summarises results from studies performed for this thesis. Detailed presentations of the results are accessible on-line from the publications and in the appendices.

4.1 Compounds determining the profile scale spatial patterns of P fractions

The data obtained at the profile scale showed that, as expected, the most important correlation variable for organic P and adsorbed P fractions (P_{CR}, P_{OX}) was SOM, represented as C_{ORG}. The interpolated maps of P_{TOT}, P_{ORG} and C_{ORG} also showed a noticeable similarity, especially in the topsoil. Organic P forms, such as to a large extent inositol phosphates (e.g. IHP), accumulate in the topsoil due to P inputs from shoot and root litter, as well as root and microbial exudates, whereas more labile organic P forms are either mineralised or translocated as dissolved organic P (DOP)[105]. Additionally, pedogenic Al minerals and poorly crystalline pedogenic Fe minerals (Al_{DCB}, Al_{OX}, Fe_{OX}) were correlated with organic P fractions, particularly in the middle and lower profile. It is well known that Al and Fe oxi-hydroxides have a high capacity to adsorb both P_{ORG}[106;107], and P_{INORG} species[4;21]. The respective contents of NaOH-EDTA extractable Al, Fe and inositol phosphates showed a positive relationship in boreal forest soils in Sweden[108]. Goethite, illite and kaolinite retain IHP in higher amounts than P_{INORG}[106], and phosphate adsorption to synthetic Al and Fe oxides is minor influenced by humic soil substances[109]. It thus can be assumed that predominantly P-bearing SOM competes with inorganic phosphate for adsorption sites on Al and Fe oxi-hydroxides. This assumption is supported by the fact that adsorption of P_{INORG} was negligible at sites CON and MIT due to competing adsorption of P_{ORG}.

Poorly crystalline metal oxides, organo-mineral complexes, mixed Fe–Al gels, goethite, gibbsite, and allophane sorb more phosphate than clay minerals (montmorillonite, illite, smectite, nontronite, kaolinite) because of the smaller surface areas of the latter compounds[21]. Additionally, clay minerals have less importance for P translocation compared to Fe and Al oxi-hydroxides, as the latter compounds often occur in the colloidal size fraction (1 – 500 nm)[105]. Clay mineral P retention, however, can be strongly intensified by Al-coverage[110]. The OX-extractable fraction includes P retained by Al-saturated expandable clay minerals, as oxalate is known to form strong complexes with Al[111]. In addition, clay minerals mainly influence P retention by Al and Fe ions bound to the silicate surfaces rather than by the

phyllosilicate lattice itself[21;24]. Thus, both the surface charging of clay minerals, and the clay type affect the surface coverage by Al and Fe cations. They determine the amount of clay mineral-bound P in the poorly crystalline pedogenic Fe and Al mineral fractions. On the other hand, organic P - which is known to have a high charge density, particularly IHP - is retained in soils by complexation, by adsorption to clays, or as precipitate with pedogenic minerals[112]. Thus, especially in loamy soils (as e.g. at BBR and CON site), some P is retained by clay minerals.

Dissolution of apatite is the primary P source in soils[2]. However, small P amounts can be preserved as inclusion, e.g. in slowly weathering silicates[113]. At sites CON, MIT, and LUE, correlations of predominantly inorganic P fractions with contents of Al_{MI} and Fe_{MI} were detected, especially high at MIT and LUE. This suggests that, even at later stages of pedogenesis, the remaining unweathered primary rock, e.g. slowly weathering silicate rock, bears some inorganic P forms. During soil development, adsorbed P_{INORG} can desorb when displaced by other soil solution anions[21;111]. This desorption was illustrated in the spatial pattern of easily available orthophosphate ($P_{OX.INORG}$) at sites CON and MIT, where $P_{OX.INORG}$ showed maxima in the upper (CON) and the lower profile (MIT).

The horizontal, i.e. lateral, variability of soil properties is is commonly assumed to be rather low compared to the vertical, i.e. depth, distribution, which is typically studied by core sampling[29;51]. However, heterogeneous soil P distribution is known to affect plant rooting patterns[30] and mycorrhizal symbiosis[31]. Thus, it is important to assess the horizontal, as well as the vertical profile scale variability when: i) detecting zones where e.g. P_{TOT} and P_{ORG} are relatively enriched or depleted, ii) investigating soil parameters to study soil processes enduring decades or even centuries.

4.2 Effects of podsolisation on spatial patterns of P fractions at the profile scale

At site BBR, podsolisation was not developed, due to slow weathering of the basalt bedrock, the hill-top location, and oxide-richness in this soil[114]. Calcium was depleted in the acidic

BBR topsoil, but its contents increased from the top- to the subsoil. However, Al- and Fe oxi-hydroxide contents were largest in the upper profile, compared to lower profile compartments. A higher P_{INORG} content was detected in the upper and lower profile, whereas its content was particularly low in the middle profile.

At site CON, an early stage of podsolisation was found. The hill-side soil showed many rock outcrops from the regolith bedrock[73]. Significant translocation of pedogenic Al minerals was detected; however, their contents were still high in the upper profile. In contrast, the contents of Fe bound in poorly crystalline pedogenic minerals was highest in the uppermost topsoil. In addition, SOM contents decreased gradually from the topsoil to a depth of 20 cm, and the vertical variation was larger than the horizontal. These compound distributions indicate initial podsolisation, as characterised by mobilisation of Al, either as Al–Si hydroxy sols or complexed by dissolved organic acids[115]. In the middle part of the CON profile, pedogenic Al minerals and poorly crystalline pedogenic Fe minerals showed increased importance for P retention, supposedly because Al and Fe oxi-hydroxides and Al- and/or Fe-covered clays have adsorbed P-rich SOM and P_{INORG}. Mineral Al and Fe contents showed maxima at depths of 40 – 70 cm, probably as result of ongoing Al and Fe mobilisation from the primary parent material. At these depths, additional enrichment zones of P_{INORG}, $P_{OX.INORG}$, and P_{MI} were detected. This can be explained by formation of secondary crystalline $AlPO_4$ which probably has formed after weathering of primary apatites[116].

The Cambisol at site MIT was characterised by more advanced podsolisation, compared to sites BBR and CON. This podsolisation was detected visibly by bleached sand grains in the topsoil (Nechic subqualifier), and analytically by the distribution of pedogenic Al minerals in the topsoil. Compared to BBR and CON, dissolution of Al oxi-hydroxides was advanced, although poorly crystalline pedogenic Fe minerals were still abundant in the topsoil. At MIT, contents of P_{INORG} and especially $P_{OX.INORG}$ increased gradually from the top- to the subsoil. However, the hill-top MIT soil - also formed from regolith[73] - lacked the rock outcrops that retarded podsolisation of the hill-side CON and the basaltic BBR soil. The highest contents of pedogenic Al minerals were detected in the middle profile at site MIT, indicating constant dissolution of these minerals in the upper profile, translocation, and precipitation

in the middle profile.. As a result of pedogenic Al mineral dissolution and translocation, many P fractions showed low total and vertical variability. In general, the distribution patterns of many P fractions were identified as comparably homogeneously distributed, characterising intermediate stages of podsolisation. Additionally, the soil at MIT showed this podsolisation also as a result of former large industrial, atmospheric S deposition[117] and recent large N deposition. This is in accordance with results of a temperate forest soil study of six watersheds in the eastern United States and Europe. The authors of this study found that the dominant chemical fraction of P was (i) associated with secondary Al and organic phases and (ii) responsive to experimental acidification[118].

At site LUE, Al and Fe primary minerals were not provided abundantly by the sandy parent material, resulting in pronounced podsolisation at this site, visible e.g. in the eluvial horizon. However, small amounts of enriched pedogenic, and unweathered primary Al and Fe in silicate minerals were detected at depths below 10 cm in a (proto-) spodic horizon. In this region, the contribution of poorly crystalline Fe was largest just below the eluvial horizon, whereas the contents of Fe_{CR}, and of pedogenic Al minerals were highest at greater depths. This pattern is expected, as (i) organic acids and Al/Fe ions form strong, water-soluble complexes[114], and as (ii) Fe-SOM complexes are less soluble than Al-SOM complexes and thus precipitate earlier[29]. Additionally, DOP is effectively retained by subsoils, in which DOP was enriched in the mobile hydrophilic fraction, as shown for five acidic forest sites in Germany[119]. It can therefore be assumed that the P enrichment in the middle profile of site LUE is due to illuviation and retention of P-rich SOM. After dislocation of this P-rich SOM from the upper and its retention in the middle and lower profile, it was probably adsorbed to first mainly pedogenic Fe- (15 – 50 cm depth), and at 30 – 50 cm depth to pedogenic Al minerals. High contents of many P fractions were detected in the uppermost LUE topsoil, accumulated due to increased SOM contents in the topsoil. This highlights the importance of topsoil P_{ORG} mineralisation and microbial litter for plant nutrition in P-deficient organic soils, as e.g. demonstrated for boreal forest[120]. Diffusive P (P species transported into the soil solution due to a concentration gradient) has supposedly an increasing importance with increasing soil depth, as shown in a temperate forest soil study[121].

4.3 Improvement of linear combination fitting accuracy

Chemical soil fractionation techniques only reveal operationally-defined P species, though do not allow for direct P speciation. Even though P *K*-edge XANES spectroscopy has been used for P speciation in soils for over two decades[54], the quantities of different P species as determined by LCF is still discussed controversially[59]. Phosphorus speciation was tested in dilute (2 mg P g^{-1}) mixtures of the major P species present in soils ($AlPO_4$, $FePO_4$, Hydap, and IHP).

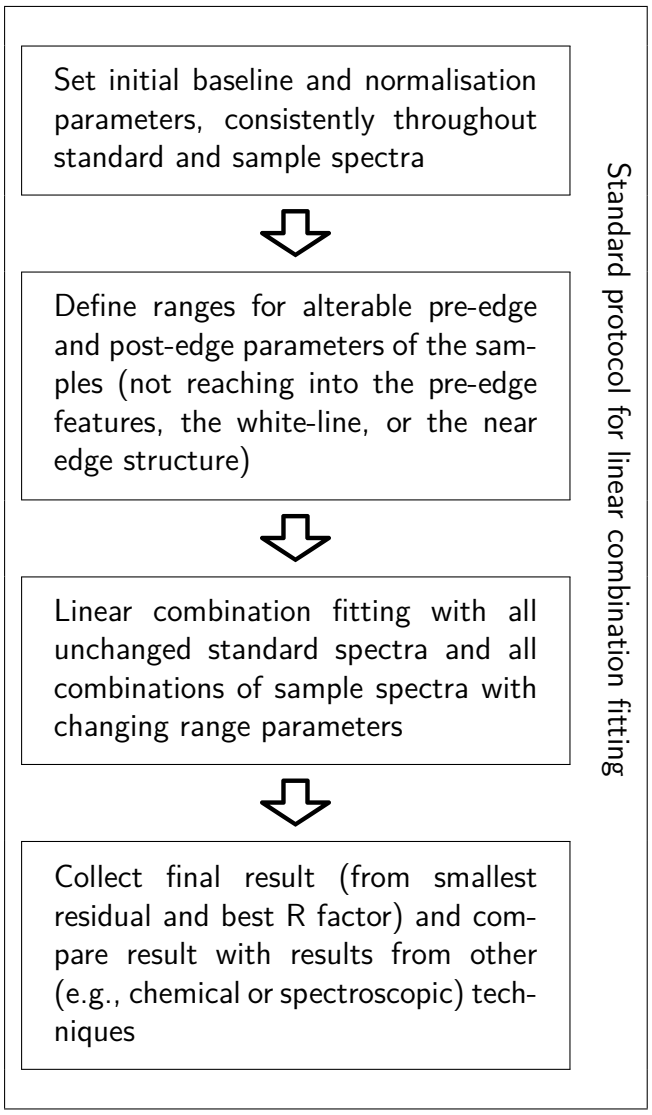

Figure 2: Flowchart of the standard protocol for linear combination fitting. The protocol has been tested on P *K*-edge XANES spectra of standard compound mixtures and soil samples. Printed with courtesy of ACS.

After applying baseline correction and edge-step normalisation according to the newly established standard protocol LCF (Fig. 2), P species were reproduced with a mean deviation between 3 and 9% (of total P) and a mean absolute deviation of 5%. This approached considerably improved traditional LCF with the widely-used X-ray absorption data analysis software ATHENA[103]. Furthermore, LCF was also enhanced using the new standard protocol for spectrum deconvolution and subsequent LCF on P *K*-edge XANES spectra on soil spectra. The accuracy of the LCF was improved mainly because the procedure did not follow the often cited[56] advice to apply normalisation "as consistently as possible" between samples and standards[122]. Linear combination fits obtained using this rule were sometimes obviously incorrect, and sample-specific adjustment of baseline-correction and edge-step normalisation energy parameters markedly enhanced the fitting results, even when performed manually in ATHENA.

The new standard protocol (Fig. 2) answers the call for urgently needed "systematic studies to directly validate and improve the precision and accuracy of XAS fitting results"[38]. Inorganic P species were quantified more accurately than IHP in most cases. The procedure can generally be transferred to any XANES spectrum representing a mixture of different P species, provided that all reasonable standard compound spectra have been included to create the fit. There was no difference between using short or long energy range parameters with respect to P speciation results. In general, small changes in baseline and normalisation parameters, not variation in range parameters lead to more accurate fits. Using ATHENA, LCF fitting can also be optimised, adjusting baseline and edge-step fitting parameters and repeatedly inspect the fit visually to minimise the residual of the fit. When doing so, special care has to be taken, examining the pre-edge region and the energy range between the white-line and 2190 eV. The results indicate that the newly established standard protocol is broadly applicable for P *K*-edge XANES spectroscopy. However, some pitfalls associated with the assessment of LCF results from unknown samples have to be taken care of: (i) small proportions of a compound to total P, (ii) the fitting statistics, (iii) the selection and plausibility of LCF standards, and (iv) difficulty to measure organic P.

4.4 Linear combination fitting pitfalls

In some cases, small proportions (1 – 4% of total P) of a particular P species were claimed erroneously by LCF. As good scientific practice, P amounts smaller than 5%, as identified with LCF, are not reliable and should be confirmed with other methods or excluded from the reported P speciation results. As XANES spectra can generally not be investigated as black boxes without any knowledge of its origin, LCF results should always be interpreted cautiously when additional information is lacking[56].

The LCF statistics (χ^2 and R factor) were used to compare adjustment of the baseline and edge-step fitting parameters. However, they were unreliable as an absolute measure of goodness-of-fit when comparing fits from different samples, because mean absolute deviation of the respective fitting results and R factor did not correlate significantly. The fitting statistics presumably are a poor indicator for the fitting quality because residuum information is integrated over energy regions that are relevant for an accurate LCF result (e.g., pre-edge peak, white-line, post-edge features), but also over less relevant energy regions.

Besides carefully increasing the fitting quality and validating small P species amounts, the plausibility of LCF results should still be examined critically because adding many different P standard compound spectra may result in improved fitting statistics, even if some P species are unlikely to occur in a given sample. The actual presence of a stated species can additionally be questionable as the existence of a fitted amount can be chemically impossible[56]. Gathering additional information about unknown samples from any available source is thus strongly recommended.

Particulary organic P, which was reproduced with lowest accuracy in the mixtures, should be cross-checked with other techniques, as e.g. solution ^{31}P NMR spectroscopy[81]. The unfocused X-ray radiation did probably not damage the samples, as observed for IHP with a focused X-ray beam[69] because the spectra did not show specific beam damage effects when repeated. Organic P was reproduced best when no $FePO_4$ was present. Both spectra exhibit similar post-edge features at 2160 eV, probably influencing the fitting results of these two standards, whereas the standard spectra of Hydap and $AlPO_4$ differed distinctly from

the latter two in this region. Nonetheless, even small changes in baseline and normalisation parameters were the main drivers for more accurate fits.

4.5 Soil depth considerably influences micro scale P heterogeneity at advanced stage of podsolisation

Phosphorus speciation using P *K*-edge XANES spectroscopy with a focused beam was applied at 15 P-rich micro sites (definition: see Section 3.4.4) of four aggregates from the low-P LUE and the high-P BBR top- and subsoil, respectively. The distribution and micro site speciation of P varied more pronouncedly for the low-P top- and subsoil at site LUE, than for the high-P aggregates at BBR. The speciation results from LUE suggest that soil depth more strongly determines P speciation at the micro scale at later stages of podsolisation. Using µ-XANES spectroscopy, spatially-resolved P speciation results at P micro sites revealed that the low-P topsoil aggregate mostly comprised organic P (0 – 55% of total P: free organic P, 9 – 38% of total P: Ca-bound organic P). Micro scale Ca-P complexation processes probably formed this Ca-bound organic P in the topsoil aggregate[123]. Additionally, orthophosphate adsorbed to Al oxi-hydroxides and organic P adsorbed to Fe oxi-hydroxides were detected in substantial amounts. All soil compounds were to a greater proportion co-located with P in the top- than in the subsoil, because P was relatively abundant at shallow soil depths compared to the subsoil horizons.

In the low-P subsoil aggregate sample at LUE, quartz grains encompassed with and agglutinated by a finer-grained matrix were identified using scanning electron microscope imaging. The P present in this sample was incorporated in the fine matrix of SOM and the mineral coatings, and the retained P was predominantly inorganic. At this site, spatially-resolved P µ-XANES speciation conducted on P micro subsoil sites revealed that P was predominantly bound as $AlPO_4$ and $FePO_4$. It has been reported that strengite or variscite (Fe and Al phosphates, respectively) can persist in soil environments with moderately acidic pH[124], however, these results are questionable. For example, crystalline $AlPO_4$ (berlinite) was identified to be more resistant against dissolution at pH 6 – 7 than at pH 3[45]. Addition-

ally, it must be emphasised that the reference standard compound spectrum of amorphous $AlPO_4$ is close to identical with the spectrum of Al hydroxy phosphate, which is known to be thermodynamically stable at less acidic pH values. Lastly, up to about a quarter of total P was clay mineral- or Fe oxi-hydroxide-bound in the low-P subsoil aggregate. This highlights the importance of Al- and Fe-bearing pedogenic minerals in micro sites of sandy subsoil aggregates for retaining P that has already been described at the profile scale.

4.6 Soil substrate influence on micro scale P heterogeneity is stronger during early stages of podsolisation

The clayey-silty soil substrate at the high-P BBR site profoundly defined the micro scale P speciation and distribution patterns. This substrate originates from ongoing intense weathering of basalt rock and rock fragments into Al and Fe oxi-hydroxides and 2:1 clay minerals[125]. In the high-P topsoil aggregate, micro sites of P were characterised by orthophosphate adsorbed to Al-saturated SOM and Al oxi-hydroxides, as well as by $AlPO_4$ and $FePO_4$. Although Fe oxi-hydroxides strongly adsorb both inorganic[21] and organic[106] P under moderately acidic conditions, as present at this site, P binding was only marginally influenced by Fe oxi-hydroxides in the high-P topsoil aggregate. Interestingly, just little P was detected as organically-bound P compounds (0 – 13%). This is probably due to intensive mineralisation of organic P in the topsoil at site BBR[15]. Up to about a quarter of total P was assigned to easily bioavailable $MgHPO_4$, which was only, but consistently detected in the high-P topsoil aggregate. The existence of this P species is surprising, because $MgHPO_4$ is unstable below pH 5. Presumably, $MgHPO_4$ has been stabilised in less acidic interior regions of soil aggregates. These results emphasise not only how important sorbed and mineral P phases are at early stages of podsolisation, but also how important investigating micro scale P heterogeneity is for assessing P availability and accessibility in soils.

In the BBR subsoil aggregate, Hydap was detected consistently at all micro sites. Additionally, percentages of $AlPO_4$ and $FePO_4$ were similar to those found in the topsoil

aggregate. This underlines that the influence of soil substrate on micro scale P heterogeneity in siliceous aggregates is stronger at the little developed high-P BBR soil than at the pedogenetically older low-P LUE soil. Unexpectedly, clay mineral-bound P percentages were relatively low. Exchanger-sites of expandable clay-minerals are predominantly covered with Al hydroxy polymer cations at pH values between 4 and 5, which are present in the BBR subsoil[73]. Thus, these clay-minerals have a sorption efficiency similar to that of Al oxi-hydroxides[91], which have been identified as important P species in the high-P subsoil aggregate. However, the results from the micro site study revealed that P adsorbed to Al-saturated clay minerals contributed only secondarily to P speciation in the BBR subsoil aggregate.

4.7 Micro scale soil P distribution patterns are soil-dependent

Not only micro scale P speciation, but also the amount, distribution, and form of P-rich areas (definition: see Section 3.5.3) differed strongly among the investigated aggregates. Expectedly, the spatial P distribution was characterised by pronounced heterogeneity, as revealed using raster imaging performed with NanoSIMS and μ-XRF. In the aggregates of the high-P BBR soil, P-rich areas were relatively abundant and distributed less loosely than the relatively few and more distant P-rich areas in the aggregates of the low-P LUE soil. In these areas, P was mostly co-located with Al and Fe (mostly oxi-hydroxides) and to a lesser extent with clay minerals.

In the LUE aggregate, P-rich areas were predominantly co-located with Al/Fe oxi-hydroxides in the subsoil. However, topsoil Al/Fe oxi-hydroxides were more frequently co-located with P than those in the subsoil. If SOM was present, co-localisation of P increased for both Al/Fe oxi-hydroxides and clay minerals. In addition, SOM was strongly co-located with P in the low-P LUE topsoil, which indicates that in the sandy LUE topsoil, the few Al and Fe oxi-hydroxides and clay minerals play a pivotal role in retaining P. It can be assumed that P-rich SOM is complex-bound at the surfaces of these Al and Fe oxi-hydroxides and Al-/Fe-saturated clay minerals[21], especially in the topsoil of this site.

In contrast, the aggregates of the high-P BBR soil showed different P distribution patterns due to the finer-grained, clayey-silty soil substrate. At this site, the most important compounds for P binding were Al and Fe oxi-hydroxides. In the topsoil, both Al/Fe oxi-hydroxides and clay minerals were frequently co-located with P. The influence on P sorption by cationic Al hydroxy polymer clusters on 2:1 clay mineral surfaces[91;126] and by Al and Fe oxi-hydroxides under acidic conditions[21] is well known. Nonetheless, the results from the micro scale aggregate study implies that a robust mechanistic understanding of micro scale P retention and P release must account for the heterogeneous P distribution in soil aggregates.

4.8 Conceptual model of P distribution during podsolisation

The results presented in this thesis indicate that the micro and profile scale P distribution is affecting P acquisition strategies of plants and soil microorganisms. They allow for deducing of a conceptual model of relationships between the stage of podsolisation and the distribution of different P forms. This model takes into account the distribution of pedogenic Al and Fe minerals in a soil profile, important P fluxes, and the concept of P-acquiring and P-recycling systems[14]. The model is in accordance with the results of numerous field studies of soil profiles with different degree of podsolisation[16;108;118]. The conceptual model refines the often cited model describing trends of soil P amounts and forms with time[2] by visualising the zonation of P pools in acidic temperate soils on siliceous parent material, and adds a geochemical description of the spatial distribution of P in soils during podsolisation.

During initial stages of pedogenesis, primary P-bearing minerals (e.g. apatite) are weathered and the released P is taken up directly by plants and microbes[14]. Apatite weathering can be promoted by ectomycorrhizal fungi[127]. Phosphorus retention is increased in the topsoil after initial soil acidification, as result of increased contents of plant-available P[128], protonation of oxi-hydroxides, and after saturation of SOM and clay cation exchanger sites with Al^{3+}. In the mineral topsoil, biocycled P is retained by newly formed pedogenic oxi-hydroxides,

however, P also leaches as DOP and/or in colloids through the soil, as described for site CON[72]. Fast lateral flows can promote P losses[105], as e.g. present at site CON.

Intermediate stages of podsolisation are characterised by progressive soil acidification. As result, in the topsoil, Al oxi-hydroxides dissolve, clay minerals are destructed and Al-bound P is mobilised. The dislocation of P, as e.g. at site MIT, results in rather homogeneous vertical variation of C_{ORG} and P_{TOT}. However, SOM in general, and thereby P_{ORG}, is protected in the interior of soil aggregates[129], and its mineralisation by microorganisms is hampered when adsorbed to minerals[130]. Thus, P binding partners (SOM, clay-bound Fe and Al, Al and Fe oxi-hydroxides, and SOM-Al/Fe oxi-hydroxide complexes) highly govern P availability in this stage of podsolisation by P desorption, dissolution or mobilisation[131]. Topsoil P is constantly being depleted by leaching of DOP and colloidal P, or even drastically during heavy rainfall events[105].

Only at later stages of podsolisation, Fe oxi-hydroxides are dissolved in the topsoil. This dissolution further decreases topsoil P sorption[132]. The horizontal and vertical variability of P fractions is large and P-rich patches occur due to SOM enrichment in the topsoil and Al- and Fe-P_{ORG} complexes in the illuvial horizons, where highly stable SOM-Al/Fe oxi-hydroxide complexes still retain P. At this stage, atmospheric dust deposition, as e.g. desert dust[133] or from anthropogenic combustion emissions[134], can be a pivotal source of mineral P.

5 Conclusions

The work presented here highlights that assessing the micro and profile scale heterogeneity of soil P is important when investigating soil processes in general and the spatial P distribution in temperate forest soils in particular. The different mechanisms governing this small scale P distribution are affecting P acquisition strategies of plants and soil microorganisms in temperate forest ecosystems with siliceous parent material. Zones with potentially high P uptake are indicated by enrichment zones of P, as identified in the soils at CON, MIT, and LUE as SOM-bound P, Fe and Al oxi-hydroxide-bound P, clay-bound P, and P in

unweathered parent material.

The investigated sites showed a gradient of increasing stage of podsolisation (BBR < CON < MIT < LUE) as indicated by the distribution of pedogenic Al and Fe minerals in the soil profiles. Predominantly, spatial patterns of SOM and pedogenic Al and Fe oxi-hydroxides contents determined the spatial patterns of organic P and different P fractions at the profile scale. However, sampling more than one profile per site would have been beneficial for more robust explanations. Additionally, other methods, as e.g. P isotope approaches, are needed to adequately translate the results into an unambiguous identification of the key pools responsible for ecosystem P nutrition. Direct methods of P speciation (e.g. NMR, XANES spectroscopy) and fractionation techniques should be combined to appropriately investigate soil P speciation.

Micro scale P distribution and speciation patterns revealed that Al/Fe oxi-hydroxides and clay minerals are major binding partners of P in siliceous aggregates. In these aggregates, P species diversity and micro scale distribution is predominantly dependent on soil substrate and soil depth. The identification and explanation of how P accumulates in the investigated soils (both at the micro and profile) has implications on plant and microbial studies in temperate forest ecosystems with soils formed from siliceous parent material. The research in this thesis not only effectively combined distribution and speciation analysis for soil aggregate studies, but also opened new perspectives on P accessibility and availability in soils at the profile scale. Three factors governing P availability are well-known: i) parent material, ii) weathering intensity, and iii) erosion (as P input)[105]. I was able to demonstrate in this thesis that, as fourth factor, assessing the micro and profile scale spatial and chemical heterogeneity of soil P is inevitable for understanding the governing factors of P accessibility and availability in soils.

Bibliography

1. Elser, J. J. Phosphorus: a limiting nutrient for humanity? *Curr. Opin. Biotechnol.* **23**, 833–838 (2012).

2. Walker, T. W. & Syers, J. K. The fate of phosphorus during pedogenesis. *Geoderma* **15**, 1–19 (1976).

3. Crews, T. E. *et al.* Changes in Soil-Phosphorus Fractions and Ecosystem Dynamics across a Long Chronosequence in Hawaii. *Ecology* **76**, 1407–1424 (1995).

4. Parfitt, R. L. *et al.* N and P in New Zealand soil chronosequences and relationships with foliar N and P. *Biogeochemistry* **75**, 305–328 (2005).

5. Turner, B. L., Condron, L. M., Richardson, S. J., Peltzer, D. A. & Allison, V. J. Soil organic phosphorus transformations during pedogenesis. *Ecosystems* **10**, 1166–1181 (2007).

6. Yang, X. & Post, W. M. Phosphorus transformations as a function of pedogenesis: A synthesis of soil phosphorus data using hedley fractionation method. *Biogeosciences* **8**, 2907–2916 (2011).

7. Turner, B. L. *et al.* Soil microbial biomass and the fate of phosphorus during long-term ecosystem development. *Plant Soil* **367**, 225–234 (2013).

8. Föllmi, K. B., Hosein, R., Arn, K. & Steinmann, P. Weathering and the mobility of phosphorus in the catchments and forefields of the Rhône and Oberaar glaciers, central Switzerland: Implications for the global phosphorus cycle on glacial–interglacial timescales. *Geochim. Cosmochim. Acta* **73**, 2252–2282 (2009).

9. Richardson, S. J., Peltzer, D. A., Allen, R. B., McGlone, M. S. & Parfitt, R. L. Rapid development of phosphorus limitation in temperate rainforest along the Franz Josef soil chronosequence. *Oecologia* **139**, 267–276 (2004).

10. Allison, V. J., Condron, L. M., Peltzer, D. A., Richardson, S. J. & Turner, B. L. Changes in enzyme activities and soil microbial community composition along carbon and nutrient gradients at the Franz Josef chronosequence, New Zealand. *Soil Biol. Biochem.* **39**, 1770–1781 (2007).

11. Tamburini, F. *et al.* Oxygen isotopes unravel the role of microorganisms in phosphate cycling in soils. *Environ. Sci. Technol.* **46**, 5956–5962 (2012).

12. Richter, D. D., Allen, H. L., Li, J., Markewitz, D. & Raikes, J. Bioavailability of slowly cycling soil phosphorus: major restructuring of soil P fractions over four decades in an aggrading forest. *Oecologia* **150**, 259–271 (2006).

13. Wardle, D. A., Walker, L. R. & Bardgett, R. D. Ecosystem properties and forest decline in contrasting long-term chronosequences. *Science* **305**, 509–513 (2004).

14. Lang, F. *et al.* Phosphorus in forest ecosystems: New insights from an ecosystem nutrition perspective. *J. Plant Nutr. Soil Sci.* **179**, 129–135 (2016).

15. Zavišić, A. *et al.* Phosphorus availabilities in beech (*Fagus sylvatica* L.) forests impose habitat filtering on ectomycorrhizal communities and impact tree nutrition. *Soil Biol. Biochem.* **98**, 127–137 (2016).

16. Ilg, K., Wellbrock, N. & Lux, W. Phosphorus supply and cycling at long-term forest monitoring sites in Germany. *Eur. J. Forest Res.* **128**, 483–492 (2009).

17. Jonard, M. *et al.* Tree mineral nutrition is deteriorating in Europe. *Glob. Change Biol.* **21**, 418–430 (2015).

18. Vitousek, P. M. & Farrington, H. Nutrient limitation and soil development: Experimental test of a biogeochemical theory. *Biogeochemistry* **37**, 63–75 (1997).

19. Mohren, G. M. J., Vandenburg, J. & Burger, F. W. Phosphorus deficiency induced by nitrogen input in Douglas fir in the Netherlands. *Plant Soil* **95**, 191–200 (1986).

20. Laliberté, E. *et al.* Experimental assessment of nutrient limitation along a 2-million-year dune chronosequence in the south-western Australia biodiversity hotspot. *J. Ecol.* **100**, 631–642 (2012).

21. Violante, A. & Pigna, M. Competitive sorption of arsenate and phosphate on different clay minerals and soils. *Soil Sci. Soc. Am. J.* **66**, 1788–1796 (2002).

22. Sims, J. T. & Pierzynski, G. M. Chemistry of Phosphorus in Soils. In Tabatabai, M. A. & Sparks, D. L. (eds.) *Chemical Processes in Soils*, vol. 8 of *SSSA Book Series*, 151–192 (Soil Science Society of America, Madison, 2005).

23. Gerke, J. & Hermann, R. Adsorption of Orthophosphate to Humic-Fe-Complexes and to Amorphous Fe-Oxide. *Z. Pflanzenernähr. Bodenkd.* **155**, 233–236 (1992).

24. Arai, Y. & Sparks, D. L. Phosphate Reaction Dynamics in Soils and Soil Components: A Multiscale Approach. In Sparks, D. L. (ed.) *Adv. Agron.*, vol. 94, 135–179 (Academic Press, Burlington, 2007).

25. Stevenson, F. & Cole, M. *Cycles of Soil: Carbon, Nitrogen, Phosphorus, Sulfur, Micronutrients* (John Wiley and Sons, New York, 1999), 2nd edn.

26. Condron, L. M. & Newman, S. Revisiting the fundamentals of phosphorus fractionation of sediments and soils. *J. Soils Sed.* **11**, 830–840 (2011).

27. Hinsinger, P. Bioavailability of soil inorganic P in the rhizosphere as affected by root-induced chemical changes: a review. *Plant Soil* **237**, 173–195 (2001).

28. Richardson, A. E., Barea, J. M., McNeill, A. M. & Prigent-Combaret, C. Acquisition of phosphorus and nitrogen in the rhizosphere and plant growth promotion by microorganisms. *Plant Soil* **321**, 305–339 (2009).

29. Ferro Vázquez, C., Nóvoa Muñoz, J. C., Costa Casais, M., Klaminder, J. & Martínez Cortizas, A. Metal and organic matter immobilization in temperate podzols: A high resolution study. *Geoderma* **217–218**, 225–234 (2014).

30. Jackson, R. B. & Caldwell, M. M. Geostatistical patterns of soil heterogeneity around individual perennial plants. *J. Ecol.* **81**, 683–692 (1993).

31. Facelli, E. & Facelli, J. M. Soil phosphorus heterogeneity and mycorrhizal symbiosis regulate plant intra-specific competition and size distribution. *Oecologia* **133**, 54–61 (2002).

32. Liptzin, D., Sanford, R. L. & Seastedt, T. R. Spatial patterns of total and available N and P at alpine treeline. *Plant Soil* **365**, 127–140 (2013).

33. Totsche, K. U. *et al.* Biogeochemical interfaces in soil: The interdisciplinary challenge for soil science. *J. Plant Nutr. Soil Sci.* **173**, 88–99 (2010).

34. Hesterberg, D., Duff, M. C., Dixon, J. B. & Vepraskas, M. J. X-ray microspectroscopy and chemical reactions in soil microsites. *J. Environ. Qual.* **40**, 667–678 (2011).

35. Lehmann, J., Kinyangi, J. & Solomon, D. Organic matter stabilization in soil microaggregates: implications from spatial heterogeneity of organic carbon contents and carbon forms. *Biogeochemistry* **85**, 45–57 (2007).

36. Baveye, P. C. & Laba, M. Moving away from the geostatistical lamppost: Why, where, and how does the spatial heterogeneity of soils matter? *Ecol. Model.* **298**, 24–38 (2015).

37. Vogel, C. *et al.* Determination of phosphorus fertilizer soil reactions by Raman and synchrotron infrared microspectroscopy. *Appl. Spectrosc.* **67**, 1165–1170 (2013).

38. Kruse, J. *et al.* Innovative methods in soil phosphorus research: A review. *J. Plant Nutr. Soil Sci.* **178**, 43–88 (2015).

39. Tiessen, H. & Moir, J. Characterization of available P by sequential extraction. In Carter, M. R. & Gregorich, E. G. (eds.) *Soil Sampling and Methods of Analysis*, chap. 25, 75–86 (CRC Press 2007, Boca Raton, 2007), 2nd edn.

40. Sherman, J., Fernandez, I. J., Norton, S. A., Ohno, T. & Rustad, L. E. Soil aluminum, iron, and phosphorus dynamics in response to long-term experimental nitrogen and sulfur additions at the Bear Brook Watershed in Maine, USA. *Environ. Monit. Assess.* **121**, 421–429 (2006).

41. Hedley, M. J., Stewart, J. W. B. & Chauhan, B. S. Changes in Inorganic and Organic Soil-Phosphorus Fractions Induced by Cultivation Practices and by Laboratory Incubations. *Soil Sci. Soc. Am. J.* **46**, 970–976 (1982).

42. Johnson, A. H., Frizano, J. & Vann, D. R. Biogeochemical implications of labile phosphorus in forest soils determined by the Hedley fractionation procedure. *Oecologia* **135**, 487–499 (2003).

43. Schwertmann, U. Differenzierung der Eisenoxide des Bodens durch Extraktion mit Ammoniumoxalat-Lösung. *Z. Pflanzenernähr. Düng. Bodenk.* **105**, 194–202 (1964).

44. Mehra, O. P. & Jackson, M. L. Iron Oxide Removal from Soils and Clays by a Dithionite-Citrate System Buffered with Sodium Bicarbonate. *Clays Clay Miner.* **7**, 317–327 (1958).

45. Prietzel, J. Mobilization of X-ray amorphous and crystalline aluminum and iron phosphates by common soil extraction procedures. *J. Plant Nutr. Soil Sci.* (2016).

46. Turner, B. L., Cade-Menun, B. J., Condron, L. M. & Newman, S. Extraction of soil organic phosphorus. *Talanta* **66**, 294–306 (2005).

47. Negassa, W. & Leinweber, P. How does the Hedley sequential phosphorus fractionation reflect impacts of land use and management on soil phosphorus: A review. *J. Plant Nutr. Soil Sci.* **172**, 305–325 (2009).

48. Kruse, J., Negassa, W., Appathurai, N., Zuin, L. & Leinweber, P. Phosphorus speciation in sequentially extracted agro-industrial by-products: evidence from X-ray absorption near edge structure spectroscopy. *J. Environ. Qual.* **39**, 2179–2184 (2010).

49. Negassa, W. *et al.* Phosphorus Speciation in Agro-Industrial Byproducts: Sequential Fractionation, Solution ^{31}P NMR, and P k-and $l_{2,3}$-Edge XANES Spectroscopy. *Environ. Sci. Technol.* **44**, 2092–2097 (2010).

50. Liu, J. *et al.* Complementary Phosphorus Speciation in Agricultural Soils by Sequential Fractionation, Solution 31P Nuclear Magnetic Resonance, and Phosphorus K-edge X-ray Absorption Near-Edge Structure Spectroscopy. *J. Environ. Qual.* **42**, 1763–1770 (2013).

51. Eriksson, A. K., Gustafsson, J. P. & Hesterberg, D. Phosphorus speciation of clay fractions from long-term fertility experiments in Sweden. *Geoderma* **241**, 68–74 (2015).

52. Kruse, J. *et al.* Phosphorus $l_{2,3}$-edge XANES: overview of reference compounds. *J. Synchrotron Radiat.* **16**, 247–259 (2009).

53. Regelink, I. C., Koopmans, G. F., van der Salm, C., Weng, L. & van Riemsdijk, W. H. Characterization of colloidal phosphorus species in drainage waters from a clay soil using asymmetric flow field-flow fractionation. *J. Environ. Qual.* **42**, 464–473 (2013).

54. Hesterberg, D., Zhou, W., Hutchison, K. J., Beauchemin, S. & Sayers, D. E. XAFS study of adsorbed and mineral forms of phosphate. *J. Synchrotron Radiat.* **6**, 636–638 (1999).

55. Ingall, E. D. *et al.* Phosphorus K-edge XANES spectroscopy of mineral standards. *J. Synchrotron Radiat.* **18**, 189–197 (2011).

56. Kelly, S. D., Hesterberg, D. & Ravel, B. Analysis of soils and minerals using X-ray absorption spectroscopy. In Ulery, A. L. & Drees, L. R. (eds.) *Methods of soil analysis. Part 5. Mineralogical Methods*, vol. 5 of *SSSA Book Series*, chap. 14, 387–464 (Soil Science Society of America, Madison, 2008).

57. Beauchemin, S. *et al.* Speciation of phosphorus in phosphorus-enriched agricultural soils using X-ray absorption near-edge structure spectroscopy and chemical fractionation. *J. Environ. Qual.* **32**, 1809–1819 (2003).

58. Siebers, N., Kruse, J. & Leinweber, P. Speciation of Phosphorus and Cadmium in a Contaminated Soil Amended with Bone Char: Sequential Fractionations and XANES Spectroscopy. *Water Air Soil Poll.* **224**, 1–13 (2013).

59. Liu, J. *et al.* Molecular Speciation of Phosphorus Present in Readily Dispersible Colloids from Agricultural Soils. *Soil Sci. Soc. Am. J.* **78**, 47–53 (2014).

60. Toor, G. S., Peak, J. D. & Sims, J. T. Phosphorus speciation in broiler litter and turkey manure produced from modified diets. *J. Environ. Qual.* **34**, 687–697 (2005).

61. Hashimoto, Y., Takamoto, A., Kikkawa, R., Murakami, K. & Yamaguchi, N. Formations of hydroxyapatite and inositol hexakisphosphate in poultry litter during the composting period: sequential fractionation, P K-edge XANES and solution ^{31}P NMR investigations. *Environ. Sci. Technol.* **48**, 5486–5492 (2014).

62. Sato, S., Solomon, D., Hyland, C., Ketterings, Q. M. & Lehmann, J. Phosphorus speciation in manure and manure-amended soils using XANES spectroscopy. *Environ. Sci. Technol.* **39**, 7485–7491 (2005).

63. Güngör, K., Jürgensen, A. & Karthikeyan, K. G. Determination of phosphorus speciation in dairy manure using XRD and XANES spectroscopy. *J. Environ. Qual.* **36**, 1856–1863 (2007).

64. Kruse, J. & Leinweber, P. Phosphorus in sequentially extracted fen peat soils: A K-edge X-ray absorption near-edge structure (XANES) spectroscopy study. *J. Plant Nutr. Soil Sci.* **171**, 613–620 (2008).

65. Ajiboye, B., Akinremi, O. O., Hu, Y. & Flaten, D. N. Phosphorus speciation of sequential extracts of organic amendments using nuclear magnetic resonance and X-ray absorption near-edge structure spectroscopies. *J. Environ. Qual.* **36**, 1563–1576 (2007).

66. Lombi, E. *et al.* Speciation and distribution of phosphorus in a fertilized soil: A synchrotron-based investigation. *Soil Sci. Soc. Am. J.* **70**, 2038–2048 (2006).

67. Ajiboye, B., Akinremi, O. O., Hu, Y. & Jürgensen, A. XANES speciation of phosphorus in organically amended and fertilized vertisol and mollisol. *Soil Sci. Soc. Am. J.* **72**, 1256–1262 (2008).

68. Prietzel, J., Dümig, A., Wu, Y. H., Zhou, J. & Klysubun, W. Synchrotron-based P K-edge XANES spectroscopy reveals rapid changes of phosphorus speciation in the topsoil of two glacier foreland chronosequences. *Geochim. Cosmochim. Acta* **108**, 154–171 (2013).

69. Brandes, J. A., Ingall, E. & Paterson, D. Characterization of minerals and organic phosphorus species in marine sediments using soft X-ray fluorescence spectromicroscopy. *Mar. Chem.* **103**, 250–265 (2007).

70. Giguet-Covex, C. *et al.* XANES spectroscopy as a tool to trace phosphorus transformation during soil genesis and mountain ecosystem development from lake sediments. *Geochim. Cosmochim. Acta* **118**, 129–147 (2013).

71. Prietzel, J., Thieme, J. & Paterson, D. Phosphorus speciation of forest-soil organic surface layers using P K-edge XANES spectroscopy. *J. Plant Nutr. Soil Sci.* **173**, 805–807 (2010).

72. Missong, A., Bol, R., Willbold, S., Siemens, J. & Klumpp, E. Phosphorus forms in forest soil colloids as revealed by liquid-state ^{31}P-NMR. *J. Plant Nutr. Soil Sci.* **179**, 159–167 (2016).

73. Prietzel, J., Klysubun, W. & Werner, F. Speciation of phosphorus in temperate zone forest soils as assessed by combined wet-chemical fractionation and XANES spectroscopy. *J. Plant Nutr. Soil Sci.* **179**, 168–185 (2016).

74. Khare, N., Hesterberg, D., Beauchemin, S. & Wang, S. L. XANES determination of adsorbed phosphate distribution between ferrihydrite and boehmite in mixtures. *Soil Sci. Soc. Am. J.* **68**, 460–469 (2004).

75. Khare, N., Hesterberg, D. & Martin, J. D. XANES investigation of phosphate sorption in single and binary systems of iron and aluminum oxide minerals. *Environ. Sci. Technol.* **39**, 2152–2160 (2005).

76. Ajiboye, B., Akinremi, O. O. & Jürgensen, A. Experimental validation of quantitative XANES analysis for phosphorus speciation. *Soil Sci. Soc. Am. J.* **71**, 1288–1291 (2007).

77. Harrison, A. *Soil organic phosphorus: a review of world literature* (CAB International, Wallingford, 1987).

78. Rivard, C., Lanson, B. & Cotte, M. Phosphorus speciation and micro-scale spatial distribution in North-American temperate agricultural soils from micro X-ray fluorescence and X-ray absorption near-edge spectroscopy. *Plant Soil* **401**, 7–22 (2015).

79. Majumdar, S. *et al.* Applications of synchrotron μ-XRF to study the distribution of biologically important elements in different environmental matrices: A review. *Anal. Chim. Acta* **755**, 1–16 (2012).

80. Bertrand, I., Grignon, N., Hinsinger, P., Souche, G. & Jaillard, B. The use of secondary ion mass spectrometry coupled with image analysis to identify and locate chemical elements in soil minerals: The example of phosphorus. *Scanning* **23**, 279–291 (2001).

81. Cade-Menun, B. J. & Liu, C. W. Solution phosphorus-31 nuclear magnetic resonance spectroscopy of soils from 2005 to 2013: A review of sample preparation and experimental parameters. *Soil Sci. Soc. Am. J.* **78**, 19–37 (2014).

82. Mueller, C. W. *et al.* Advances in the analysis of biogeochemical interfaces: NanoSIMS to investigate soil microenvironments. In Sparks, D. L. (ed.) *Adv. Agron.*, vol. 121, 1–46 (Academic Press, Burlington, 2013).

83. Eriksson, A. K., Hesterberg, D., Klysubun, W. & Gustafsson, J. P. Phosphorus dynamics in Swedish agricultural soils as influenced by fertilization and mineralogical properties: Insights gained from batch experiments and XANES spectroscopy. *Sci. Total Environ.* **566-567**, 1410–1419 (2016).

84. IUSS Working Group WRB. World Reference Base for Soil Resources 2014, update 2015. International soil classification system for naming soils and creating legends for soil maps. World Soil Resources Reports 106, FAO (2015).

85. Webster, R. & Oliver, M. A. Reliability of the Experimental Variogram and Nested Sampling. In Webster, R. & Oliver, M. A. (eds.) *Geostatistics for Environmental Scientists*, chap. 6, 109–138 (John Wiley & Sons, Ltd., Chichester, 2008).

86. Hornburg, V. & Lüer, B. Vergleich zwischen Total- und königswasserextrahierbaren Elementgehalten in natürlichen Böden und Sedimenten. *J. Plant Nutr. Soil Sci.* **162**, 131–137 (1999).

87. Saunders, W. M. H. & Williams, E. G. Observations on the Determination of Total Organic Phosphorus in Soils. *J. Soil Sci.* **6**, 254–267 (1955).

88. Holmgren, G. G. A Rapid Citrate-Dithionite Extractable Iron Procedure. *Soil Sci. Soc. Am. J.* **31**, 210–211 (1967).

89. Murphy, J. & Riley, J. P. A modified single solution method for the determination of phosphate in natural waters. *Anal. Chim. Acta* **27**, 31–36 (1962).

90. John, M. K. Colorimetric Determination of Phosphorus in Soil and Plant Materials with Ascorbic Acid. *Soil Sci.* **109**, 214–220 (1970).

91. Prietzel, J. *et al.* Reference spectra of important adsorbed organic and inorganic phosphate binding forms for soil P speciation using synchrotron-based K-edge XANES spectroscopy. *J. Synchrotron Radiat.* **23**, 532–544 (2016).

92. Klysubun, W., Sombunchoo, P., Deenan, W. & Kongmark, C. Performance and status of beamline BL8 at SLRI for X-ray absorption spectroscopy. *J. Synchrotron Radiat.* **19**, 930–936 (2012).

93. Herrmann, A. M. *et al.* A novel method for the study of the biophysical interface in soils using nano-scale secondary ion mass spectrometry. *Rapid Commun. Mass Spectrom.* **21**, 29–34 (2007).

94. Gianoncelli, A., Kourousias, G., Merolle, L., Altissimo, M. & Bianco, A. Current status of the TwinMic beamline at elettra: a soft x-ray transmission and emission microscopy station. *J. Synchrotron Radiat.* **23**, 1526–1537 (2016).

95. Salomé, M. *et al.* The ID21 Scanning X-ray Microscope at ESRF. *J. Phys.: Conf. Ser.* **425**, 182004 (2013).

96. Solé, V. A., Papillon, E., Cotte, M., Walter, P. & Susini, J. A multiplatform code for the analysis of energy-dispersive X-ray fluorescence spectra. *Spectrochim. Acta B* **62**, 63–68 (2007).

97. R Core Team. *R: A Language and Environment for Statistical Computing*. R Foundation for Statistical Computing, Vienna (2016).

98. Ribeiro Jr., P. & Diggle, P. geoR: A package for geostatistical analysis. *R-News* **1**, 15–18 (2001).

99. Diggle, P. J. & Ribeiro Jr., P. J. Bayesian Inference in Gaussian Model-based Geostatistics. Tech. Rep. 2, Department of Mathematics and Statistics, Lancaster University (2002).

100. Cressie, N. A. C. Statistics for Spatial Data. In Cressie, N. A. C. (ed.) *Statistics for Spatial Data, Revised Edition*, chap. 1, 1–26 (John Wiley & Sons, Inc., Hoboken, 2015).

101. Pebesma, E. J. Multivariable geostatistics in S: the gstat package. *Comput. Geosci.* **30**, 683–691 (2004).

102. Revelle, W. psych: Procedures for Personality and Psychological Research (2015).

103. Ravel, B. & Newville, M. ATHENA, ARTEMIS, HEPHAESTUS: data analysis for X-ray absorption spectroscopy using IFEFFIT. *J. Synchrotron Radiat.* **12**, 537–541 (2005).

104. Shober, A. L., Hesterberg, D. L., Sims, J. T. & Gardner, S. Characterization of phosphorus species in biosolids and manures using XANES spectroscopy. *J. Environ. Qual.* **35**, 1983–1993 (2006).

105. Bol, R. *et al.* Dissolved and colloidal phosphorus fluxes in forest ecosystems-an almost blind spot in ecosystem research. *J. Plant Nutr. Soil Sci.* **179**, 425–438 (2016).

106. Celi, L., Lamacchia, S., Marsan, F. A. & Barberis, E. Interaction of inositol hexaphosphate on clays: Adsorption and charging phenomena. *Soil Sci.* **164**, 574–585 (1999).

107. Yan, Y. P. *et al.* Sorption and desorption characteristics of organic phosphates of different structures on aluminium (oxyhydr)oxides. *Eur. J. Soil Sci.* **65**, 308–317 (2014).

108. Vincent, A. G. *et al.* Changes in organic phosphorus composition in boreal forest humus soils: the role of iron and aluminium. *Biogeochemistry* **108**, 485–499 (2012).

109. Borggaard, O. K., Raben-Lange, B., Gimsing, A. L. & Strobel, B. W. Influence of humic substances on phosphate adsorption by aluminium and iron oxides. *Geoderma* **127**, 270–279 (2005).

110. Shang, C., Caldwell, D. E., Stewart, J. W. B., Tiessen, H. & Huang, P. M. Bioavailability of organic and inorganic phosphates adsorbed on short-range ordered aluminum precipitate. *Microb. Ecol.* **31**, 29–39 (1996).

111. Bhatti, J. S., Comerford, N. B. & Johnston, C. T. Influence of oxalate and soil organic matter on sorption and desorption of phosphate onto a spodic horizon. *Soil Sci. Soc. Am. J.* **62**, 1089–1095 (1998).

112. Condron, L. M., Turner, B. L. & Cade-Menun, B. J. Chemistry and Dynamics of Soil Organic Phosphorus. In Sims, J. T. & Sharpley, A. N. (eds.) *Phosphorus: Agriculture and the Environment*, vol. 46 of *Agronomy Monograph*, chap. 4, 87–121 (American Society of Agronomy, Crop Science Society of America, and Soil Science Society of America, Madison, 2005).

113. Syers, J. K., Williams, J. D. H., Campbell, A. S. & Walker, T. W. The significance of apatite inclusions in soil phosphorus studies. *Soil Sci. Soc. Am. J.* **31**, 752–756 (1967).

114. Sauer, D. *et al.* Podzol: Soil of the year 2007. a review on its genesis, occurrence, and functions. *J. Plant Nutr. Soil Sci.* **170**, 581–597 (2007).

115. Lundström, U., van Breemen, N. & Bain, D. The podzolization process. A review. *Geoderma* **94**, 91–107 (2000).

116. Lichter, J. Rates of weathering and chemical depletion in soils across a chronosequence of Lake Michigan sand dunes. *Geoderma* **85**, 255–282 (1998).

117. Erkenberg, A., Prietzel, J. & Rehfuess, K.-E. Schwefelausstattung ausgewählter europäischer Waldböden in Abhängigkeit vom atmogenen S-Eintrag. *Z. Pflanzenernähr. Bodenkd.* **159**, 101–109 (1996).

118. SanClements, M. D., Fernandez, I. J. & Norton, S. A. Phosphorus in Soils of Temperate Forests: Linkages to Acidity and Aluminum. *Soil Sci. Soc. Am. J.* **74**, 2175–2186 (2010).

119. Kaiser, K. Dissolved organic phosphorus and sulphur as influenced by sorptive interactions with mineral subsoil horizons. *Eur. J. Soil Sci.* **52**, 489–493 (2001).

120. Vincent, A. G., Turner, B. L. & Tanner, E. V. J. Soil organic phosphorus dynamics following perturbation of litter cycling in a tropical moist forest. *Eur. J. Soil Sci.* **61**, 48–57 (2010).

121. Achat, D. L. *et al.* Evaluation of the phosphorus status of P-deficient podzols in temperate pine stands: combining isotopic dilution and extraction methods. *Biogeochemistry* **92**, 183–200 (2009).

122. Sayers, D. E. & Bunker, B. A. Data Analysis. In Koningsberger, D. C. & Prins, R. (eds.) *X-ray absorption: principles, applications, techniques of EXAFS, SEXAFS, and XANES*, vol. 10 of *Chemical analyis: a series of monographs on analytical chemistry and its applications*, chap. 6, 211–253 (John Wiley and Sons, New York, 1988).

123. Celi, L., Lamacchia, S. & Barberis, E. Interaction of inositol phosphate with calcite. *Nutr. Cycl. Agroecosys.* **57**, 271–277 (2000).

124. Bache, B. W. Aluminum and iron phosphate studies relating to soils. *J. Soil Sci.* **14**, 113–123 (1963).

125. Eggleton, R. A., Foudoulis, C. & Varkevisser, D. Weathering of basalt: Changes in rock chemistry and mineralogy. *Clays Clay Miner.* **35**, 161–169 (1987).

126. Kasama, T., Watanabe, Y., Yamada, H. & Murakami, T. Sorption of phosphates on Al-pillared smectites and mica at acidic to neutral pH. *Appl. Clay Sci.* **25**, 167–177 (2004).

127. Blum, J. D. *et al.* Mycorrhizal weathering of apatite as an important calcium source in base-poor forest ecosystems. *Nature* **417**, 729–731 (2002).

128. Ohno, T. & Amirbahman, A. Phosphorus availability in boreal forest soils: A geochemical and nutrient uptake modeling approach. *Geoderma* **155**, 46–54 (2010).

129. von Lützow, M. *et al.* Stabilization of organic matter in temperate soils: mechanisms and their relevance under different soil conditions - a review. *Eur. J. Soil Sci.* **57**, 426–445 (2006).

130. Han, L., Sun, K., Jin, J. & Xing, B. Some concepts of soil organic carbon characteristics and mineral interaction from a review of literature. *Soil Biol. Biochem.* **94**, 107–121 (2016).

131. Haygarth, P. M., Condron, L. M., Heathwaite, A. L., Turner, B. L. & Harris, G. P. The phosphorus transfer continuum: Linking source to impact with an interdisciplinary and multi-scaled approach. *Sci. Total Environ.* **344**, 5–14 (2005).

132. Zhang, W., Faulkner, J. W., Giri, S. K., Geohring, L. D. & Steenhuis, T. S. Effect of Soil Reduction on Phosphorus Sorption of an Organic-Rich Silt Loam. *Soil Sci. Soc. Am. J.* **74**, 240–249 (2010).

133. Okin, G. S., Mahowald, N., Chadwick, O. A. & Artaxo, P. Impact of desert dust on the biogeochemistry of phosphorus in terrestrial ecosystems. *Global Biogeochem. Cy.* **18**, GB2005 (2004).

134. Wang, R. *et al.* Significant contribution of combustion-related emissions to the atmospheric phosphorus budget. *Nat. Geosci.* **8**, 48–54 (2014).

List of publications

Werner F. and Prietzel J. (2015): Standard Protocol and Quality Assessment of Soil Phosphorus Speciation by P *K*-Edge XANES Spectroscopy. Environmental Science & Technology, 49 (17), pp 10521–10528, DOI: 10.1021/acs.est.5b03096.

Werner F., de la Haye T. R., Spielvogel S., and Prietzel J. (2017): Small-scale spatial distribution of phosphorus fractions in soils from silicate parent material with different degree of podzolization. Geoderma, 302, pp. 52–65, DOI: 10.1016/j.geoderma.2017.04.026.

Werner F., Mueller C. W., Thieme J., Gianoncelli A., Rivard C., Höschen C., and Prietzel J. (2017): Micro-scale heterogeneity of soil phosphorus depends on soil substrate and depth. Accepted for publication by Nature Scientific Reports 2017.

Related co-authored research articles:

Prietzel J., Klysubun W., **Werner F.** (2016): Speciation of phosphorus in temperate zone forest soils as assessed by combined wet-chemical fractionation and XANES spectroscopy. Journal of Plant Nutrition and Soil Science, 179 (2), pp 168–185,
DOI: 10.1002/jpln.201500472.

Prietzel J., Harrington G., Häusler W., Heister K., **Werner F.**, Klysubun W. (2016): Reference spectra of important adsorbed organic and inorganic phosphate binding forms for soil P speciation using synchrotron-based *K*-edge XANES spectroscopy. Journal of Synchrotron Radiation, 23 (2), pp 532–544, DOI: 10.1107/S1600577515023085.

Standard Protocol and Quality Assessment of Soil Phosphorus Speciation by P *K*-Edge XANES Spectroscopy

by

Florian Werner and Jörg Prietzel

DOI: 10.1021/acs.est.5b03096

Published in **Environmental Science & Technology 49**, pp. 10521–10528

Title: Standard Protocol and Quality Assessment of Soil Phosphorus Speciation by P K-Edge XANES Spectroscopy

Author: Florian Werner, Jörg Prietzel

Publication: Environmental Science & Technology

Publisher: American Chemical Society

Date: Sep 1, 2015

PERMISSION/LICENSE IS GRANTED FOR YOUR ORDER AT NO CHARGE

This type of permission/license, instead of the standard Terms & Conditions, is sent to you because no fee is being charged for your order. Please note the following:

- Permission is granted for your request in both print and electronic formats, and translations.
- If figures and/or tables were requested, they may be adapted or used in part.
- Please print this page for your records and send a copy of it to your publisher/graduate school.
- Appropriate credit for the requested material should be given as follows: "Reprinted (adapted) with permission from (COMPLETE REFERENCE CITATION). Copyright (YEAR) American Chemical Society." Insert appropriate information in place of the capitalized words.
- One-time permission is granted only for the use specified in your request. No additional uses are granted (such as derivative works or other editions). For any other uses, please submit a new request.

Environmental Science & Technology

Article

pubs.acs.org/est

Standard Protocol and Quality Assessment of Soil Phosphorus Speciation by P *K*-Edge XANES Spectroscopy

Florian Werner* and Jörg Prietzel

Lehrstuhl für Bodenkunde, Research Department Ecology and Ecosystem Management, Technische Universität München, Emil-Ramann-Straße 2, 85354 Freising, Germany

Supporting Information

ABSTRACT: Phosphorus (P) in soils is most often bound as phosphate to one or more of the following four elements or compounds: calcium, aluminum, iron, and soil organic matter. A promising method for direct P speciation in soils is synchrotron-based X-ray absorption near edge structure (XANES) spectroscopy at the *K*-edge of P. However, the quality of this method is debated controversially, partly because a standard protocol for reproducible spectrum deconvolution is lacking and minor modifications of the applied deconvolution procedure can lead to considerable changes in the P speciation results. On the basis of the observation that appropriate baseline correction and edge-step normalization are crucial for correct linear combination (LC) fitting results, we established a standard protocol for the deconvolution and LC fitting of P *K*-edge XANES spectra. We evaluated the quality of LC fits obtained according to this standard protocol with 16 defined dilute (2 mg P g^{-1}) ternary mixtures of aluminum phosphate, iron phosphate, hydroxyapatite, and phytic acid in a quartz matrix. The LC fitting results were compared with the contribution of the different P compounds to total P in the various mixtures. Compared to using a traditional LC fitting procedure, our standard protocol reduced the fitting error by 6% (absolute). However, P portions smaller than 5% should be confirmed with other methods or excluded from the P speciation results. A publicly available database of P *K*-edge XANES reference spectra was initiated.

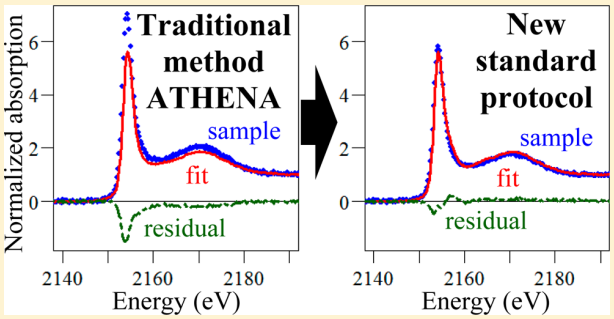

INTRODUCTION

Inorganic phosphorus (P) in soils is most often associated with calcium (Ca), aluminum (Al), or iron (Fe).[1] Organic P in soils is to a large fraction present as inositol phosphate.[1] Much of the organic and inorganic P is not in bioavailable form,[2] and to investigate the bioavailability of P, it is necessary to identify different P species in soils and sediments.[3] At the moment, direct P speciation in soils is still difficult to achieve, and P speciation in soils and sediments is mostly assessed indirectly with sequential chemical fractionation methods.[4,5] Indirect soil P speciation, however, is characterized by two disadvantages: First, the reagents used in the fractionation procedures may change P-binding forms and therefore bias P speciation results.[3,6] Second, to assign the operationally defined P fractions to distinct P species is a major problem of all P fractionation methods.[7] To overcome this problem, recent studies[8,9] have combined sequential P fractionation in soils with direct methods, namely, solution ^{31}P NMR spectroscopy (mainly used to study organically bound P)[10] and/or synchrotron-based X-ray absorption near edge structure (XANES) spectroscopy at the *K*-edge[11] and $L_{2,3}$-edge[12] of P. Kruse et al.[8] concluded that even though fractionation techniques remain indispensable when studying P speciation only a combination of indirect and direct methods provides sufficient information about P species in plants and soils.[9] In another recent study, Liu et al.[13] came to the same conclusion when also using combined sequential fractionation, solution ^{31}P NMR spectroscopy, and P *K*-edge XANES spectroscopy to characterize soil P in agricultural soils.

Synchrotron-based XANES spectroscopy at the P *K*-edge has been used to study P speciation in soils for 20 years.[14] XANES spectra of different P species vary in one or more spectral features, such as white-line intensity and position, as well as pre-edge and postedge structures.[15] These differences have been used to "fingerprint" distinct P species in 59 mineral standard specimens,[15] binary mineral standard mixtures,[16] and in studies on P sorption onto iron and aluminum oxide minerals.[17,18] Furthermore, fingerprinting was used in manure,[19,20] poultry litter,[21,22] sequential extracts of organic substances[23] and fen peat soils,[24] sediments,[25,26] soils,[27−30] organic soil surface layers,[31] and soil colloids.[32] Most often, the spectra were analyzed quantitatively by linear combination (LC) fitting.[21,30,32] Sometimes, principal component analysis[33] or partial least-squares regression[27] was used. During LC fitting, proportions of given spectra of P standards are summed to

Received: June 26, 2015
Revised: August 13, 2015
Accepted: August 13, 2015
Published: August 13, 2015

DOI: 10.1021/acs.est.5b03096
Environ. Sci. Technol. 2015, 49, 10521−10528

Table 1. Phosphorus Speciation of 16 Ternary Mixtures Comprised of Aluminum Phosphate, Iron Phosphate, Hydroxyapatite, and Phytic Acid Diluted with Fine-Ground Quartz to a Total Phosphorus Concentration of 2 mg g^{-1} and Results of Linear Combination Fitting Conducted on Baseline-Corrected and Edge-Step-Normalized P *K*-Edge XANES Spectra[a]

	portion of total P				LC fitting results (fraction of 1)				fitting statistics		deviation from total P (relative and mean of absolute)				
mixture	$AlPO_4$	$FePO_4$	HydAp	PhyAc	$AlPO_4$	$FePO_4$	HydAp	PhyAc	χ^2	*R* factor	$AlPO_4$	$FePO_4$	HydAp	PhyAc	mean
1:1:1:0	0.35	0.32	0.34	0	0.25	0.36	0.35	0.04	0.09	0.00014	−0.10	+0.04	+0.01	+0.04	0.05
2:1:1:0	0.52	0.23	0.25	0	0.40	0.32	0.27	0.02	0.12	0.00019	−0.12	+0.09	+0.02	+0.02	0.06
1:2:1:0	0.26	0.48	0.26	0	0.20	0.51	0.29	0.00	0.09	0.00015	−0.06	+0.03	+0.03	0.00	0.03
1:1:2:0	0.26	0.24	0.50	0	0.17	0.28	0.55	0.00	0.10	0.00017	−0.09	+0.04	+0.05	0.00	0.04
1:1:0:1	0.34	0.31	0	0.35	0.26	0.45	0.00	0.29	0.13	0.00021	−0.08	+0.14	0.00	−0.06	0.07
2:1:0:1	0.51	0.23	0	0.26	0.55	0.31	0.00	0.14	0.10	0.00016	+0.04	+0.08	0.00	−0.12	0.06
1:2:0:1	0.26	0.47	0	0.27	0.25	0.61	0.00	0.15	0.12	0.00018	−0.01	+0.14	0.00	−0.12	0.07
1:1:0:2	0.25	0.23	0	0.52	0.28	0.37	0.01	0.34	0.20	0.00032	+0.03	+0.14	+0.01	−0.18	0.09
1:0:1:1	0.33	0	0.32	0.35	0.30	0.00	0.42	0.28	0.08	0.00014	−0.03	0.00	+0.10	−0.07	0.05
2:0:1:1	0.50	0	0.24	0.26	0.51	0.00	0.31	0.18	0.10	0.00017	+0.01	0.00	+0.07	−0.08	0.04
1:0:2:1	0.25	0	0.49	0.26	0.17	0.00	0.53	0.29	0.13	0.00023	−0.08	0.00	+0.04	+0.03	0.04
1:0:1:2	0.25	0	0.24	0.51	0.21	0.00	0.31	0.47	0.10	0.00018	−0.04	0.00	+0.07	−0.04	0.04
0:1:1:1	0	0.31	0.33	0.36	0.00	0.32	0.40	0.28	0.13	0.00022	0.00	+0.01	+0.07	−0.08	0.04
0:2:1:1	0	0.48	0.25	0.27	0.00	0.55	0.30	0.15	0.09	0.00015	0.00	+0.07	+0.05	−0.12	0.06
0:1:2:1	0	0.23	0.50	0.27	0.00	0.25	0.60	0.15	0.09	0.00016	0.00	+0.02	+0.10	−0.12	0.06
0:1:1:2	0	0.23	0.25	0.52	0.00	0.28	0.36	0.36	0.12	0.00020	0.00	+0.05	+0.11	−0.16	0.08

[a]Furthermore, LC fitting statistics (χ^2 and *R* factor) from the fitting procedure and relative deviations of the LC fitting results from the actual proportions are shown.

yield a fitted spectrum that represents an unknown spectrum with least-squares deviance.[34] The validity of the quantities of different P species as determined by LC fitting on P XANES spectra is debated controversially.[32]

At present, it is not clear how accurately LC fitting exercises can reproduce P speciation in an environmental sample because the set of standard spectra to fit unknown spectra with least-squares deviance simplifies complex environmental systems like soils and sediments. Furthermore, it has to be particularly taken into account that minor modifications in the applied baseline correction and edge-step normalization procedure can lead to considerable changes of the P speciation results. Because synchrotron-based P *K*-edge XANES spectroscopy is increasingly used for P speciation in soils and other environmental samples, there is a strong need for a standardized procedure to ensure unequivocal and accurate results of P speciation by LC fittings on P XANES spectra. Ajiboye et al.[16] reported on the accuracy of LC fitting results for P XANES spectroscopy applications. They compared the results from LC fitting on P *K*-edge XANES spectra obtained from various defined binary mixtures (diluted with boron nitride to a P content of about 5%) of three reference compounds (hydroxyapatite, variscite, and phosphosiderite). They reproduced their mixtures with a relative error of 0.8−17%, being especially accurate when the proportion of hydroxyapatite was large. However, often more than three major components for P binding in soils are claimed: Apart from calcium, aluminum, and iron phosphates, soil organic matter (SOM) is an additional important contributor to soil P.[35,36] The quality of LC fitting techniques used for P speciation on XANES spectra with mixtures of all major components (Al-, Fe-, and Ca-bound P as well as organically bound P) has not yet been examined nor has there been given a detailed description of how to obtain accurate LC fits with reproducible P speciation results after appropriate spectrum baseline correction and edge-step normalization. In this paper, we present a standard protocol for spectrum deconvolution and subsequent LC fitting on P *K*-edge XANES spectra of soils. Our objective is to test the quality of our protocol on dilute ternary mixtures of the four major P compounds present in soils.

■ MATERIALS AND METHODS

Standards and Mixtures. Four P standards, each representing a major soil P species, were used: Iron(III) phosphate dihydrate ($FePO_4{\cdot}2H_2O$; abbreviation: $FePO_4$), aluminum phosphate ($AlPO_4$), calcium phosphate tribasic (hydroxyapatite; $Ca_5(PO_4)_3(OH)$; abbreviation: HydAp), and phytic acid sodium salt hydrate ($C_6H_{18}(PO_4)_6{\cdot}x$Na + yH_2O; abbreviation: PhyAc). All compounds were purchased from Sigma-Aldrich (St. Louis, MO, USA) and tested for purity by XRD analysis. To test the accuracy of our procedure at P concentrations close to natural soil abundances and to avoid self-absorption during XANES spectroscopy, we diluted the standards with fine-ground, high-purity quartz (SiO_2; Merck KGaA, Darmstadt, Germany) to a concentration of 2 mg P g^{-1}. Quartz was used as a diluent instead of the often-used boron nitride[34] so as to more adequately mimic soil matrices. We produced a total mass of standard compound of 25 g (proportion of pure P species without quartz: 301.61 mg $FePO_4$, 196.88 mg $AlPO_4$, 270.30 mg HydAp, and 247.23 mg PhyAc). The diluted standards were finely ground and homogenized with agate milling stones (Planetary ball mill Pulverisette 5, Fritsch GmbH, Idar-Oberstein, Germany). To avoid cross contamination, we flushed the equipment with deionized water, applied ultrasound to the milling equipment, and reground one time with pure quartz after every grinding step. To obtain data on the concentration of total P in the standards, we conducted a total digestion of all standards with hydrofluoric acid (HF) and perchloric acid ($HClO_4$) and subsequent element analysis using inductively coupled plasma optical emission spectrometry (ICP-OES; Vista-PRO Simultaneous ICP-OES, Varian Inc., Palo Alto, CA, USA).

Various defined ternary mixtures of all four standards were produced by weighing different amounts of the standard compounds in various combinations to 1 g of sample and

DOI: 10.1021/acs.est.5b03096
Environ. Sci. Technol. 2015, 49, 10521−10528

mixing them manually with agate mortar and pestle. The mixtures were prepared to represent concentration distributions of three equal P proportions (e.g., P in $AlPO_4$, P in $FePO_4$, P in HydAp, and no P in PhyAc; mixing ratio 1:1:1:0) as well as P proportion distributions in which one P species proportion is enriched compared to the remaining two species by a factor of 2 (e.g., 2:1:1:0). We proceeded in this way to validate accuracy in general and concentration disparities in particular. In total, 16 dilute ternary mixtures of the standards were produced (Table 1).

P *K*-Edge XANES Spectroscopy. All XANES spectra were acquired in fluorescence mode at Beamline 8 of the Synchrotron Light Research Institute (SLRI) in Nakhon Ratchasima, Thailand.[37] The storage ring had an energy of 1.2 GeV and a stored current of 150 mA. The X-ray photon energy was scanned by an InSb(111) double-crystal monochromator with an energy resolution of $1-3 \times 10^{-4}$ (i.e., at the *K*-edge of P: ∼ 0.4 eV). The monochromator at Beamline 8 was calibrated with pure elemental P (2145.5 eV) every 12 h. There was no indication of movement of the edge energy (E_0) throughout the entire beamtime. The X-ray fluorescence at each energy was recorded with a 13-element germanium detector. We distributed the fine-ground samples as thin, homogeneous film on P-free Kapton tape (Lanmar Inc., Northbrook, IL, USA), mounted the tape to a sample holder, and placed the sample holder in a 45° angle from the incident monochromatic beam (beam size = 10 mm × 1 mm) to increase fluorescence yield. The sample chamber was constantly purged with helium gas to decrease X-ray absorption by the gas that surrounds the sample. Measurements were conducted at energy ranges from −100 to +350 eV with respect to E_0 of elemental P (2145.5 eV) with a 2 s dwell time per energy step. The ranges were chosen to account for the good practice, recommended by Kelly et al.,[34] to collect data in longer ranges (>200 eV). Energy steps were chosen as follows: from −100 to −40 eV and from +100 to +350 eV, energy step of 5 eV; from −40 to −10 eV and from +50 to +100 eV, energy step of 1 eV; and from −10 to +50 eV, energy step of 0.25 eV. A minimum of four spectra for the standards and two spectra for the samples was acquired.

Spectrum Deconvolution and Data Processing. Initial spectrum deconvolution was performed with the program ATHENA of the software package DEMETER.[38] At first, E_0 of all raw spectra was calibrated to the zero crossing of the second derivative of the absorption. Replicate spectra of a given sample were then examined visibly for glitches, drifts, noise, and general quality before merging them. The data was further processed using the statistical software *R* (Version 3.2.0).[39] Baseline correction and edge-step normalization of P *K*-edge XANES spectra followed by LC fitting had never been performed before using *R*, but the large amount of LC fittings required an automated procedure. The code we programmed followed the approach for LC fitting applied by ATHENA. All merged spectra were initially baseline-corrected from −80 to −20 eV (linear regression) and normalized and flattened to an absorption (edge-step) of 1 from +140 to +340 eV (linear regression) with respect to E_0. These values reproduced a longer spectrum (up to +850 eV) of PhyAc in the best way to make sure that our spectra were not biased by small normalization ranges. LC fitting, using the Levenberg−Marquardt nonlinear least-squares algorithm, was conducted from −14 to +46 eV (with respect to E_0) with the function *nlsLM* of package *minpack.LM*.[40] All four standards were used to create the fit, allowing their proportions to vary between 0 and 1 (maximum number of iterations: 1000).

Because in the past no standard protocol existed for the deconvolution of P *K*-edge XANES spectra, we concluded that the starting values for baseline correction and edge-step normalization could be set personally. However, we allowed the baseline and normalization parameters of the samples to be modified, on the basis of the observation that minor modifications of these parameters can lead to considerable changes in the P speciation results. Computerized combination of all possible baseline correction and edge-step normalization parameters using *R* code resulted in over 65 000 baseline-corrected and edge-step-normalized sample spectra. Among these spectra, the lower energy level used for baseline correction varied between −80 and −40 eV (2.5 eV step), and the upper energy level varied between −30 and −10 eV (2.5 eV step) with respect to E_0. The lower energy level used for edge-step normalization varied between +120 and +170 eV (2.5 eV step), and the upper level varied between +290 and +340 eV (2.5 eV step) with respect to E_0. All spectra were automatically LC fitted, using the initially baseline-corrected and edge-step-normalized standard spectra as predictor compounds. To mimic the function "force weighting factors to sum one" in the ATHENA LC fitting procedure, all those fits were selected where the sum of the standard proportions was deviating from 1 by less than 0.0005 (fraction of 1). From these, the best fit was chosen, as seen by the lowest *R* factor (χ^2 divided by the sum of the squared sample data; same as in ATHENA). Deviations, means, correlations, and regressions were also calculated using *R*.

Fitting of Spectra with Smaller Energy Ranges. We also fitted our data with baseline correction and edge-step normalization energy values closer to E_0 to test the applicability of our standard protocol for P K-edge XANES spectra acquired in a smaller energy range. These ranges (e.g., between 2140 and 2200 eV) have mostly been used for LC fitting in earlier studies,[20,41] partly to avoid the superposition of P XANES spectra by the sulfur *K*-edge (+326.5 eV, with respect to the P *K*-edge) in soils and sediments. In this approach initial baseline correction of all spectra was performed from −40 to −10 eV and edge-step normalization from +35 to +65 eV with respect to E_0. These values were chosen from corrected and normalized standard spectra that represented best the spectra of the respective standard compound obtained with the larger energy ranges described above. For LC fitting, parameters of the samples were allowed to vary between −48 and −28 eV (baseline parameter at the lower energy level) and between −18 and −8 eV (baseline parameter at the upper energy level) with respect to E_0, both with a 1 eV step. The edge-step normalization parameter at the lower energy level varied between +29 and +39 eV (0.5 eV step); the edge-step normalization parameter at the upper energy level varied between +60 and +70 eV (1 eV step) with respect to E_0. All other data processing was performed as already described before for the deconvolution of XANES spectra with the larger energy ranges.

Exemplary Soil Samples. To test the applicability of our standard protocol on environmental samples, three exemplary soil samples were chosen. A sample from a calcareous topsoil (Ah horizon) near Tuttlingen, Germany (TUT), a sample from an acidic topsoil (Ah) near Mitterfels, Germany (MIT), and a sample from an acidic subsoil (Bw horizon) near Bad Brückenau, Germany (BBR). As seen from the chemical soil

DOI: 10.1021/acs.est.5b03096
Environ. Sci. Technol. 2015, 49, 10521−10528

characteristics, the soil samples most likely differ in P speciation (Table S1). Spectra of all samples were also collected at Beamline 8 of SLRI. Spectrum deconvolution was performed as described for the standard and mixture spectra.

RESULTS

Chemical Analysis of Standards. Results from total digestion and subsequent element analysis by ICP-OES confirmed that we created standard compounds with P concentrations occurring similar to those in soils. The compounds showed the following concentrations: $AlPO_4$, 1.81 mg P g^{-1}; HydAp, 1.76 mg P g^{-1}; $FePO_4$, 1.65 mg P g^{-1}; and PhyAc, 1.88 mg P g^{-1}. We found no P in $HF/HClO_4$ digests of high-purity quartz; additionally, the XANES spectrum of the pure quartz did not show any P fluorescence. According to the ICP-OES results, we corrected the expected concentrations of P species in the mixtures to the P concentrations for the standard mixtures as presented in Table 1 as proportions of total P. In all ternary mixtures, the portion of different P species deviated only slightly (1−3% of total P) from the expected portion of the respective P species.

Standard Protocol for LC Fitting. In this paper, we present a standard protocol for how to baseline-correct and edge-step-normalize P *K*-edge XANES spectra to yield accurate and precise P speciation results from LC fitting applications (Figure 1). We found from visual inspection that LC fitting with our initial baseline and normalization parameters often resulted in fits that were obviously incorrect. On the basis of this observation, we allowed the initial parameters of the samples to vary within reasonable ranges before fitting. The points defining the baseline did not interfere with the white-line or pre-edge features, and the normalization parameters were chosen to be far enough to not reach into the near edge structures. We identified optimum values as follows: Only those LC fitting results were collected where the sum of the standard proportions deviated from 1 by less than 0.0005. The best fit was chosen from these results by the smallest *R* factor; the resulting energy ranges can be found in Table S2.

Simple linear regression revealed that there was no difference between the LC fitting results of a given spectrum that had been baseline-corrected and edge-step-normalized using larger energy ranges and those of a given spectrum after baseline-correction and edge-step normalization with smaller energy ranges (Table S3). In the following section and in Table 1, the P speciation results using parameters close to E_0 (i.e., the smaller energy ranges) are described. The respective results obtained by LC fitting of the same spectra deconvoluted in a larger energy range are presented in Table S4.

Comparison with Traditional LC Fitting. Our approach improved LC fits considerably, as evident both in visual inspection and in the fitting statistics. When compared to LC fitting results after traditional baseline correction and edge-step normalization with fixed parameter values performed with ATHENA, the LC fitting using our standard protocol yielded 6% (absolute) more accurate results. In detail, linear regression showed that the compounds were fitted better by the following (absolute) percents using our protocol than by applying traditional, consistent baseline correction and edge-step normalization with ATHENA (Table S5): $AlPO_4$, 10%; $FePO_4$, 11%; HydAp, 1%; and PhyAc, 4%. Additionally, using our standard protocol improved LC fitting of three exemplary soil spectra compared to results from fitting these spectra with the traditional approach using ATHENA (Table S1; abstract graphics: TUT sample).

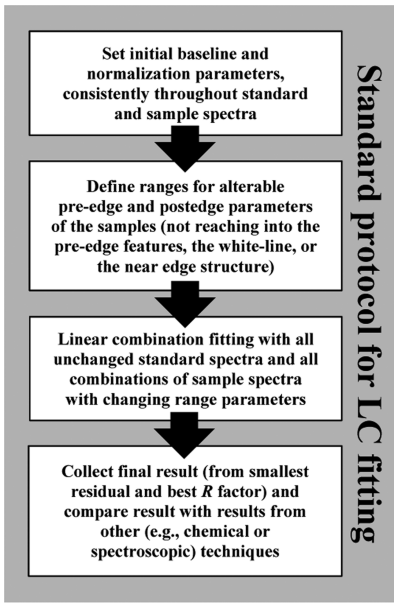

Figure 1. Flowchart of our standard protocol for baseline correction, edge-step normalization, and linear combination (LC) fitting performed on P *K*-edge XANES spectra of soils and sediments. (1) As starting values, all standards and sample spectra are baseline-corrected and edge-step-normalized consistently (e.g., baseline from −40 to −10 eV and normalization from +35 to +65 eV, with respect to E_0). (2) Ranges for adjusting pre-edge and postedge parameters of the fitted sample are defined. Care has to be taken so that the ranges do not interfere with the pre-edge features, the white-line, or the near postedge structure. (3) The actual fitting is performed with all predefined, consistently normalized standard spectra. The sample spectra are fitted with all changing range parameters. (4) The final fitting result is collected from the smallest residual and the best *R* factor of a fitting procedure of a sample. Fitting results (especially stated portions < 5%) should be compared and/or double-checked with, for example, chemical or other spectroscopic techniques.

LC Fitting Results. Phosphorus speciation according to our standard protocol for baseline correction and edge-step normalization on the spectra of our 16 mixtures followed by LC fitting reproduced the P speciation of the mixtures with a mean absolute deviation of 5% (of total P; $n = 64$), ranging from 3% ($AlPO_4$−P/$FePO_4$−P/HydAp-P/PhyAc-P = 1:2:1:0; $n = 4$) to 9% ($AlPO_4$−P/$FePO_4$−P/HydAp-P/PhyAc-P = 1:1:0:2; $n = 4$). We found no significant correlation (Spearman's rank correlation rho: 0.27, $p > 0.05$) between the *R* factor from the LC fitting and the absolute mean deviation.

LC fitting results of the mixtures without PhyAc (Figure 2A−D) generally underestimated $AlPO_4$ (6−12%), whereas $FePO_4$ was moderately overestimated (3−9%) and HydAp was slightly overestimated (1−5%). PhyAc was twice claimed erroneously by LC fitting, however only with small proportions: For mixture 1:1:1:0, a portion of 4% was calculated, whereas for mixture 2:1:1:0, a portion of 2% was calculated. In all mixtures without HydAp (Figure 2E−H), PhyAc was underestimated (6−12% of total P). In contrast, $FePO_4$ was overestimated (8−14%), and $AlPO_4$ was overestimated and underestimated twice, respectively (3 and 4% and 1 and 8%). Even though not present, HydAp was erroneously detected once in a small

DOI: 10.1021/acs.est.5b03096
Environ. Sci. Technol. 2015, 49, 10521−10528

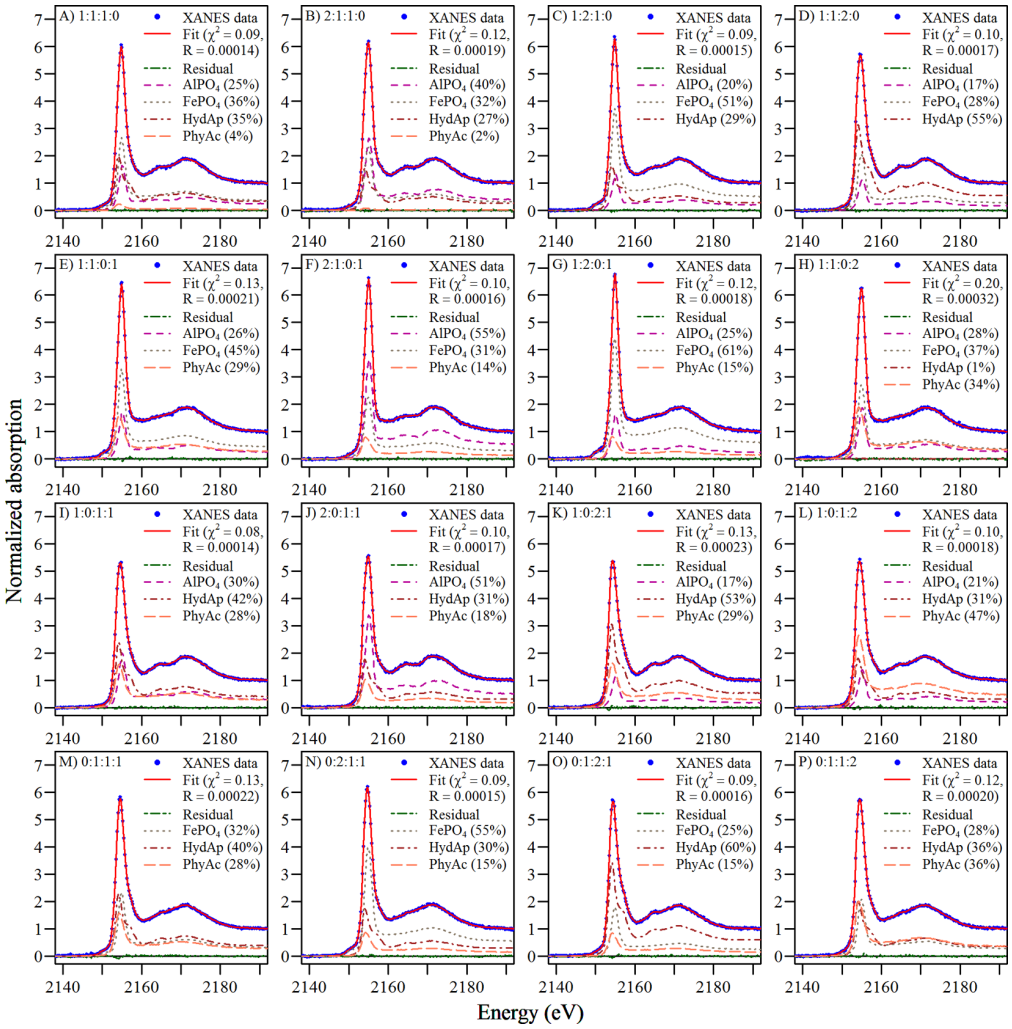

Figure 2. Linear combination fits with weighted components and residual of ternary mixtures of aluminum phosphate ($AlPO_4$), iron phosphate ($FePO_4$), hydroxyapatite (HydAp), and phytic acid (PhyAc), diluted in quartz (2 mg P g^{-1}). (A–D) Mixtures without PhyAc, (E–H) mixtures without HydAp, (I–L) mixtures without $FePO_4$, and (M–P) mixtures without $AlPO_4$. All fits in this section are selected by the least *R* factor of a fitting procedure, according to our standard protocol. Note that the residuals are almost zero in all samples.

amount (1% in mixture 1:1:0:2). Mean absolute deviations ranged from 6 to 9%. In mixtures lacking $FePO_4$ (Figure 2I–L), PhyAc was not underestimated as much (4–8% of total P) and was even slightly overestimated once (3%). Results underestimated $AlPO_4$ in three mixtures (3–8%); one overestimation was minor (1%). The results for HydAp were slightly more inaccurate than those of $AlPO_4$ and showed overestimation in all four cases (4–10%). $FePO_4$ was not detected by LC fitting. The last four mixtures (Figure 2M–P) could reproduce the lack of $AlPO_4$ very well, with no result claiming a small proportion. Regarding the other species, $FePO_4$ showed small overestimations in all mixtures (1–7% of total P). HydAp and PhyAc, however, deviated more strongly: PhyAc was again underestimated in all cases (8–16%), whereas HydAp was overestimated (5–11%).

DISCUSSION

Improvement of LC Fitting Accuracy. We showed that after applying baseline correction and edge-step normalization according to our standard protocol LC fitting can reproduce the P speciation in dilute (2 mg P g^{-1}) mixtures of the main P species supposed to be present in soils ($AlPO_4$, $FePO_4$, HydAp, and PhyAc) with a mean deviation between 3 and 9% (of total P) and a mean absolute deviation of 5%. Compared to using ATHENA with traditionally, consistently baseline-corrected and edge-step-normalized sample spectra, our standard protocol improved LC fitting by 6%. We furthermore exemplified that LC fitting of soil spectra can be enhanced when using our standard protocol for spectrum deconvolution and subsequent LC fitting on P *K*-edge XANES spectra. The improved accuracy of the P speciation results obtained by LC fitting in our study is due to the fact that our procedure does not follow the often cited[34] advice of Sayers and Bunker[42] to apply normalization "as consistently as possible" between samples and standards. Fits obtained using this rule were sometimes obviously incorrect, and sample-specific adjustment (even manually in ATHENA) of baseline-correction and edge-step-normalization energy parameters markedly improved the fits.

Selection of Energy Range Parameters. Results obtained from spectra with a larger energy range also showed the improvement of the fits. In general, there was no difference

DOI: 10.1021/acs.est.5b03096
Environ. Sci. Technol. 2015, 49, 10521–10528

between P speciation results after using short or long energy range parameters. However, we would be cautious to fit, for example, samples corrected and normalized with large energy range parameters with standards corrected and normalized with small energy range parameters first to stay close to the recommendation of Sayers and Bunker[42] and second because small changes in baseline and normalization parameters resulted in more accurate fits.

The improvement is generally, though not as automated and precise, also possible using ATHENA (not shown). Optimum baseline and edge-step fitting parameters can also be identified by repeated visual inspection, i.e., carefully minimizing the residual of the fit. Especially the pre-edge region and the energy range between the white-line energy and an energy of about 2190 eV have to be examined closely.

The results indicate that our standard protocol can be used broadly for P *K*-edge XANES spectroscopy applications. However, some pitfalls associated with the evaluation of LC fitting results from unknown samples have to be considered, namely, (i) the selection of standards used for fitting and the plausibility of their respective quantities, (ii) small contributions of a particular compound to total P, and (iii) fitting statistics.

LC Fitting Pitfalls. LC fitting statistics (χ^2 and *R* factor), as reported in Table 1, proved useful when comparing adjustment, though not as an absolute measure of goodness-of-fit when comparing fits from different samples. In our study, *R* factor and mean absolute deviation of the respective fitting results did not correlate significantly. The *R* factor hence often may be a poor indicator of the fitting quality because it integrates residuum information not only of energy regions that are particularly relevant for an accurate LC fitting result (e.g., pre-edge peak, postedge features) but also of less relevant energy regions.

Moreover, in three cases, small amounts (1−4% of total P) of a particular P species were claimed erroneously by LC fitting. We concluded that P portions smaller than 5% identified by LC fitting are not reliable and should be confirmed with other methods or excluded from the reported P speciation results. This is in line with the results of Kelly et al.,[34] who pointed out that LC fitting results should always be interpreted cautiously when additional information is lacking.

Besides validating small proportions, the plausibility of LC fitting results should still be examined critically because addition of too many different P standard spectra may result in improved fitting statistics (so-called overfitting).[34] In addition, the actual presence of a stated species can be questionable because the existence of a fitted proportion may be chemically impossible. It is therefore strongly recommended to gather additional information about unknown samples from any available source. We concluded that direct methods and fractionation techniques should be combined to appropriately investigate soil P speciation. Organic P, which was reproduced with lowest accuracy in our study, especially should be additionally examined with other methods, such as solution ^{31}P NMR spectroscopy.[10]

Organic P. With the procedure documented in our standard protocol, we were generally able to produce LC fits on P *K*-edge XANES spectra with good overall accuracy, although inorganic P species in most cases were quantified more accurately than phytic acid. Brandes et al.[26] observed radiation damage resulting in mass loss when repeating measurements on phytic acid with a focused X-ray beam. However, our measurements, which have been conducted with unfocused X-rays, did not show specific beam damage effects when repeated (not shown). Our results indicated that PhyAc was reproduced best when no $FePO_4$ was present. This may be due to the fact that both spectra showed a similar postedge feature at an energy of about 2160 eV that influenced the fitting results of these two compounds. The standard spectra of HydAp and $AlPO_4$ differed distinctly from the spectra of PhyAc and $FePO_4$ in this region. However, even small changes in baseline and normalization parameters were the main drivers for more accurate LC fits. Discussing physical changes of properties of our standard compounds is thus difficult.

Relevance of a Standard Protocol. Our standard protocol answers the call for urgently required "systematic studies to directly validate and improve the precision and accuracy of XAS fitting results".[43] The procedure can generally be transferred to any XANES spectrum representing a mixture of different P species, given that all reasonable standard spectra have been included to create the fit. To foster and strengthen P *K*-edge XANES spectroscopy for assessing P speciation in soils, we recommend (i) to use our standard protocol to ensure appropriate spectrum deconvolution and LC fitting as well as (ii) to establish a publicly available database with reference spectra of different soil P species, including mineral and organic P standards as well as P (as phosphate and as organic P) adsorbed to soil minerals and SOM. As a first step, we present data on the raw spectra for the reference compounds used in our study in the Supporting Information.

■ ASSOCIATED CONTENT

Supporting Information

The Supporting Information is available free of charge on the ACS Publications website at DOI: 10.1021/acs.est.5b03096.

Tables showing optimized ranges, linear regression results between long- and short-range and between short-range and traditional fitting, and LC fitting results of the long-range and of exemplary soil samples. (PDF)

Four raw standard spectra used in our study. (ZIP)

■ AUTHOR INFORMATION

Corresponding Author

*E-mail: florian.werner@wzw.tum.de. Tel.: +498161715266. Fax: +498161714466.

Notes

The authors declare no competing financial interest.

■ ACKNOWLEDGMENTS

We thank Wantana Klysubun and her technician team for assistance during acquisition of the P XANES spectra at Beamline 8 of SLRI. Moreover, we are grateful for the helpful comments of the reviewers that improved our manuscript. This study was funded by the German Research Foundation (DFG), as part of the Priority Program SPP 1685, grant Pr 543/6-1.

■ ABBREVIATIONS

BBR	Bad Brückenau
E_0	edge energy
HydAp	hydroxyapatite
ICP-OES	inductively coupled plasma optical emission spectrometry
LC	linear combination
MIT	Mitterfels

DOI: 10.1021/acs.est.5b03096
Environ. Sci. Technol. 2015, 49, 10521−10528

NMR	nuclear magnetic resonance
PhyAc	phytic acid
SOM	soil organic matter
TUT	Tuttlingen
XANES	X-ray absorption near edge structure

REFERENCES

(1) Sims, J. T.; Pierzynski, G. M. Chemistry of Phosphorus in Soils. In *Chemical Processes in Soils*; Tabatabai, M. A., Sparks, D. L., Eds.; Soil Science Society of America: Madison, WI, 2005; pp 151−192.

(2) Stevenson, F. J.; Cole, M. A. *Cycles of Soil: Carbon, Nitrogen, Phosphorus, Sulfur, Micronutrients*, 2nd ed.; John Wiley and Sons: New York, 1999.

(3) Condron, L. M.; Newman, S. Revisiting the fundamentals of phosphorus fractionation of sediments and soils. *J. Soils Sediments* **2011**, *11* (5), 830−840.

(4) Hedley, M. J.; Stewart, J. W. B.; Chauhan, B. S. Changes in Inorganic and Organic Soil-Phosphorus Fractions Induced by Cultivation Practices and by Laboratory Incubations. *Soil Sci. Soc. Am. J.* **1982**, *46* (5), 970−976.

(5) Tiessen, H.; Moir, J., Characterization of available P by sequential extraction. In *Soil Sampling and Methods of Analysis*; Carter, M. R., Ed.; CRC Press LLC: Boca Raton, FL, 1993; pp 75−86.

(6) Turner, B. L.; Cade-Menun, B. J.; Condron, L. M.; Newman, S. Extraction of soil organic phosphorus. *Talanta* **2005**, *66* (2), 294−306.

(7) Negassa, W.; Leinweber, P. How does the Hedley sequential phosphorus fractionation reflect impacts of land use and management on soil phosphorus: A review. *J. Plant Nutr. Soil Sci.* **2009**, *172* (3), 305−325.

(8) Kruse, J.; Negassa, W.; Appathurai, N.; Zuin, L.; Leinweber, P. Phosphorus speciation in sequentially extracted agro-industrial by-products: evidence from X-ray absorption near edge structure spectroscopy. *J. Environ. Qual.* **2010**, *39* (6), 2179−2184.

(9) Negassa, W.; Kruse, J.; Michalik, D.; Appathurai, N.; Zuin, L.; Leinweber, P. Phosphorus Speciation in Agro-Industrial Byproducts: Sequential Fractionation, Solution ^{31}P NMR, and P *K*-and $L_{2,3}$-Edge XANES Spectroscopy. *Environ. Sci. Technol.* **2010**, *44*, 2092−2097.

(10) Cade-Menun, B. J.; Liu, C. W. Solution Phosphorus-31 Nuclear Magnetic Resonance Spectroscopy of Soils from 2005 to 2013: A Review of Sample Preparation and Experimental Parameters. *Soil Sci. Soc. Am. J.* **2014**, *78* (1), 19−37.

(11) Franke, R.; Hormes, J. The P K-near edge absorption spectra of phosphates. *Phys. B* **1995**, *216* (1−2), 85−95.

(12) Kruse, J.; Leinweber, P.; Eckhardt, K. U.; Godlinski, F.; Hu, Y.; Zuin, L. Phosphorus $L_{2,3}$-edge XANES: overview of reference compounds. *J. Synchrotron Radiat.* **2009**, *16* (2), 247−259.

(13) Liu, J.; Yang, J.; Cade-Menun, B. J.; Liang, X.; Hu, Y.; Liu, C. W.; Zhao, Y.; Li, L.; Shi, J. Complementary Phosphorus Speciation in Agricultural Soils by Sequential Fractionation, Solution ^{31}P Nuclear Magnetic Resonance, and Phosphorus K-edge X-ray Absorption Near-Edge Structure Spectroscopy. *J. Environ. Qual* **2013**, *42*, 1763−1770.

(14) Hesterberg, D.; Zhou, W.; Hutchison, K. J.; Beauchemin, S.; Sayers, D. E. XAFS study of adsorbed and mineral forms of phosphate. *J. Synchrotron Radiat.* **1999**, *6* (3), 636−638.

(15) Ingall, E. D.; Brandes, J. A.; Diaz, J. M.; de Jonge, M. D.; Paterson, D.; McNulty, I.; Elliott, W. C.; Northrup, P. Phosphorus *K*-edge XANES spectroscopy of mineral standards. *J. Synchrotron Radiat.* **2011**, *18* (2), 189−197.

(16) Ajiboye, B.; Akinremi, O. O.; Jurgensen, A. Experimental validation of quantitative XANES analysis for phosphorus speciation. *Soil Sci. Soc. Am. J.* **2007**, *71* (4), 1288−1291.

(17) Khare, N.; Hesterberg, D.; Martin, J. D. XANES investigation of phosphate sorption in single and binary systems of iron and aluminum oxide minerals. *Environ. Sci. Technol.* **2005**, *39* (7), 2152−2160.

(18) Khare, N.; Hesterberg, D.; Beauchemin, S.; Wang, S. L. XANES determination of adsorbed phosphate distribution between ferrihydrite and boehmite in mixtures. *Soil Sci. Soc. Am. J.* **2004**, *68* (2), 460−469.

(19) Güngör, K.; Jürgensen, A.; Karthikeyan, K. G. Determination of phosphorus speciation in dairy manure using XRD and XANES spectroscopy. *J. Environ. Qual.* **2007**, *36* (6), 1856−1863.

(20) Sato, S.; Solomon, D.; Hyland, C.; Ketterings, Q. M.; Lehmann, J. Phosphorus speciation in manure and manure-amended soils using XANES spectroscopy. *Environ. Sci. Technol.* **2005**, *39* (19), 7485−7491.

(21) Hashimoto, Y.; Takamoto, A.; Kikkawa, R.; Murakami, K.; Yamaguchi, N. Formations of hydroxyapatite and inositol hexakisphosphate in poultry litter during the composting period: sequential fractionation, P K-edge XANES and solution ^{31}P NMR investigations. *Environ. Sci. Technol.* **2014**, *48* (10), 5486−5492.

(22) Toor, G. S.; Peak, J. D.; Sims, J. T. Phosphorus speciation in broiler litter and turkey manure produced from modified diets. *J. Environ. Qual.* **2005**, *34* (2), 687−697.

(23) Ajiboye, B.; Akinremi, O. O.; Hu, Y.; Flaten, D. N. Phosphorus speciation of sequential extracts of organic amendments using nuclear magnetic resonance and X-ray absorption near-edge structure spectroscopies. *J. Environ. Qual.* **2007**, *36* (6), 1563−1576.

(24) Kruse, J.; Leinweber, P. Phosphorus in sequentially extracted fen peat soils: A K-edge X-ray absorption near-edge structure (XANES) spectroscopy study. *J. Plant Nutr. Soil Sci.* **2008**, *171* (4), 613−620.

(25) Giguet-Covex, C.; Poulenard, J.; Chalmin, E.; Arnaud, F.; Rivard, C.; Jenny, J. P.; Dorioz, J. M. XANES spectroscopy as a tool to trace phosphorus transformation during soil genesis and mountain ecosystem development from lake sediments. *Geochim. Cosmochim. Acta* **2013**, *118*, 129−147.

(26) Brandes, J. A.; Ingall, E.; Paterson, D. Characterization of minerals and organic phosphorus species in marine sediments using soft X-ray fluorescence spectromicroscopy. *Mar. Chem.* **2007**, *103* (3−4), 250−265.

(27) Siebers, N.; Kruse, J.; Leinweber, P. Speciation of Phosphorus and Cadmium in a Contaminated Soil Amended with Bone Char: Sequential Fractionations and XANES Spectroscopy. *Water, Air, Soil Pollut.* **2013**, *224* (5), 1−13.

(28) Lombi, E.; Scheckel, K. G.; Armstrong, R. D.; Forrester, S.; Cutler, J. N.; Paterson, D. Speciation and distribution of phosphorus in a fertilized soil: A synchrotron-based investigation. *Soil Sci. Soc. Am. J.* **2006**, *70* (6), 2038−2048.

(29) Ajiboye, B.; Akinremi, O. O.; Hu, Y.; Jurgensen, A. XANES speciation of phosphorus in organically amended and fertilized vertisol and mollisol. *Soil Sci. Soc. Am. J.* **2008**, *72* (5), 1256−1262.

(30) Prietzel, J.; Dümig, A.; Wu, Y. H.; Zhou, J.; Klysubun, W. Synchrotron-based P *K*-edge XANES spectroscopy reveals rapid changes of phosphorus speciation in the topsoil of two glacier foreland chronosequences. *Geochim. Cosmochim. Acta* **2013**, *108*, 154−171.

(31) Prietzel, J.; Thieme, J.; Paterson, D. Phosphorus speciation of forest-soil organic surface layers using P *K*-edge XANES spectroscopy. *J. Plant Nutr. Soil Sci.* **2010**, *173*, 805−807.

(32) Liu, J.; Yang, J. J.; Liang, X. Q.; Zhao, Y.; Cade-Menun, B. J.; Hu, Y. F. Molecular Speciation of Phosphorus Present in Readily Dispersible Colloids from Agricultural Soils. *Soil Sci. Soc. Am. J.* **2014**, *78* (1), 47−53.

(33) Beauchemin, S.; Hesterberg, D.; Chou, J.; Beauchemin, M.; Simard, R. R.; Sayers, D. E. Speciation of phosphorus in phosphorus-enriched agricultural soils using X-ray absorption near-edge structure spectroscopy and chemical fractionation. *J. Environ. Qual.* **2003**, *32* (5), 1809−1819.

(34) Kelly, S.; Hesterberg, D.; Ravel, B. Analysis of soils and minerals using X-ray absorption spectroscopy. In *Methods of soil analysis. Part 5. Mineralogical Methods*; Ulery, A. L.; Drees, L. R., Eds.; No. 5 in the Soil Science Society of America book series; Soil Science Society of America: Madison, WI 2008; pp 387−464.

(35) Turner, B. L.; Condron, L. M.; Richardson, S. J.; Peltzer, D. A.; Allison, V. J. Soil organic phosphorus transformations during pedogenesis. *Ecosystems* **2007**, *10* (7), 1166−1181.

(36) Harrison, A. F. *Soil organic phosphorus: a review of world literature*; CAB International: Wallingford, U.K., 1987.

DOI: 10.1021/acs.est.5b03096
Environ. Sci. Technol. 2015, 49, 10521−10528

(37) Klysubun, W.; Sombunchoo, P.; Deenan, W.; Kongmark, C. Performance and status of beamline BL8 at SLRI for X-ray absorption spectroscopy. *J. Synchrotron Radiat.* **2012**, *19* (6), 930−936.
(38) Ravel, B.; Newville, M. ATHENA, ARTEMIS, HEPHAESTUS: data analysis for X-ray absorption spectroscopy using IFEFFIT. *J. Synchrotron Radiat.* **2005**, *12* (4), 537−541.
(39) R Core Team *R: A Language and Environment for Statistical Computing*; R Foundation for Statistical Computing: Vienna, Austria, 2015.
(40) Elzhov, T. V.; Mullen, K. M.; Spiess, A.-N.' Bolker, B. *minpack.lm: R interface to the Levenberg-Marquardt nonlinear least-squares algorithm found in MINPACK, plus support for bounds*; 2013.
(41) Shober, A. L.; Hesterberg, D. L.; Sims, J. T.; Gardner, S. Characterization of phosphorus species in biosolids and manures using XANES spectroscopy. *J. Environ. Qual.* **2006**, *35* (6), 1983−1993.
(42) Sayers, D. E.; Bunker, B. A. Data Analyis. In *X-ray absorption: principles, applications, techniques of EXAFS, SEXAFS, and XANES*; Koningsberger, D. C., Prins, R., Eds.; John Wiley and Sons: New York, 1988; Vol. *10*, pp 211−253.
(43) Kruse, J.; Abraham, M.; Amelung, W.; Baum, C.; Bol, R.; Kuhn, O.; Lewandowski, H.; Niederberger, J.; Oelmann, Y.; Ruger, C.; Santner, J.; Siebers, M.; Siebers, N.; Spohn, M.; Vestergren, J.; Vogts, A.; Leinweber, P. Innovative methods in soil phosphorus research: A review. *J. Plant Nutr. Soil Sci.* **2015**, *178* (1), 43−88.

DOI: 10.1021/acs.est.5b03096
Environ. Sci. Technol. 2015, 49, 10521−10528

Reprinted with permission from

Small-scale spatial distribution of phosphorus fractions in soils from silicate parent material with different degree of podzolization

by

Florian Werner, Tilman René de la Haye,
Sandra Spielvogel, and Jörg Prietzel

DOI: 10.1016/j.geoderma.2017.04.026

Published in **Geoderma 302**, pp. 52–65

ELSEVIER LICENSE
TERMS AND CONDITIONS

May 11, 2017

This Agreement between Florian Werner ("You") and Elsevier ("Elsevier") consists of your license details and the terms and conditions provided by Elsevier and Copyright Clearance Center.

License Number	4105360449849
License date	
Licensed Content Publisher	Elsevier
Licensed Content Publication	Geoderma
Licensed Content Title	Small-scale spatial distribution of phosphorus fractions in soils from silicate parent material with different degree of podzolization
Licensed Content Author	Florian Werner,Tilman René de la Haye,Sandra Spielvogel,Jörg Prietzel
Licensed Content Date	15 September 2017
Licensed Content Volume	302
Licensed Content Issue	n/a
Licensed Content Pages	14
Start Page	52
End Page	65
Type of Use	reuse in a thesis/dissertation
Portion	full article
Format	both print and electronic
Are you the author of this Elsevier article?	Yes
Will you be translating?	No
Order reference number	
Title of your thesis/dissertation	Spatial heterogeneity of phosphorus concentration and speciation at the micro and profile scale in German forest soils
Expected completion date	May 2017
Estimated size (number of pages)	58
Elsevier VAT number	GB 494 6272 12
Requestor Location	Florian Werner Chair of Soil Science Emil-Ramann-Str. 2 Freising, other 85354 Germany Attn: Florian Werner
Publisher Tax ID	GB 494 6272 12
Total	0.00 EUR
Terms and Conditions	

Authors can share their preprints anywhere at any time. Preprints should not be added to or enhanced in any way in order to appear more like, or to substitute for, the final versions of articles however authors can update their preprints on arXiv or RePEc with their Accepted Author Manuscript (see below).
If accepted for publication, we encourage authors to link from the preprint to their formal publication via its DOI. Millions of researchers have access to the formal publications on ScienceDirect, and so links will help users to find, access, cite and use the best available version. Please note that Cell Press, The Lancet and some society-owned have different preprint policies. Information on these policies is available on the journal homepage.
Accepted Author Manuscripts: An accepted author manuscript is the manuscript of an article that has been accepted for publication and which typically includes author-incorporated changes suggested during submission, peer review and editor-author communications.
Authors can share their accepted author manuscript:

- immediately
    - via their non-commercial person homepage or blog
    - by updating a preprint in arXiv or RePEc with the accepted manuscript
    - via their research institute or institutional repository for internal institutional uses or as part of an invitation-only research collaboration work-group
    - directly by providing copies to their students or to research collaborators for their personal use
    - for private scholarly sharing as part of an invitation-only work group on commercial sites with which Elsevier has an agreement
- After the embargo period
    - via non-commercial hosting platforms such as their institutional repository
    - via commercial sites with which Elsevier has an agreement

In all cases accepted manuscripts should:

- link to the formal publication via its DOI
- bear a CC-BY-NC-ND license - this is easy to do
- if aggregated with other manuscripts, for example in a repository or other site, be shared in alignment with our hosting policy not be added to or enhanced in any way to appear more like, or to substitute for, the published journal article.

Published journal article (JPA): A published journal article (PJA) is the definitive final record of published research that appears or will appear in the journal and embodies all value-adding publishing activities including peer review co-ordination, copy-editing, formatting, (if relevant) pagination and online enrichment.
Policies for sharing publishing journal articles differ for subscription and gold open access articles:
Subscription Articles: If you are an author, please share a link to your article rather than the full-text. Millions of researchers have access to the formal publications on ScienceDirect, and so links will help your users to find, access, cite, and use the best available version.
Theses and dissertations which contain embedded PJAs as part of the formal submission can be posted publicly by the awarding institution with DOI links back to the formal publications on ScienceDirect.
If you are affiliated with a library that subscribes to ScienceDirect you have additional private sharing rights for others' research accessed under that agreement. This includes use for classroom teaching and internal training at the institution (including use in course packs

and courseware programs), and inclusion of the article for grant funding purposes.
Gold Open Access Articles: May be shared according to the author-selected end-user license and should contain a CrossMark logo, the end user license, and a DOI link to the formal publication on ScienceDirect.
Please refer to Elsevier's posting policy for further information.
18. **For book authors** the following clauses are applicable in addition to the above: Authors are permitted to place a brief summary of their work online only. You are not allowed to download and post the published electronic version of your chapter, nor may you scan the printed edition to create an electronic version. **Posting to a repository:** Authors are permitted to post a summary of their chapter only in their institution's repository.
19. **Thesis/Dissertation**: If your license is for use in a thesis/dissertation your thesis may be submitted to your institution in either print or electronic form. Should your thesis be published commercially, please reapply for permission. These requirements include permission for the Library and Archives of Canada to supply single copies, on demand, of the complete thesis and include permission for Proquest/UMI to supply single copies, on demand, of the complete thesis. Should your thesis be published commercially, please reapply for permission. Theses and dissertations which contain embedded PJAs as part of the formal submission can be posted publicly by the awarding institution with DOI links back to the formal publications on ScienceDirect.

Elsevier Open Access Terms and Conditions
You can publish open access with Elsevier in hundreds of open access journals or in nearly 2000 established subscription journals that support open access publishing. Permitted third party re-use of these open access articles is defined by the author's choice of Creative Commons user license. See our open access license policy for more information.
Terms & Conditions applicable to all Open Access articles published with Elsevier:
Any reuse of the article must not represent the author as endorsing the adaptation of the article nor should the article be modified in such a way as to damage the author's honour or reputation. If any changes have been made, such changes must be clearly indicated.
The author(s) must be appropriately credited and we ask that you include the end user license and a DOI link to the formal publication on ScienceDirect.
If any part of the material to be used (for example, figures) has appeared in our publication with credit or acknowledgement to another source it is the responsibility of the user to ensure their reuse complies with the terms and conditions determined by the rights holder.
Additional Terms & Conditions applicable to each Creative Commons user license:
CC BY: The CC-BY license allows users to copy, to create extracts, abstracts and new works from the Article, to alter and revise the Article and to make commercial use of the Article (including reuse and/or resale of the Article by commercial entities), provided the user gives appropriate credit (with a link to the formal publication through the relevant DOI), provides a link to the license, indicates if changes were made and the licensor is not represented as endorsing the use made of the work. The full details of the license are available at http://creativecommons.org/licenses/by/4.0.
CC BY NC SA: The CC BY-NC-SA license allows users to copy, to create extracts, abstracts and new works from the Article, to alter and revise the Article, provided this is not done for commercial purposes, and that the user gives appropriate credit (with a link to the formal publication through the relevant DOI), provides a link to the license, indicates if changes were made and the licensor is not represented as endorsing the use made of the work. Further, any new works must be made available on the same conditions. The full details of the license are available at http://creativecommons.org/licenses/by-nc-sa/4.0.
CC BY NC ND: The CC BY-NC-ND license allows users to copy and distribute the Article, provided this is not done for commercial purposes and further does not permit distribution of

Geoderma 302 (2017) 52–65

Contents lists available at ScienceDirect

Geoderma

journal homepage: www.elsevier.com/locate/geoderma

Small-scale spatial distribution of phosphorus fractions in soils from silicate parent material with different degree of podzolization

Florian Werner[a,*], Tilman René de la Haye[b], Sandra Spielvogel[b], Jörg Prietzel[a]

[a] Chair of Soil Science, Chair of Soil Science, Research Department Ecology and Ecosystem Management, Technical University of Munich, Emil-Ramann-Straße 2, 85354 Freising, Germany

[b] Soil Science Section, Institute of Geography, Faculty of Science, University of Bern, Hallerstrasse 12, 3012 Bern, Switzerland

ARTICLE INFO

Keywords:
Cambisol
Geostatistics
Organic carbon
Oxyhydroxides
Pedogenesis
P fractions

ABSTRACT

The spatial heterogeneity of phosphorus (P) and different P forms in soils has implications for plant, microbial, and ecosystem P supply. Little information is available concerning the small-scale vertical and horizontal distributions of P and important variables for P binding at the soil profile scale. We assessed spatial patterns of total P and different P fractions, and of major P binding partners (e.g. soil organic matter: SOM, pedogenic Fe and Al minerals) with geostatistical methods in soil profiles and soil profile compartments formed from siliceous parent material and stocked with mature *Fagus sylvatica* forest to describe spatial and pedogenetic changes of P distribution and to address mechanisms for these changes. As expected, we found that the distribution of total P was generally best matched by the distribution pattern of organic P, both showing decreasing contents from the top- to the subsoil. Inorganic P was mainly ascribed as bound in primary silicate minerals at all sites, but with decreasing importance in later stages of podzolization. SOM, Al and Fe oxyhydroxides as well as SOM-Al/Fe oxyhydroxide complexes were identified as main binding partners of organic P at all sites. With increasing depth, correlations of various P fractions with SOM decreased, whereas those with pedogenic Fe and Al oxyhydroxides increased. This pattern is assigned to the mobilization of first pedogenic Al minerals, and in later stages of podzolization, also of pedogenic Fe minerals in the topsoil. Our results support the concept of different ecosystem P nutrition strategies at each of our sites: ranging from acquiring inorganic P from weathered parent material to minimizing loss of organic P by recycling. Assessing the small-scale soil variability enables investigating the influence of podzolization intensity in temperate forest soils on the spatial P distribution at the profile scale.

1. Introduction

Temperate forest ecosystems rely on the availability of phosphorus (P) from the soil. The small-scale (μm to cm) vertical and horizontal distribution of soil variables like pH, metal cations (especially Ca, Fe and Al), and P can be a crucial factor governing plant root activity (Hinsinger, 2001). In most cases spatial patterns of soil P contents were assessed unidimensional by depth gradients, not addressing the question of horizontal variation of P in soil profiles (e.g., Ferro Vázquez et al., 2014). This is striking, as also the horizontal spatial heterogeneity of P has been identified as an important factor controlling P availability years ago for plants (Facelli and Facelli, 2002; Jackson and Caldwell, 1993), or recently for an alpine treeline (Liptzin et al., 2013). Consequently, the two-dimensional (i.e. vertical and horizontal) small-scale spatial distribution patterns of P and important P-binding elements in soils are still unclear. However, the presence or absence of P accumulation patterns (hot spots) in soils and specific soil fractions have implications for plant P acquisition and plant P supply (Facelli and Facelli, 2002). Hereby, geostatistics offers the possibility to produce high resolution maps for total P and different P fractions, and important variables for P binding.

Even though most soils in central Europe are young, the P status of European forests is often low or insufficient (Ilg et al., 2009; Jonard et al., 2015). Apart from nitrogen, P is expected to become (co-) limiting to net primary production of plants as well as ecosystems (Elser, 2012; Vitousek and Farrington, 1997). Soil acidification and N eutrophication, intensified by anthropogenic deposits, reduce plant-available P (Mohren et al., 1986). Thus, strong P sorption, e.g. by humic-mineral complexes (Gerke and Hermann, 1992), Al and Fe oxides and hydroxides (oxyhydroxides) (Sims and Pierzynski, 2005),

* Corresponding author.
E-mail addresses: florian.werner@wzw.tum.de (F. Werner), tilman.delahaye@giub.unibe.ch (T.R. de la Haye), sandra.spielvogel@giub.unibe.ch (S. Spielvogel), prietzel@wzw.tum.de (J. Prietzel).

http://dx.doi.org/10.1016/j.geoderma.2017.04.026
Received 13 July 2016; Received in revised form 10 January 2017; Accepted 27 April 2017

or clay minerals (Violante and Pigna, 2002), increased formation of P-fixing short-range order Al or Fe phosphates (Arai and Sparks, 2007), as well as retarded mineralization of organic P may limit forest growth in many ecosystems (Laliberté et al., 2012; Richardson et al., 2004). Studying P availability in soil therefore implies accounting for the spatial distribution of different P species in soils, as assessed by wet-chemical fractionation of soil, and/or by advanced spectroscopic/−metric techniques (Kruse et al., 2015). Fractionation techniques have proven useful to answer questions about P bioavailability, e.g. as reported by Sherman et al. (2006) in a study about long-term acidification effects in spodic forest soils in Maine, USA. However, advanced techniques can provide additional valuable information: organic P speciation can be assessed by nuclear magnetic resonance (NMR) spectroscopy (e.g., Cade-Menun and Liu, 2014), a general P speciation by *K*-edge (e.g., Eriksson et al., 2015) or *L*-edge (Kruse et al., 2015) X-ray absorption near-edge structure (XANES) spectroscopy, or particle investigation after field flow fractionation techniques (e.g., Regelink et al., 2013).

A current research program in Germany, which our subproject is a part of, focuses on the mechanisms that allow temperate forests on silicate bedrock to sufficiently supply the trees with P (Lang et al., 2016). The sites are characterized by a P availability gradient, as characterized in pre-studies by nutrient P contents of beech foliage. Two of the three sites investigated in this study were also included in a recent study by Prietzel et al. (2016) using *K*-edge XANES spectroscopy. However, they concentrated on discussing P speciation methodologically, the relationship of the P species with parent material and solely studied soil horizons, but not different soil compartments. Thus, at the moment no information can be found on the two-dimensional heterogeneity of physical and chemical soil properties of P content and P fractions in soils with different stages of pedogenesis at the profile scale.

In an often cited publication, Walker and Syers (1976) introduced a model describing changes of soil P forms and contents with time. After > 22.000 years of soil development at the Franz-Josef chronosequence, P is stated to be either occluded or organic P and to reach a steady state in which P losses from the system equal gains. Here, we aim at refining the model of Walker and Syers (1976) for soils from siliceous parent material by (1) determining the small-scale horizontal and vertical spatial distribution of P by grid sampling and geostatistical methods, (2) distinguishing different P binding forms by wet-chemical fractionation, and (3) examining the relations of different P fractions to other important explanatory soil variables (e.g. SOM, Al and Fe oxyhydroxides). In addition, we (4) perform analyses for different soil depths.

2. Materials and methods

2.1. Soil sampling and sample preparation

Soil samples were taken from three sites in Germany stocked with mature European beech (*Fagus sylvatica*) stands of about 120 years with differing P contents in the beech leaves and differing total P contents in the soils (Zavišić et al., 2016). One site is located in the Black Forest near Freiburg (site Conventwald: CON), Gauss-Krüger-coordinates: 3,422,803 E, 5,321,010 N. The second site is located in the Bavarian Forest near Mitterfels (MIT), Gauss-Krüger-coordinates: 4,564,502 E, 5,426,906 N, and the last near Lüss (LUE), Gauss-Krüger-coordinates: 3,585,473 E, 5,857,057 N. All soils were formed under temperate climate from siliceous parent material and are classified as Cambisols (IUSS Working Group WRB, 2015). More detailed information on site and soil properties is presented in Table 1 and Table S1, respectively. Additional information on the site stand properties can be found in Zavišić et al. (2016), information for specific soil horizons is presented in Table S2, and general information about the sites can be found online at http://www.ecosystem-nutrition.uni-freiburg.de/standorte.

At each site, a soil profile was excavated at a representative pure beech location. Samples were taken from the mineral soil in a 70 × 100 cm rectangle at every 10 cm intersection (Fig. 1) with a steel tube (ø 2 cm, sampling depth 3 cm). Depending on profile depth and stone content, 63, 71, and 68 (CON, MIT, and LUE) samples were obtained. Within this grid, up to five smaller gridded nests (up to 6 samples with a distance of 3 cm, taken with the same steel tube, Fig. 1) were included to improve geostatistical models (Webster and Oliver, 2008). Soil samples were dried at 60 °C for 48 h and subsequently sieved (< 2 mm). Sieved and finely ground subsamples were digested with $HF/HClO_4$ to analyze the contents of total P (P_{tot}), Ca (Ca_{tot}), Fe (Fe_{tot}), and Al (Al_{tot}) by ICP-OES (Vista-PRO Simultaneous ICP-OES, Varian Inc., Palo Alto, CA, USA). This digestion was favored over the *aqua regia* digestion to ensure complete digestion of silicate minerals and prevent underestimation of total P (Hornburg and Lüer, 1999). Organic P (P_{org}) was determined using the ignition loss method of Saunders and Williams (1955), and inorganic P was calculated by subtracting P_{org} from P_{tot}. Total C and N contents were analyzed with an Elementar VarioEL CN analyzer (Elementar GmbH, Hanau, Germany). Because all soils were acidic and free of carbonate, total C content can be accounted for total organic C (C_{org}). Contents of Al and Fe bound in pedogenic minerals were analyzed by extraction with bicarbonate-buffered dithionite-citrate solution (Al_{di} and Fe_{di}) according to Mehra and Jackson (1958), as modified by Holmgren (1967). Contents of Fe in poorly crystalline pedogenic minerals (Fe_{pc}), and of Al in $Al(OH)_3$, interlayer Al hydroxy polymers, imogolite, and allophane, were assessed by extraction with acidic NH_4 oxalate solution (Al_{ox}) using the method of Schwertmann (1964). By subtracting Fe_{pc} from Fe_{di} we calculated the content of Fe in crystalline pedogenic minerals (Fe_{cr}). The respective amounts of oxalate-extractable P (P_{pc}), i.e. P bound by Fe_{pc} and Al_{ox}, and dithionite-citrate-extractable P (P_{di}) were quantified in the same way. The content of P bound by crystalline pedogenic Fe minerals and by Al in crystalline and amorphous Fe minerals (P_{cr}) was obtained by subtracting P_{pc} from P_{di}. Contents of Fe, Al, and P in primary silicate minerals (Fe_{mi}, Al_{mi}, P_{mi}) were calculated by subtracting Fe_{di}, Al_{di} and P_{di} from Fe_{tot}, Al_{tot} and P_{tot}, respectively. In addition, oxalate extracts were analyzed for orthophosphate P ($P_{pc.inorg}$) by colorimetry using the ascorbic acid method of Murphy and Riley (1962), as modified by John (1970). The difference between P_{pc} and $P_{pc.inorg}$ was assigned to organic P forms ($P_{pc.org}$).

2.2. Statistical data analysis

The data were analyzed statistically with the software package *R*, version 3.3.1 (R Core Team, 2015). To characterize and compare the magnitudes of spatial variation of the investigated soil properties among the three profiles, coefficient of variations (CV) were calculated for the variables C_{org}, Ca_{tot}, Fe_{mi}, Fe_{cr}, Fe_{pc}, Al_{mi}, Al_{di}, Al_{ox}, P_{tot}, P_{org}, P_{mi}, P_{inorg}, P_{cr}, P_{pc}, $P_{pc.org}$, and $P_{pc.inorg}$. Additionally, in order to specifically address the horizontal and vertical variation of the variables, a vertical and a horizontal CV were calculated (CV_{ver} and CV_{hor}). These were the medians of the coefficients for every column and row, respectively, if the profile is imagined as a table consisting of rows (i.e. left to right part of the profile) and columns (depth increments). The proportion of horizontal CV by vertical CV ($CV_{hor/ver}$) served as a measure of variability in profile width and depth; i.e. values below 1 expressed a greater variation in vertical than in horizontal direction of the profile, and vice versa. Correlation patterns among the studied variables were analyzed using the Spearman rank coefficient ρ. An upper profile region was defined by all sample points starting from the mineral soil surface to those of 25 cm depth (Fig. 1). The middle profile region included points < 25 cm depth down to 55 cm depth, and the lower profile region contained points from < 55 cm depth and reached until 70 cm (CON), 80 cm (LUE), or 90 cm (MIT) of depth. Additionally, factor analysis was performed on all variables of a given soil profile using *psych* package, version 1.6.9 (Revelle, 2015) to infer explanatory constructs from the observed variables. The *Optimal Coordinate* method

Table 1
General properties of the three study sites Conventwald (CON), Mitterfels (MIT), and Lüss (LUE). MAT: mean annual temperature, MAP: mean annual precipitation.

	CON	MIT	LUE
Soil profile			
Parent material[a]	Paragneiss	Paragneiss	Pleistocene glacifluvial sands
P content (parent material)	0.29 mg P g^{-1}[b]	1.38 mg P g^{-1}[b]	0.17 mg P g^{-1}[c]
Soil type (WRB 2015)	Hyperdystric Skeletic Folic Cambisol (Hyperhumic, Loamic)	Hyperdystric Chromic Folic Cambisol (Humic, Loamic, Nechic)	Hyperdystric Folic Cambisol (Arenic, Loamic, Nechic, Protospodic)
Elevation [m a.s.l.][a]	884	1023	115
MAT [°C][a]	6.6	4.9	8.0
MAP [mm][a]	1749	1229	779
Forest type[b]	Mature *Fagus sylvatica* forest	Mature *Fagus sylvatica* forest	Mature *Fagus sylvatica* forest

[a] Zavišić et al. (2016).
[b] Prietzel et al. (2016).
[c] Yang et al. (2016).

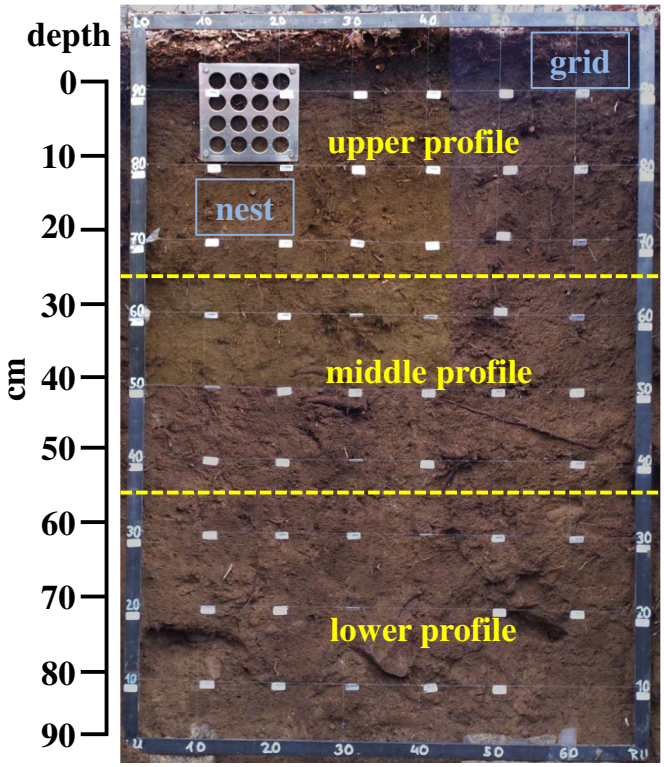

Fig. 1. Sampling grid with nest for smaller gridded sampling and scheme of soil region compartmentation. The steel grid is 70 × 100 cm with intersections every 10 cm. For nested sampling, a steel plate with holes of a diameter of 2 cm and a distance of 3 cm between the hole centers was used. The soil was divided into three regions: upper profile (0–25 cm depth), middle profile (> 25–55 cm depth), and lower profile (> 55 cm depth). The profile is from the site Mitterfels.

was used to select the number of factors. For rotation *varimax* and as factoring method *principal axis factoring* was determined. Factor scores were identified using *Thurstone* regression.

For geostatistical analysis, Bayesian Kriging was performed using *geoR* package, version 1.7–5.2 (Ribeiro and Diggle, 2001). This approach was preferred over ordinary or universal kriging because covariance parameters do not have to be considered known and to allow parameter uncertainty in the prediction (Diggle and Ribeiro, 2002). However, the default Bayesian approach of treating the parameters as random variables often resulted in poor posterior distribution estimates due to small numbers of support points. In these cases, we calculated covariance parameters from empirical variograms to define the prior parameters. First, data were analyzed for a depth trend. This was performed by testing the data values and the y-coordinates for correlation using the Kendall rank correlation coefficient and a scatter plot with a linear regression model. As second step, the data were checked for normal distribution using the Shapiro-Wilk test. When the assumption of normal distribution was rejected, the variogram estimator suggested by Cressie (2015) was used to build robust variograms. In all other cases the classical method of moment estimator was applied. All variograms were computed using the *geoR*-Package (ordinary kriging) and the *gstat*-Package (universal kriging), version 1.1–3 (Pebesma, 2004). Each variogram was calculated for the maximum distance between all samples, half of the maximum distance and one third of the maximum distance. For each distance, variograms were computed for six through thirteen bins in each variogram. For map computation, the variogram parameters with the lowest root mean squared errors were set as prior parameter for Bayesian Kriging. Afterwards, Bayesian Kriging was performed using a 1 cm prediction grid.

3. Results

3.1. Soil profile maps derived from Bayesian Kriging

As expected, the interpolated maps did not reveal a uniform distribution of any P fraction in any of the studied soils (Figs. 2 and 3). Total P showed high contents in the upper part of the profiles and decreased systematically with soil depth at site CON (Fig. 2). At MIT, total P decreased less strongly with depth and at LUE, P_{tot} was distributed more patchily and characterized by a secondary maximum at 40–60 cm depth. Organic P generally showed the same trends, however, was confined to the uppermost topsoil at sites CON and MIT. Phosphorus bound in primary silicate minerals was distributed particularly patchily at sites CON and MIT. At CON, high contents were found in the upper profile at 30–50 cm depth, whereas at MIT, P_{mi}

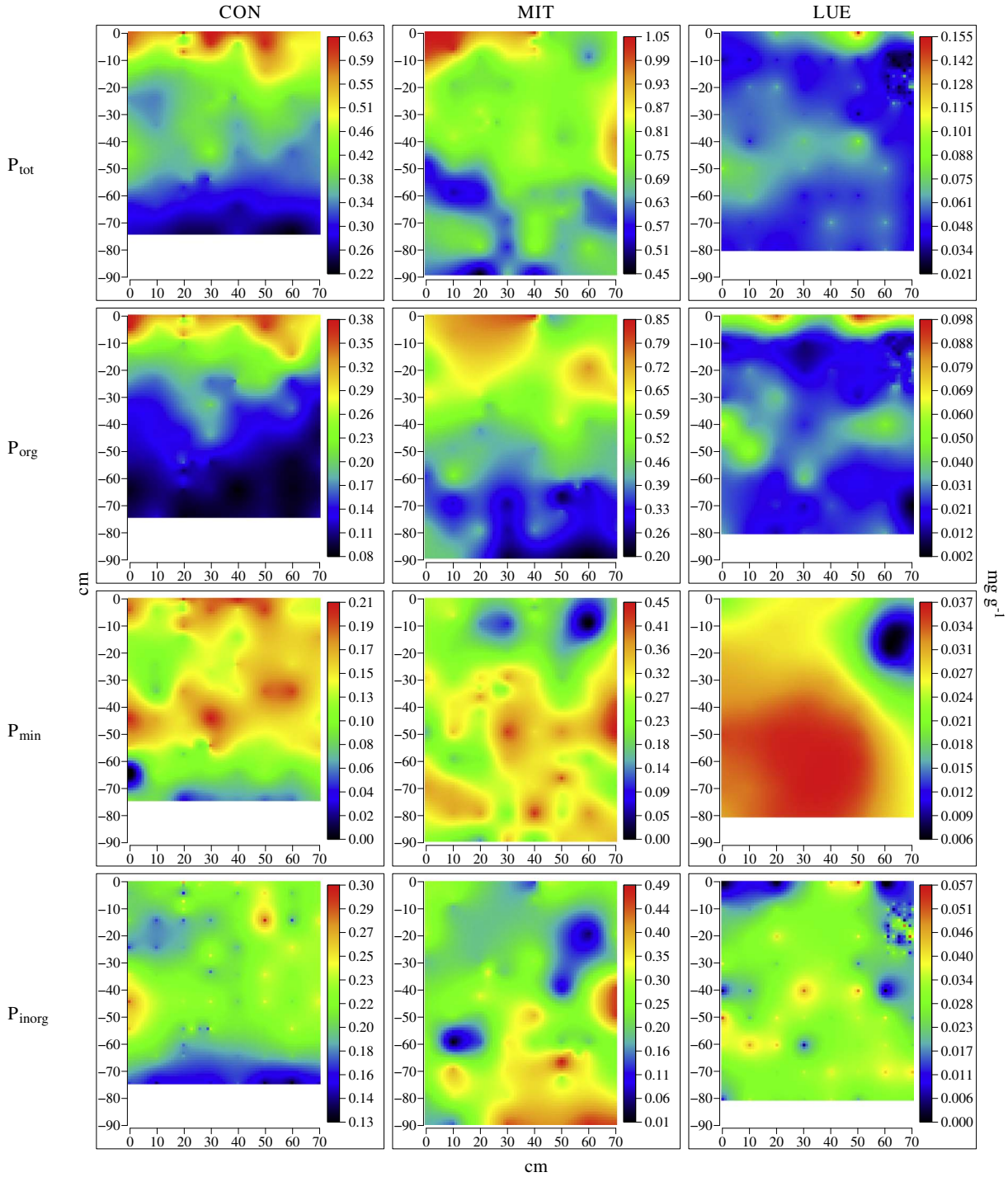

Fig. 2. Interpolated distribution patterns of total phosphorus (P) and different P fractions in soil profiles at the study sites Conventwald (CON), Mitterfels (MIT), and Lüss (LUE). Bayesian Kriging predictions (grid: 1 cm) of total P (P_{tot}), organic P (P_{org}), P bound in primary silicate minerals (P_{mi}), and inorganic P (P_{inorg}). Scales differ among maps.

contents were patchily elevated at depths > 40 cm. In contrast, at site LUE, P_{mi} showed a more homogenous distribution at depths below 40 cm. Inorganic P was particularly enriched in the upper and middle profile at CON, in the lower profile at MIT, and in the middle and lower profile at LUE.

As for P_{cr} (Fig. 3), at sites CON and MIT, this fraction showed higher contents in the upper profile, decreasing with depth. Additionally, a secondary maximum was found at 60–70 cm depth at site CON. At LUE, P_{cr} showed a patch of maximum content at 20 cm depth. Phosphorus bound by poorly crystalline pedogenic Al/Fe minerals was generally distributed differently than P_{cr}. At CON and MIT, P_{pc} showed a depth trend from higher contents in the upper profile to lower contents in the lower profile. In addition, all sites showed secondary maxima of P_{pc} at about 40 cm depth. For CON and MIT, separation of inorganic and organic P bound by poorly crystalline pedogenic Al/Fe minerals revealed a systematic change from a dominance of $P_{pc.org}$ in the uppermost 30 to 40 cm to a dominance of $P_{pc.inorg}$ below that depth. In all soils, the spatial distribution of $P_{pc.org}$ strongly resembled the distribution of P_{org}. Additionally, the spatial distribution of $P_{pc.inorg}$ resembled the distribution of P_{inorg}, however, at LUE, $P_{pc.inorg}$ was distributed more patchily.

Major P-bearing soil compounds, i.e. SOM, represented by C_{org}, and

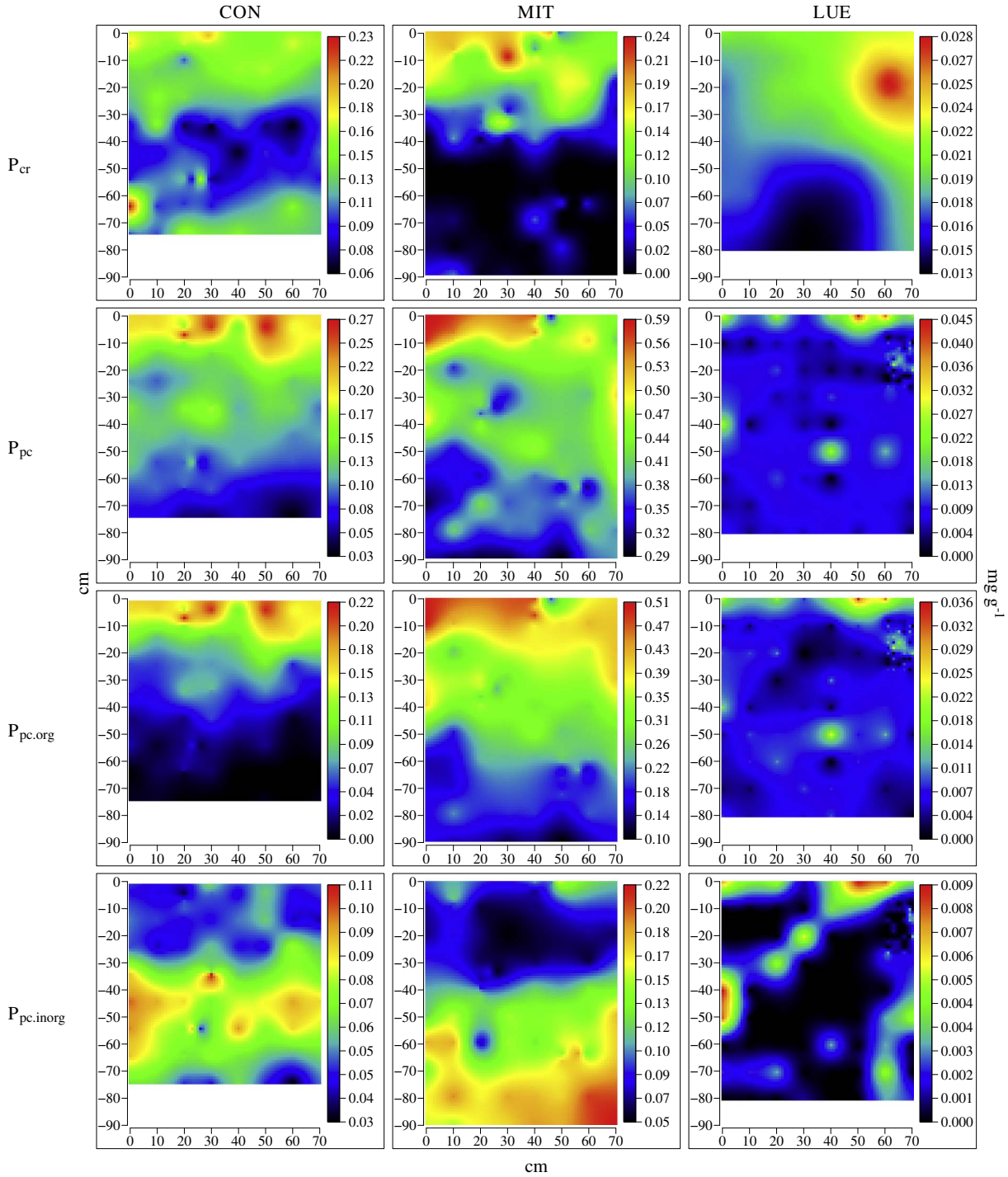

Fig. 3. Interpolated distribution patterns of different phosphorus (P) fractions in soil profiles at the study sites Conventwald (CON), Mitterfels (MIT), and Lüss (LUE). Bayesian Kriging predictions (grid: 1 cm) of P bound by crystalline (P_{cr}) and poorly crystalline (P_{pc}) pedogenic Al/Fe minerals, and organic and inorganic P bound by poorly crystalline pedogenic Al/Fe minerals ($P_{pc.org}$, $P_{pc.inorg}$) are shown. Scales differ among maps.

pedogenic Fe and Al minerals with different crystallinity, also showed an expected heterogeneous distribution (Figs. 4 and 5). In particular, C_{org} was enriched in the upper profile, particularly in the uppermost 10 cm, and showed a strong systematic decrease with depth (Fig. 4). Iron in primary silicate minerals increased with depth at sites CON and MIT. In contrast, at LUE, soil Fe_{mi} contents showed an enrichment zone at 40–60 cm depth. At all sites, the distribution of pedogenic Fe with differing crystallinity (Fe_{cr} and Fe_{pc}) differed significantly from each other. At site CON, Fe_{cr} content increased, whereas Fe_{pc} content slightly decreased with depth. In contrast, at MIT, Fe_{pc} showed highest contents in the upper 10 cm, whereas Fe_{cr} showed a patch of maximum content at 10–30 cm depth. Site LUE showed a pronounced enrichment of Fe_{cr} and Fe_{pc} at soil depths between 20 and 50 cm. The zone of maximum Fe_{cr} enrichment (40 cm depth) was below the zone of maximum Fe_{cr} enrichment (20 cm).

Aluminum in primary silicate minerals was depleted in the upper profile at all sites, showing a rather homogenous lateral distribution at MIT and CON, but patchiness at LUE (Fig. 5). A zone of maximum Al_{mi} content was prominent at 40–60 cm depth at sites CON and LUE, and at 70–90 cm depth at MIT. Dithionite- and oxalate-extractable Al in

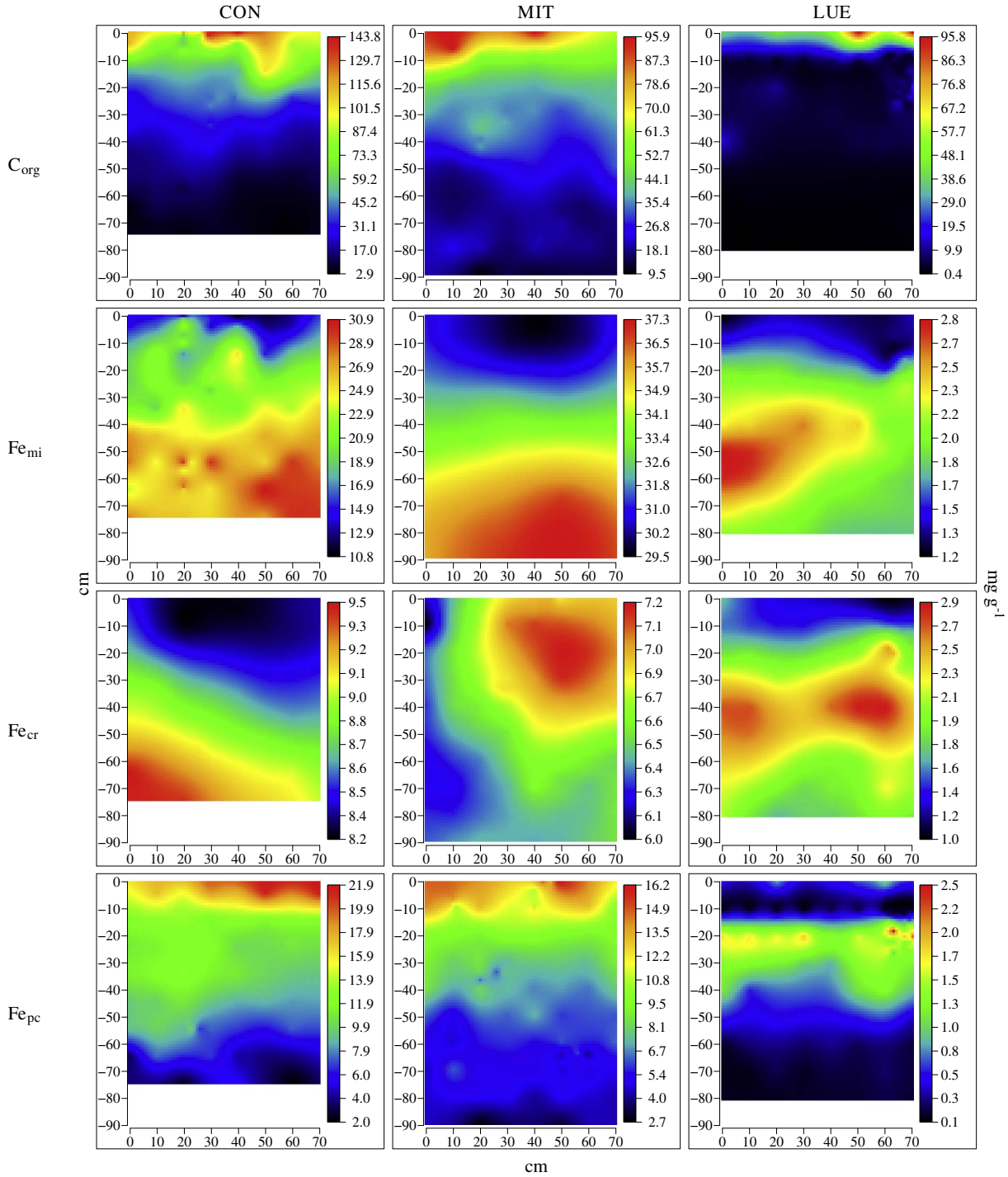

Fig. 4. Interpolated distribution patterns of organic carbon (C) and iron (Fe) fractions in soil profiles at the study sites Conventwald (CON), Mitterfels (MIT), and Lüss (LUE). Bayesian Kriging predictions (grid: 1 cm) of organic C (C_{org}), and Fe in primary silicate minerals (Fe_{mi}), crystalline pedogenic Fe minerals (Fe_{cr}), and poorly crystalline pedogenic Fe minerals (Fe_{pc}). Scales differ among maps.

general did not differ markedly from each other in distribution and nearly the same contents were extracted. At CON and MIT both variables showed a general decrease with depth. This general trend was superimposed by an upper profile depletion of Al_{di} and Al_{ox} which was more pronounced and deep-reaching at site MIT than at site CON, associated with formation of an enrichment zone at 20 (CON) or 40 cm depth (MIT). At LUE, a band of patched pedogenic Al minerals was found from a depth of 30 cm to 50 cm, with patches of maximum Al_{di} and Al_{ox} contents at 40 cm depth.

At site CON, the C:P ratio ranged from 33 to 445, showing values below 200 at about 40 cm depth (Fig. 6). At MIT, no significant depth trend was detected, and the C:P ratio was largest in the upper profile (213.7), but mainly showing ratios below 200. At site LUE, the profile was divided at about 40 cm depth. At shallower depth we found a depth trend of a C:P ratio ranging from about 200 (40 cm) to over 1300 (topsoil). Below 40 cm depth, the C:P ratio was predominantly below 200.

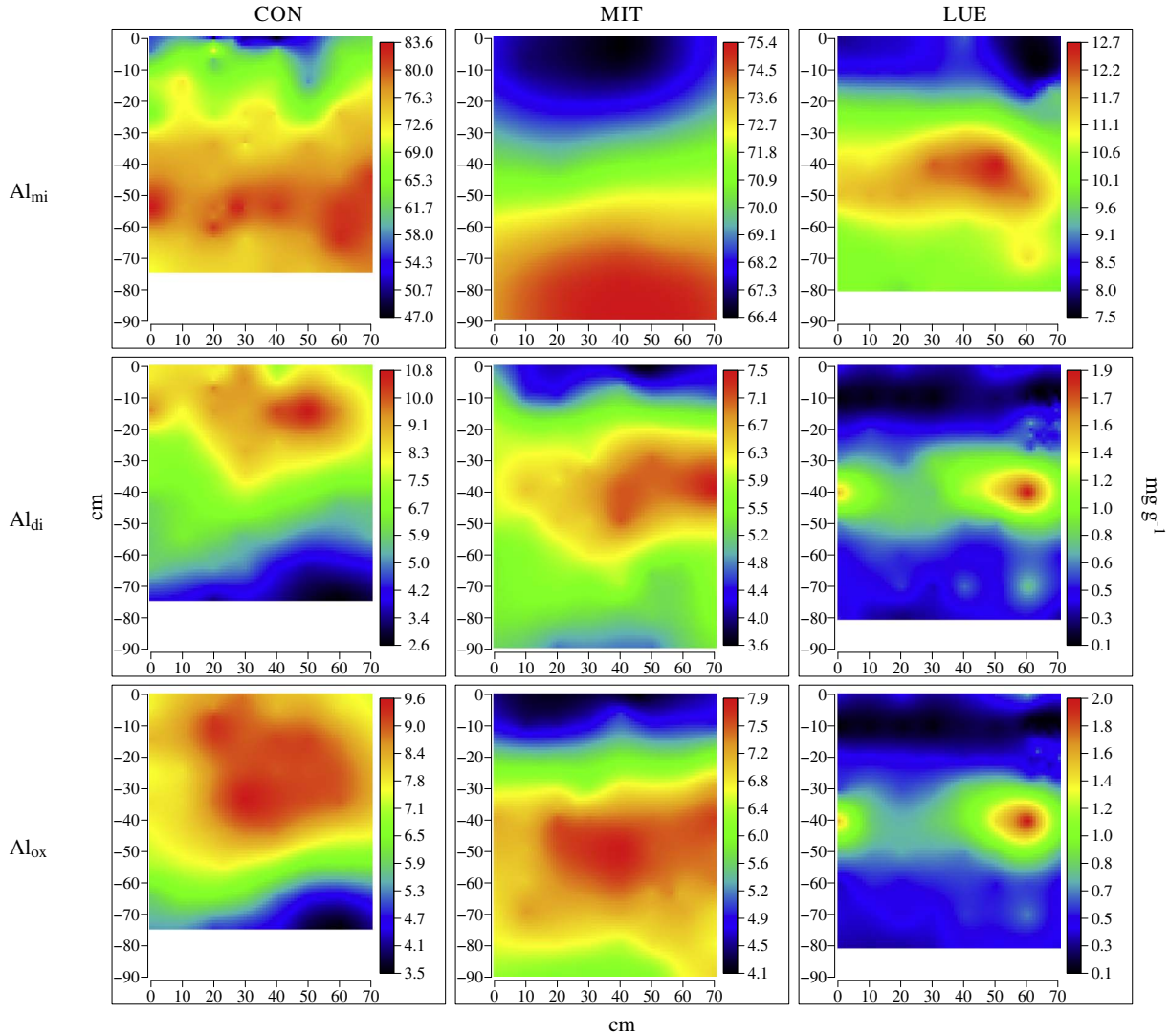

Fig. 5. Interpolated distribution patterns of aluminum (Al) fractions in soil profiles at the study sites Conventwald (CON), Mitterfels (MIT), and Lüss (LUE). Bayesian Kriging predictions (grid: 1 cm) of Al in primary silicate minerals (Al_{mi}), and dithionite-citrate-extractable, and oxalate-extractable Al (Al_{di}, Al_{ox}) are shown. Scales differ among maps.

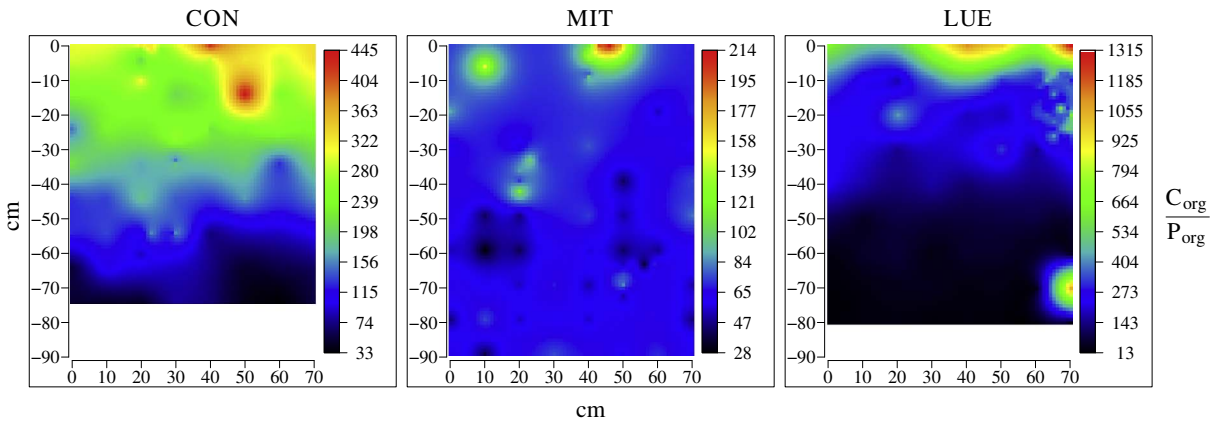

Fig. 6. Ratios of organic carbon (C_{org}) over organic phosphorus (P_{org}) in soil profiles at the study sites Conventwald (CON), Mitterfels (MIT), and Lüss (LUE). Bayesian Kriging predictions (grid: 1 cm) of the proportion C_{org}/P_{org}. Scales differ among maps.

3.2. Coefficient of variation analysis

In nearly all cases, CV analysis revealed a larger vertical than horizontal variation of all studied soil properties (Table 2). Major P-bearing soil compounds and many P fractions showed largest total variation at site LUE, and lowest total variation at site MIT. The site CON had intermediate CVs. Both horizontal and vertical variation showed trends similar to total variation at all sites. At LUE, we found the largest vertical variation for all P-bearing soil compounds and for some P fractions, compared to the other soils. Due to the large

Table 2
Coefficient of Variation (CV) analysis results for the sites Conventwald (CON), Mitterfels (MIT), and Lüss (LUE). CV of all grid data points (CV_{tot}), median of all horizontal and vertical CVs (CV_{hor} and CV_{ver}), and respective proportion of CV_{hor} / CV_{ver} are portrayed. Proportion values below 1 indicate a larger vertical than horizontal variation. Variables are organic C (C_{org}), total Ca (Ca_{tot}), Fe in primary silicate minerals (Fe_{mi}), Fe in crystalline pedogenic minerals (Fe_{cr}), and in poorly crystalline pedogenic minerals (Fe_{pc}), Al in primary silicate minerals (Al_{mi}), and dithionite-citrate-extractable, and oxalate-extractable Al (Al_{di}, Al_{ox}), total P (P_{tot}), organic P (P_{org}), P bound in primary silicate minerals (P_{mi}), inorganic P (P_{inorg}), P bound by crystalline (P_{cr}) and poorly crystalline (P_{pc}) pedogenic Al/Fe minerals, and organic and inorganic P bound by poorly crystalline pedogenic Al/Fe minerals ($P_{pc.org}$, $P_{pc.inorg}$).

	CON				MIT				LUE			
Variable	CV_{tot}	CV_{hor}	CV_{ver}	$CV_{hor/ver}$	CV_{tot}	CV_{hor}	CV_{ver}	$CV_{hor/ver}$	CV_{tot}	CV_{hor}	CV_{ver}	$CV_{hor/ver}$
C_{org}	91.4	25.0	94.9	0.26	49.7	17.4	48.4	0.36	201.9	33.4	181.5	0.18
Ca_{tot}	11.9	7.7	11.2	0.69	11.6	6.8	12.1	0.56	19.8	12.3	17.4	0.71
Fe_{mi}	19.7	8.7	19.9	0.44	13.3	5.8	12.4	0.47	41.9	29.8	36.3	0.82
Fe_{cr}	18.1	12.3	14.4	0.85	16.9	11.7	13.1	0.89	38.5	19.6	34.2	0.57
Fe_{pc}	46.0	12.5	44.1	0.28	36.9	10.4	39.3	0.26	91.6	25.1	93.8	0.27
Al_{mi}	8.6	3.2	8.4	0.38	11.9	4.6	12.1	0.38	19.2	8.8	18.9	0.46
Al_{di}	31.8	11.5	30.8	0.38	17.0	9.6	16.8	0.57	59.8	20.8	54.7	0.38
Al_{ox}	26.2	10.1	26.1	0.39	18.0	8.3	19.6	0.42	65.1	20.3	49.6	0.41
P_{tot}	23.7	8.5	23.7	0.36	14.6	10.4	14.5	0.72	30.7	17.7	21.9	0.80
P_{org}	44.9	16.5	43.6	0.38	32.7	19.6	26.4	0.74	59.6	30.4	56.3	0.54
P_{mi}	32.7	19.0	31.0	0.61	32.1	22.8	31.2	0.73	51.8	38.0	38.9	0.98
P_{inorg}	17.6	11.1	16.6	0.67	47.1	36.0	42.3	0.85	44.1	30.8	39.9	0.77
P_{cr}	27.7	14.8	27.0	0.55	129.4	127.3	137.7	0.92	72.7	75.7	88.8	0.85
P_{pc}	42.9	18.5	42.5	0.43	14.5	11.0	14.2	0.77	91.3	50.7	87.5	0.58
$P_{pc.org}$	101.6	41.5	102.4	0.41	32.0	12.9	31.7	0.41	91.8	65.9	90.8	0.73
$P_{pc.inorg}$	29.2	16.5	30.4	0.54	38.2	13.9	39.6	0.35	147.7	155.3	147.5	1.05

horizontal and vertical variation at LUE, the proportion of horizontal to vertical CV ($CV_{hor/ver}$) was sometimes large compared to the other sites (e.g. Ca_{tot}, Fe_{mi}, Al_{mi}, P_{mi}). However, C_{org}, Fe_{cr}, and Al_{di} showed a considerably larger vertical than horizontal variation at this site. At both MIT and CON, all Fe compounds, Al_{mi} and Al_{ox} showed nearly the same $CV_{hor/ver}$. In contrast, at site CON we found small $CV_{hor/ver}$ for many P fractions due to a low horizontal variation.

3.3. Correlation analysis

Spearman's rank correlation analysis of P fractions with C_{org} and Fe and Al soil compounds predominantly revealed not more than four significant results (Table 3 and Table S3). Partial correlations for every fraction were calculated, but generally did not reach significance. In general, correlation coefficients were larger at sites CON and MIT, compared to LUE. Organic P fractions (P_{org} and $P_{pc.org}$) were strongly correlated with C_{org} and Fe_{pc} at all sites, whereas inorganic P fractions (P_{inorg} and $P_{pc.inorg}$) were predominantly correlated with mineral-bound Fe and Al, as well as crystalline and poorly crystalline Fe and Al oxides (Table 3). Inorganic and primary silicate mineral-bound P showed similar correlations for the entire soil profile at all sites. At CON, these P fractions were correlated the strongest with Al_{ox}, whereas at MIT stronger correlations were found with Ca_{tot}, Al_{mi}, and Fe_{mi}. At LUE, P_{mi} and P_{inorg} showed moderate correlations with Fe_{mi}. Compared to organic P, inorganic P content was largest at site CON, and highest at site MIT (Fig. 7).

In correlation analyses conducted for different soil depth increments, results often were not significant due to smaller sample numbers. In the upper profile (Fig. 1, Table 3), C_{org} was strongly correlated with organic P fractions (Table 3), and organic P showed larger shares of total P than inorganic P at all sites (Fig. 7). Similar percentages of P_{org} were found for sites CON and LUE, whereas at site MIT, P_{org} was distinctively larger than P_{inorg} (Fig. 7). Inorganic P fractions were correlated predominantly with crystalline and poorly crystalline Al oxides. At site MIT, P_{mi} strongly correlated with Fe_{mi} and moderately with Al_{mi}. Inorganic P and P bound in primary silicate minerals correlated moderately with Fe_{mi} and Al_{mi} at LUE, respectively.

As for the middle part of the soil profile at CON, important correlation variables for organic P were pedogenic Al minerals, C_{org}, and Fe_{pc}. Only the latter two compounds correlated strongly with organic P fractions at MIT. Inorganic P fractions were correlated with Ca_{tot} (CON and MIT) and mineral-bound Al and Fe (MIT and LUE). In the middle profile at site CON, P_{inorg} content was larger than P_{org} content, whereas P_{org} was markedly larger than P_{inorg} at MIT (Fig. 7). At this site, strong correlations of P_{inorg}, P_{mi}, and $P_{pc.inorg}$ with Al_{mi} and Ca_{tot} (also partly with Fe_{mi}) were found. At site LUE, P_{mi} and P_{inorg} correlated strongly with Fe_{mi} and Al_{mi} (Table 3), and inorganic P content was slightly smaller than P_{org} content (Fig. 7).

In the lower profile, the relevance of C_{org} as correlation variable often diminished. In contrast, crystalline and poorly crystalline Fe and Al oxides showed stronger correlations with both organic and inorganic P fractions. At site CON, pedogenic Al minerals correlated strongly with P_{pc} and $P_{pc.inorg}$ (Table 3), and inorganic P was as large as in the middle profile (Fig. 7). Especially Al_{mi} was strongly correlated with P_{mi} and P_{inorg} at site MIT, whereas $P_{pc.org}$ correlated strongly (P_{pc} moderately) with pedogenic Al minerals, C_{org}, and Fe_{pc}. Organic P content was smallest compared to the upper and middle profile, however larger than in at the other sites (Fig. 7). At LUE, P_{org} and P_{cr} showed the strongest correlations with Fe_{cr} (Table 3). In addition, Ca_{tot} correlated moderately with $P_{pc.org}$ and P_{pc}.

3.4. Factor analysis

If a variable loaded highly in a factor (minimum absolute value: 0.70), we assumed that the variable strongly affected this factor. At site CON, the first factor (FA) had high positive loadings of C_{org}, Fe_{pc}, Al_{di}, Al_{ox}, P_{org}, P_{pc}, and $P_{pc.org}$ and negative loadings of depth, Fe_{mi}, and Al_{mi} (Table 4). It thus can be termed *topsoil P bound in SOM-pedogenic minerals complexes*. The second factor was loaded highly with P_{inorg}, $P_{pc.inorg}$ and negatively with P_{cr} and can be termed *inorganic P*. At MIT a similar result was found: (i) FA 1 had high positive loadings of C_{org}, Fe_{pc}, P_{org}, P_{pc}, and $P_{pc.org}$ and negative loadings of depth, Fe_{mi}, and $P_{pc.inorg}$. It thus can be termed *topsoil P bound in SOM-pedogenic Fe minerals complex*, (ii) inorganic P and P_{mi} loaded highly in FA 2, which again can be termed *inorganic P*, (iii) FA 3 had a high loading of only Al_{ox} and thus can be termed *poorly crystalline pedogenic Al minerals*. In contrast to the other soils, at LUE Al and Fe oxyhydroxides and SOM loaded on independent factors. Factor 1, explaining most variance, had high loadings of Fe_{cr}, Al_{mi}, Al_{di}, and Al_{ox} and thus can be termed *crystalline pedogenic Fe and Al minerals*. The second FA had a high positive loading of C_{org} (negative loading of depth) and thus can be termed *topsoil SOM*. Only P_{pc} and $P_{pc.org}$ highly loaded on the third FA, which is why this factor was termed *adsorbed organic P*. The last factor (FA 4) can be termed *P bound in primary silicate minerals* due to the

Table 3
Spearman's rank correlation coefficients of different P fractions in the entire soil profile and different soil compartments at the study sites Conventwald (CON), Mitterfels (MIT), and Lüss (LUE). Fractions are total P (P_{tot}), organic P (P_{org}), P bound in primary silicate minerals (P_{mi}), inorganic P (P_{inorg}), P bound by crystalline (P_{cr}) and poorly crystalline (P_{pc}) pedogenic Al/Fe minerals, and organic and inorganic P bound by poorly crystalline pedogenic Al/Fe minerals ($P_{pc.org}$, $P_{pc.inorg}$). These were correlated with organic C (C_{org}), total Ca (Ca_{tot}), Fe in primary silicate minerals (Fe_{mi}), Fe in crystalline pedogenic minerals (Fe_{cr}), and in poorly crystalline pedogenic minerals (Fe_{pc}), Al in primary silicate minerals (Al_{mi}), and dithionite-citrate-extractable, and oxalate-extractable Al (Al_{di}, Al_{ox}) and ordered by correlation coefficient size. Significance was assumed at *p*-values smaller than 0.05. Only the largest four values are shown; all values can be found in the Supporting Information (Table S3).

	Entire soil profile			Upper profile (0–25 cm)			Middle profile (25–55 cm)			Lower profile (> 55 cm)		
Variable	CON	MIT	LUE	CON	MIT	LUE	CON	MIT	LUE	CON	MIT	LUE
P_{tot}	C_{org} 0.93	C_{org} 0.73	Al_{ox} 0.51	C_{org} 0.95	ns	C_{org} 0.78	Fe_{pc} 0.69	C_{org} 0.70	Al_{mi} 0.83	Al_{di} 0.57	Al_{mi} 0.68	Fe_{cr} 0.56
	Fe_{pc} 0.89	Fe_{pc} 0.58	Fe_{pc} 0.51	Fe_{pc} 0.59	ns	Al_{ox} 0.74	C_{org} 0.65	Al_{mi} 0.45	Fe_{mi} 0.72	Al_{ox} 0.56	Ca_{tot} 0.64	ns
	Al_{di} 0.88	Al_{di} 0.39	Al_{di} 0.46	ns	ns	Al_{di} 0.62	Al_{di} 0.64	ns	ns	ns	C_{org} 0.58	ns
	Al_{ox} 0.70	Fe_{cr} 0.29	Fe_{mi} 0.44	ns	ns	Fe_{pc} 0.55	Al_{ox} 0.61	ns	ns	ns	ns	ns
P_{org}	C_{org} 0.94	C_{org} 0.77	Al_{ox} 0.50	C_{org} 0.88	ns	C_{org} 0.86	C_{org} 0.77	Fe_{pc} 0.68	Fe_{cr} 0.49	ns	C_{org} 0.55	Fe_{cr} 0.58
	Fe_{pc} 0.90	Fe_{pc} 0.73	Fe_{pc} 0.50	Fe_{pc} 0.66	ns	Al_{ox} 0.72	Al_{di} 0.75	C_{org} 0.62	ns	ns	ns	ns
	Al_{di} 0.86	Al_{di} 0.43	Al_{di} 0.48	ns	ns	Al_{di} 0.57	Fe_{pc} 0.68	ns	ns	ns	ns	ns
	Al_{ox} 0.62	ns	C_{org} 0.42	ns	ns	Fe_{pc} 0.43	Al_{ox} 0.66	ns	ns	ns	ns	ns
P_{mi}	Al_{ox} 0.66	Ca_{tot} 0.69	Fe_{mi} 0.53	C_{org} 0.52	Fe_{mi} 0.73	Fe_{mi} 0.54	Al_{ox} 0.44	Al_{mi} 0.82	Fe_{mi} 0.83	Al_{ox} 0.57	Al_{mi} 0.66	ns
	C_{org} 0.54	Al_{mi} 0.60	Al_{mi} 0.39	ns	Al_{mi} 0.51	ns	ns	Fe_{mi} 0.68	Al_{mi} 0.71	C_{org} 0.56	Ca_{tot} 0.59	ns
	Al_{di} 0.53	Fe_{mi} 0.50	Al_{ox} 0.24	ns	ns	ns	ns	Ca_{tot} 0.64	ns	Fe_{pc} 0.56	C_{org} 0.51	ns
	Fe_{pc} 0.47	Al_{ox} 0.46	ns	ns	ns	ns	ns	ns	ns	ns	ns	ns
P_{inorg}	Al_{ox} 0.51	Al_{mi} 0.62	Fe_{mi} 0.50	ns	ns	Al_{mi} 0.49	ns	Al_{mi} 0.75	Fe_{mi} 0.83	Al_{di} 0.58	Al_{mi} 0.71	Al_{ox} 0.41
	Al_{di} 0.32	Ca_{tot} 0.59	Al_{mi} 0.36	ns	ns	ns	ns	Ca_{tot} 0.73	Al_{mi} 0.70	ns	Fe_{mi} 0.50	ns
	C_{org} 0.26	Fe_{mi} 0.45	ns	ns	ns	ns	ns	ns	ns	ns	ns	ns
	Fe_{pc} 0.26	ns	ns	ns	ns	ns	ns	ns	ns	ns	ns	ns
P_{cr}	C_{org} 0.38	C_{org} 0.74	C_{org} 0.36	C_{org} 0.72	C_{org} 0.63	Al_{di} 0.43	Fe_{cr} 0.45	C_{org} 0.66	ns	ns	Fe_{mi} 0.37	Fe_{cr} 0.61
	Fe_{pc} 0.36	Fe_{pc} 0.71	Fe_{pc} 0.31	Fe_{pc} 0.62	Fe_{cr} 0.56	ns	ns	Fe_{pc} 0.50	ns	ns	ns	Al_{di} 0.43
	Al_{di} 0.28	Fe_{cr} 0.49	ns	ns	ns	ns	ns	ns	ns	ns	ns	ns
	ns	ns	ns	ns	ns	ns	ns	ns	ns	ns	ns	ns
P_{pc}	C_{org} 0.92	C_{org} 0.73	C_{org} 0.39	C_{org} 0.93	Fe_{pc} 0.60	C_{org} 0.85	Al_{ox} 0.71	Al_{ox} 0.54	ns	Al_{ox} 0.91	Al_{di} 0.56	Al_{di} 0.41
	Fe_{pc} 0.90	Fe_{pc} 0.71	Fe_{pc} 0.36	Fe_{pc} 0.67	C_{org} 0.57	Al_{ox} 0.65	C_{org} 0.66	Fe_{pc} 0.53	ns	Al_{di} 0.83	C_{org} 0.50	Ca_{tot} 0.41
	Al_{di} 0.88	Al_{di} 0.30	Ca_{tot} 0.36	Al_{di} 0.42	ns	Al_{di} 0.45	Fe_{pc} 0.64	ns	ns	C_{org} 0.57	Al_{ox} 0.42	ns
	Al_{ox} 0.74	ns	Al_{ox} 0.32	ns	ns	ns	Al_{di} 0.59	ns	ns	Fe_{pc} 0.53	Fe_{pc} 0.40	ns
$P_{pc.org}$	C_{org} 0.97	Fe_{pc} 0.93	C_{org} 0.36	C_{org} 0.94	Fe_{pc} 0.61	C_{org} 0.82	C_{org} 0.85	Fe_{pc} 0.95	ns	Al_{ox} 0.60	Al_{di} 0.71	Ca_{tot} 0.51
	Fe_{pc} 0.92	C_{org} 0.90	Ca_{tot} 0.33	Fe_{pc} 0.70	C_{org} 0.54	Al_{ox} 0.64	Al_{ox} 0.78	C_{org} 0.74	ns	C_{org} 0.54	Fe_{pc} 0.71	ns
	Al_{di} 0.90	Fe_{cr} 0.32	Fe_{pc} 0.31	ns	ns	Al_{di} 0.46	Al_{di} 0.77	ns	ns	ns	C_{org} 0.65	ns
	Al_{ox} 0.69	Al_{di} 0.29	Al_{ox} 0.26	ns	ns	ns	Fe_{pc} 0.65	ns	ns	ns	Al_{ox} 0.64	ns
$P_{pc.inorg}$	Al_{mi} 0.59	Al_{mi} 0.81	C_{org} 0.32	Al_{ox} 0.57	ns	C_{org} 0.65	Ca_{tot} 0.54	Ca_{tot} 0.70	ns	Al_{ox} 0.85	ns	ns
	Fe_{mi} 0.41	Fe_{mi} 0.74	ns	Al_{di} 0.44	ns	Al_{ox} 0.43	ns	Al_{mi} 0.67	ns	Al_{di} 0.82	ns	ns
	Ca_{tot} 0.41	Ca_{tot} 0.56	ns	ns	ns	ns	ns	Fe_{mi} 0.46	ns	ns	ns	ns
	ns	Al_{ox} 0.38	ns	ns	ns	ns	ns	ns	ns	ns	ns	ns

ns: not significant.

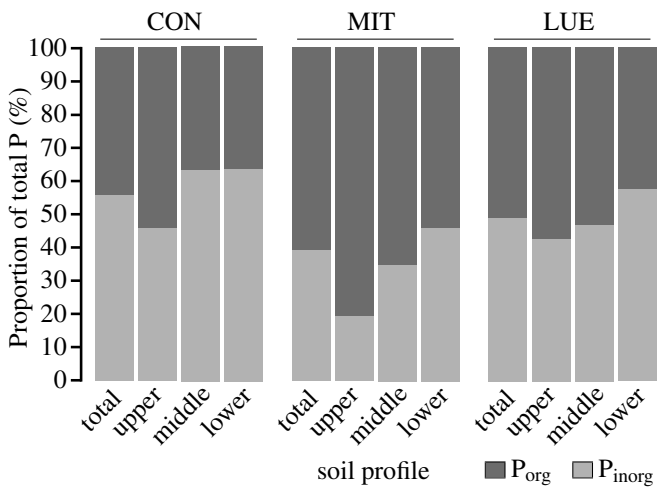

Fig. 7. Organic and inorganic phosphorus (P_{org} and P_{inorg}) as proportion or total P (in %) in different soil profile compartments at the study sites Conventwald (CON), Mitterfels (MIT), and Lüss (LUE). The soil was divided into four regions: total soil profile, upper profile (0–25 cm depth), middle profile (> 25–55 cm depth), and lower profile (> 55 cm depth). Values are provided in Table S1.

corresponding high loading of the variable P_{mi}.

4. Discussion

4.1. Compounds which determine the small-scale spatial patterns of P fractions at the profile scale

In our study, SOM, represented as C_{org}, was an important correlation variable for organic P and adsorbed P fractions (P_{cr}, P_{pc}; Table 3), and the interpolated maps of P_{tot}/P_{org} and C_{org} (Figs. 2 and 4) also show a striking similarity, especially in the topsoil, of the respective distributions of P and SOM. In addition, poorly crystalline pedogenic Fe minerals and pedogenic Al minerals (Fe_{pc}, Al_{di}, Al_{ox}) were predominantly correlated with organic P fractions, in particular in the middle and lower profile (Table 3). It has often been reported that Al and Fe oxyhydroxides have a high capacity to adsorb P_{org} (e.g., Celi et al., 1999; Yan et al., 2014), as well as P_{inorg} species (e.g., Parfitt, 1989; Violante and Pigna, 2002). Organic P predominantly accumulates as inositol phosphates (phytates) in the topsoil due to P inputs from shoot and root litter, root and microbial exudates, whereas more active forms of organic P are translocated as dissolved organic P (DOP) (Bol et al., 2016). We assume that predominantly P-bearing SOM, such as phytate, competes for adsorption sites on Al and Fe oxyhydroxides, because humic substances in soils generally have limited influence on the phosphate adsorption by synthetic Al and Fe oxides (Borggaard et al., 2005), whereas phytate is retained in higher amounts than P_{inorg} by goethite, illite and kaolinite (Celi et al., 1999). In accordance with our

Table 4
Factor loadings of predictor variables at the study sites Conventwald (CON), Mitterfels (MIT), and Lüss (LUE). Predictor variables were depth, contents of organic C (C_{org}), total Ca (Ca_{tot}), Fe in primary silicate minerals (Fe_{mi}), Fe in crystalline pedogenic minerals (Fe_{cr}), and in poorly crystalline pedogenic minerals (Fe_{pc}), Al in primary silicate minerals (Al_{mi}), and dithionite-citrate-extractable, and oxalate-extractable Al (Al_{di}, Al_{ox}), total P (P_{tot}), organic P (P_{org}), P bound in primary silicate minerals (P_{mi}), inorganic P (P_{inorg}), P bound by crystalline (P_{cr}) and poorly crystalline (P_{pc}) pedogenic Al/Fe minerals, and organic and inorganic P bound by poorly crystalline pedogenic Al/Fe minerals ($P_{pc.org}$, $P_{pc.inorg}$). Factor loadings with an absolute value of 0.7 and larger are printed in bold.

	CON		MIT			LUE			
Contribution to total variance (%)	77	23	62	25	13	35	23	22	20
Factor (FA)	FA 1	FA 2	FA 1	FA 2	FA 3	FA 1	FA 2	FA3	FA4
Variables									
Depth	− 0.96	0.14	− 0.91	0.28	− 0.05	0.32	− 0.86	− 0.13	0.23
C_{org}	0.98	− 0.12	0.93	− 0.02	− 0.10	− 0.03	0.92	0.28	− 0.27
Ca_{tot}	− 0.66	0.30	− 0.26	0.61	0.48	0.35	0.66	0.19	0.18
Fe_{mi}	− 0.83	0.33	− 0.79	0.43	− 0.11	0.46	− 0.03	− 0.02	0.63
Fe_{cr}	− 0.57	− 0.22	0.38	0.04	− 0.15	0.87	− 0.07	− 0.03	− 0.02
Fe_{pc}	0.94	− 0.11	0.92	− 0.24	0.15	0.51	0.62	0.23	− 0.05
Al_{mi}	− 0.65	0.61	− 0.69	0.65	− 0.03	0.79	− 0.10	0.05	0.41
Al_{di}	0.93	− 0.01	0.65	0.04	0.53	0.93	0.13	0.14	0.03
Al_{ox}	0.74	0.41	0.07	0.13	0.94	0.81	0.14	0.26	0.13
P_{tot}	0.97	0.07	0.87	0.53	− 0.08	0.46	0.32	0.45	0.24
P_{org}	0.94	− 0.18	0.73	− 0.45	− 0.14	0.43	0.24	0.60	− 0.23
P_{mi}	0.60	0.66	0.03	0.88	0.06	0.06	− 0.07	0.25	0.87
P_{inorg}	0.35	0.70	− 0.11	0.84	0.08	0.26	0.09	− 0.08	0.54
P_{cr}	0.26	− 0.80	0.63	− 0.17	− 0.38	0.24	0.31	− 0.10	− 0.56
P_{pc}	0.96	0.09	0.82	0.04	0.23	0.10	0.15	0.96	0.02
$P_{pc.org}$	0.98	− 0.10	0.95	− 0.15	0.14	0.02	0.16	0.84	0.13
$P_{pc.inorg}$	− 0.29	0.77	− 0.76	0.36	0.03	0.01	0.17	0.29	− 0.38

findings, a positive relationship between the respective contents of NaOH-EDTA extractable Al, Fe and inositol phosphates was reported for soils by Vincent et al. (2012) in a study of boreal forest soils in Sweden. Therefore, at sites CON and MIT, our results indicate that adsorption of P_{inorg} was negligible, probably due to competing adsorption of P_{org}.

Violante and Pigna (2002) reported that clay minerals (montmorillonite, kaolinite, nontronite, illite, smectite) sorb less phosphate than poorly crystalline metal oxides, allophane, mixed Fe–Al gels, organo-mineral complexes, goethite, and gibbsite, because of the greater surface areas of the latter compounds. However, Al-coverage of clay minerals can strongly intensify P retention (Shang et al., 1996). The P bound by Al-saturated expandable clay minerals is included in the fraction of oxalate-extractable P (P_{pc}) because oxalate forms strong complexes with Al (Bhatti et al., 1998). In addition, clay minerals mainly exert their influence on P retention by Al and Fe ions bound to the silicate surfaces rather than by the phyllosilicate lattice itself (Arai and Sparks, 2007; Violante and Pigna, 2002). Therefore, the type of clay, as well as the surface charging of clay minerals present in a soil, affect the surface coverage by Al and Fe cations and thus influence the amount of P bound in the poorly crystalline pedogenic Fe and Al mineral fractions (Fe_{pc}, Al_{ox}). In addition, especially Fe and Al oxyhydroxides occur in the colloidal size fraction (1–500 nm), resulting in a greater importance for P translocation compared to clay minerals (Bol et al., 2016). On the other hand, organic P (especially phytate) is strongly retained in soils by adsorption to clays, and by complexation, or as precipitate with pedogenic minerals due to their high charge density, as reported by Condron et al. (2005). Therefore, we assume that some P is retained by clay minerals in the studied soils, especially at site CON, which showed a loamy soil texture (Table S2) and is characterized by high correlations of P_{inorg} and P_{org} with Al_{ox} ($\rho = 0.51$ and 0.62, respectively; Table 3).

Originally, P is released from primary minerals, predominantly by dissolution of apatite (Walker and Syers, 1976). However, it can be preserved in small amounts as inclusion, e.g. in slowly weathering silicates (Syers et al., 1967). At sites CON and MIT, we named the second best factors describing the covariance of the soil variables (Table 4) as *inorganic P* due to their high loadings in these variables. In addition, at all sites correlations of predominantly inorganic P fractions with contents of Al_{mi} and Fe_{mi} were noticed, especially high at MIT and LUE (Table 3). This indicates that, even at later stages of podzolization, the remaining unweathered primary rock bears some inorganic P forms. During podzolization, adsorbed P_{inorg} can be desorbed through displacement of other soil solution anions (Bhatti et al., 1998; Violante and Pigna, 2002). The spatial pattern of $P_{pc.inorg}$ at CON and MIT illustrates this desorption during early and intermediate stages of podzolization (Fig. 2): Easily available orthophosphate ($P_{pc.inorg}$) showed maxima in the upper (CON) and the lower profile (MIT).

While the vertical, i.e. depth, distribution of soil properties is typically studied by core sampling (e.g., Eriksson et al., 2015; Ferro Vázquez et al., 2014), it is commonly assumed that horizontal, i.e. lateral, variability of soil properties is low. However, assessing both the horizontal and vertical small-scale variability is important when: i) locating zones of relative enrichment and depletion of e.g. P_{tot} and P_{org} (Fig. 2), ii) investigating total P, different P fractions and major P-bearing soil compounds at the profile scale (Tables 2–4, Fig. 2–6), and iii) studying soil parameters to derive information about soil processes that endure decades or even centuries. We assume that P enrichment zones as identified in our soils as SOM-bound P, Fe and Al oxyhydroxide-bound P, clay-bound P, and P in unweathered parent material for the different soils in our study indicate zones with potentially high P uptake. It is known that plant rooting patterns (Jackson and Caldwell, 1993) and mycorrhizal symbiosis (Facelli and Facelli, 2002) are affected by a heterogeneous soil P distribution. Therefore, we argue that the different mechanisms governing small-scale P distribution are affecting P acquisition strategies of plants and soil microorganisms in temperate forest ecosystems with siliceous parent material.

4.2. Effects of podzolization on spatial patterns of P fractions at the profile scale

The soils from our sites showed different stages of podzolization. A rather early stage was found at CON, a hill-side soil formed from regolith with many rock outcrops (Prietzel et al., 2016). In this soil, significant amounts of pedogenic Al minerals have already been mobilized from the topsoil and translocated downwards. However, their contents were still high in the upper profile, and Fe in poorly crystalline pedogenic minerals still showed the highest contents in the uppermost topsoil (Fig. 3). In addition, SOM contents decreased gradually from the topsoil to a depth of 20 cm (Fig. 3), and $CV_{hor/ver}$ values were often small (Table 2), depicting larger vertical than

horizontal variation. It is well known that these patterns indicate initial podzolization, which is characterized by mobilization of Al, either complexed by dissolved organic acids or as Al−Si hydroxy sols (Lundström et al., 2000). The contents of P_{org} and $P_{pc.org}$ were predominantly correlated with SOM, Fe_{pc} and Al_{di} (Table 3) and we combined these compounds as the factor *topsoil P bound in SOM-pedogenic minerals complexes*. This is backed by speciation results based on P *K*-edge XANES spectra of Prietzel et al. (2016) who assigned about 40% of total soil P to unbound organic P and about 60% to adsorbed mineral phases in the CON topsoil. In the middle profile at site CON, our results showed that pedogenic Al minerals and poorly crystalline pedogenic Fe minerals had increased importance for P retention, probably due to adsorption of P-rich SOM and P_{inorg} onto Al and Fe oxyhydroxides and Al- and/or Fe-covered clays. In addition, ongoing Al and Fe mobilization from primary parent material was detected in our study, as visible in the distribution of Al_{mi} and Fe_{mi}, both showing content maxima at depths of 40–70 cm (Fig. 3). Enrichment zones of P_{mi}, P_{inorg} and $P_{pc.inorg}$ were also found at these depths (40–50 cm, Fig. 2). These P fractions also loaded highly in one factor in which Al_{mi} also contributed moderately, as revealed by factor analysis (Table 4). We explain this result by the formation of crystalline $AlPO_4$ which has formed secondarily after weathering of primary apatites (Lichter, 1998). This is again backed by Prietzel et al. (2016) who reported that 17–25% of total P is bound as crystalline $AlPO_4$ in the subsoil, and 65% of total bedrock P is bound as crystalline $AlPO_4$.

Compared to CON, the Cambisol at site MIT is characterized by more advanced podzolization. This is visible by bleached sand grains in the topsoil (Nechic subqualifier), and analytically detected by the distribution of pedogenic Al minerals in the profile, showing advanced dissolution of Al oxyhydroxides in the topsoil compared to CON (Fig. 3). However, poorly crystalline pedogenic Fe minerals were still stable in the topsoil. At this intermediate stage of podzolization, the distribution patterns of many P fractions are characterized by a comparably homogeneous distribution, indicated also by the CV analysis (Table 2). At MIT, concentrations of P_{inorg} and especially $P_{pc.inorg}$ gradually increased from the top- to the subsoil. Calcium phosphate minerals were detected in the MIT bedrock by Prietzel et al. (2016), contributing about two third of total bedrock P. The remaining portion was identified as crystalline $AlPO_4$ (Prietzel et al., 2016). They explained the latter percentage by tertiary regolith formation which was associated with profound transformation of apatite into $AlPO_4$ already at depths below 15 m (Prietzel et al., 2016). However, the hill-top MIT soil lacks the rock outcrops that retarded podzolization of the hill-side CON soil, although both soils have formed from regolith (Prietzel et al., 2016). Factor and correlation analysis results (Tables 4 and 3) both indicate that P_{inorg} and P_{mi} in the MIT soil are predominantly bound by Ca and/or secondarily formed crystalline $AlPO_4$. However, we do not assume apatite to still be present in this soil due to the low soil pH that leads to rapid dissolution of apatite (Lichter, 1998). The MIT soil showed this low pH also as a product of former large industrial, atmospheric S deposition (Erkenberg et al., 1996) and ongoing large N deposition. In our study, we found the highest contents of Al_{di} and Al_{ox} in the middle profile at site MIT which indicates an ongoing dissolution of pedogenic Al minerals (Fig. 3). As a result, many P fractions showed low total and vertical variability (Table 2) due to their dislocation in the profile after pedogenic Al minerals had been dissolved. This is in accordance with results of SanClements et al. (2010). They showed that the dominant chemical fraction of P in a study of six watersheds in the eastern United States and Europe of soils under temperate forests was (i) associated with secondary Al and organic phases and (ii) responsive to experimental acidification.

Podzolization was most pronounced at site LUE. Here, the sandy parent material did not provide abundant Al and Fe primary minerals whose weathering products (especially oxyhydroxides) can retain P. At LUE, small amounts of pedogenic as well as primary Al and Fe minerals were enriched in a (proto-) spodic horizon below an eluvial horizon at depths below 10 cm. In this region, the contribution of poorly crystalline Fe was largest just below the eluvial horizon, whereas Fe_{cr}, Al_{ox} and Al_{di} showed highest contents at greater depth (Fig. 3). It is known that (i) SOM (organic acids) and Al as well as Fe ions form strong, water-soluble complexes (Sauer et al., 2007), and that (ii) Fe-SOM complexes are less soluble and thus precipitate earlier than Al-SOM complexes (Ferro Vázquez et al., 2014). Kaiser (2001) showed that DOP is enriched in the mobile hydrophilic fraction in subsoils of five acidic forest sites in Germany and highlighted that subsoils can effectively retain dissolved organic matter and thus DOP. We therefore attribute the P enrichment in the middle profile of site LUE to the illuviation and retention of P-rich SOM which was dislocated from the upper and retained in the middle and lower profile by adsorption to first mainly pedogenic Fe- (15–50 cm depth, Fig. 1), and at greater depth also to pedogenic Al minerals (30–50 cm depth, Fig. 1). Nonetheless, organic P also accumulated together with SOM in the topsoil and resulted in a significant increase of variability (Table 2). We detected high contents of many P fractions in the uppermost LUE topsoil (Fig. 2). This is in accordance with Vincent et al. (2010) who emphasized the importance of microbial litter and topsoil P_{org} mineralization for plant nutrition in P-deficient humus soils stocked with boreal forest. With increasing soil depth, Achat et al. (2009) suggested an increasing importance of diffusive P (ionic P species transported into the soil solution due to a gradient of concentration) in a temperate forest soil study. We also found highly distributed inorganic P (Fig. 2), which resulted not only in large vertical, but also in large horizontal variability of inorganic P fractions (Table 2). Additionally, we found intermediate correlations of P_{inorg} and P_{mi} with Al_{mi} and Fe_{mi}, but not with Al_{di} or Fe_{cr}, in the upper and middle profile (Table 3), indicating that some inorganic P is still present in primary Al and Fe minerals even in the strongly acidified LUE soil.

4.3. Conceptual model of P distribution changes during podzolization

In a recent publication, Lang et al. (2016) introduced a succession model of forest ecosystem nutrition – in which all our study sites are included – based on the P status of the soils. They discriminated P-acquiring systems, in which plants and microbes obtain predominantly abundant, mineral-bound P, and P-recycling systems, where mainly mineralized P ("recycled P" or "biocycled P") sustains a poor, but sufficient P supply. At our study sites, the soil P content (Table 1) did not reflect the degree of podzolization. Although it was not possible to perform formal statistics comparing the soil P status of the study sites due to just sampling one profile per site, we argue that the small-scale P distribution is affecting P acquisition strategies of plants and soil microorganisms in our soils. Based on the information presented previously, we suggest a conceptual model of relationships between the stage of podzolization as identified by the distribution of pedogenic Al and Fe minerals in a soil profile and the distribution of different P forms and important P fluxes as derived from our results (Fig. 8). Undoubtedly, investigating more profiles per site would have made our conceptual model more robust. However, our results are in accordance with numerous field studies of soil profiles with different degree of podzolization (e.g., Ilg et al., 2009; SanClements et al., 2010; Vincent et al., 2012). Decades ago, Walker and Syers (1976) introduced a model describing trends of soil P amounts and forms with time: Ca-bound P rapidly decreases while P still is retained in the soil either as organic, occluded, or non-occluded P. After about 22.000 years of soil development, a small fraction of the initial soil P is stored organically or occluded in Al/Fe oxyhydroxides (Walker and Syers, 1976). The conceptual model presented here refines the model of Walker and Syers (1976) by visualizing the zonation of P pools in acidic temperate soils on siliceous parent material. Moreover, it expands the work of Lang et al. (2016) by a geochemical description of the spatial distribution of P in soils during podzolization.

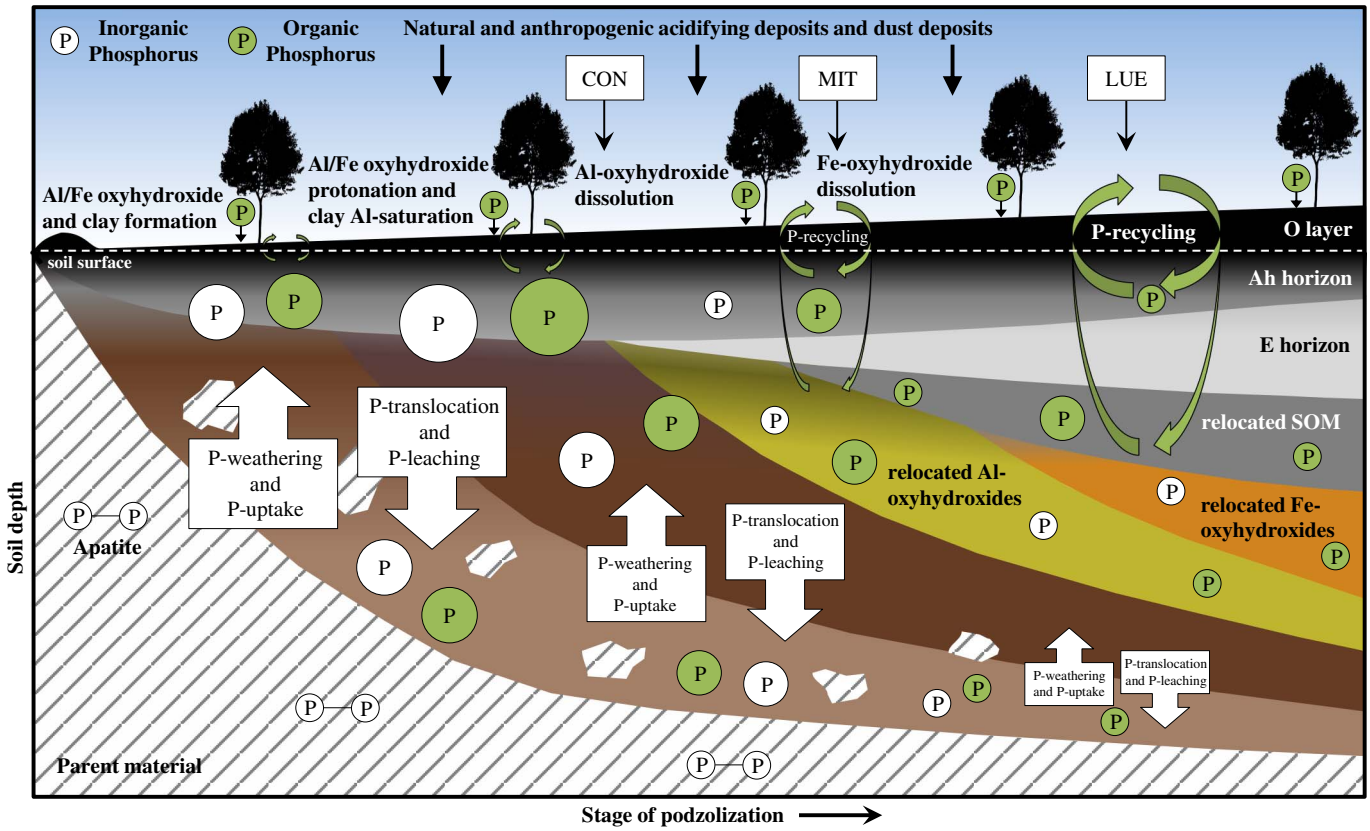

Fig. 8. Conceptual model of phosphorus (P) distribution patterns during podzolization in soils of temperate ecosystems with siliceous parent material. The studied sites Conventwald (CON), Mitterfels (MIT), and Lüss (LUE) show early, intermediate and advanced podzolization, respectively.

In accordance with Lang et al. (2016) we argue that during initial stages of podzolization P is taken up by plants and microbes after weathering of apatite and other primary P-bearing minerals. Hereby, ectomycorrhizal fungi, which are known to be associated with beech trees (Schirkonyer et al., 2013; Taylor et al., 2000), can promote apatite weathering (Blum et al., 2002). Initial soil acidification results in increased contents of plant-available P (Ohno and Amirbahman, 2010) and induces oxyhydroxide protonation and saturation of SOM and clay cation exchange sites with Al^{3+}, which in turn leads to increased P retention in the topsoil. Prevailing P immobilization is also indicated by a large C:P ratio at the CON upper profile (Fig. 4). Abundant, biocycled P is retained by newly formed pedogenic oxyhydroxides in the mineral topsoil (Fig. 7), but also leaches in colloids and/or as DOP through the soil, as described by Missong et al. (2016) for site CON. The narrow C:P ratio at depths > 40 cm supports this claim (Fig. 4). In addition, the hillslope at CON probably promotes P losses because P transport is often linked to fast lateral flows (Bol et al., 2016).

Progressive soil acidification results in topsoil dissolution of Al oxyhydroxides, clay mineral destruction, and mobilization of Al-bound P, characterizing intermediate stages of podzolization (Figs. 7 and 8). Phosphorus bound by these compounds is dislocated, resulting, e.g. at site MIT, in (i) decreasing vertical variation of C_{org} and P_{tot} (Table 2), (ii) the presence of a secondary maximum of $P_{pc.org}$ at about 30 cm depth (Fig. 2), and (iii) the homogenous distribution of the C:P ratio (Fig. 4). However, SOM in general, and thereby P_{org}, is protected against mineralization by microorganisms when adsorbed to minerals, as recently reviewed by Han et al. (2016), or protected in the interior of soil aggregates (Lützow et al., 2006). Thus, P availability in this stage of podzolization is controlled by desorption from, and by dissolution or mobilization of binding partners (Haygarth et al., 2005), i.e. SOM, clay-bound Fe and Al, Al and Fe oxyhydroxides, and SOM-Al/Fe oxyhydroxide complexes. Nonetheless, ongoing leaching of colloidal P and DOP, as well as high P losses during heavy rainfall events, are supposed to lead to increased topsoil P depletion (Bol et al., 2016).

At later stages of podzolization, also Fe oxyhydroxides are dissolved, inducing further decrease in topsoil P sorption (Zhang et al., 2010). Phosphorus fractions are distributed with large horizontal and vertical variability (Table 2), leading to patches with P accumulation by SOM enrichment in the topsoil and by Al- and Fe-P_{org} complexes in the illuvial horizons, where highly stable SOM-Al/Fe oxyhydroxide complexes still retain P (Figs. 7 and 8). Atmospheric dust deposition, as e.g. desert dust (Okin et al., 2004) or from anthropogenic combustion emissions (Wang et al., 2014), is then supposed to be an important source of unrecycled P and therefore probably of greater importance for P nutrition than at earlier stages of podzolization. In our study, P_{org} accumulated in the illuvial horizon more pronouncedly than C_{org} which indicates that the SOM in intermediate soil depths gets enriched in P during podzolization (Figs. 2 and 3). This enrichment is also indicated by the change in C:P ratio at a depth of 40–50 cm at LUE (Fig. 4).

4.4. Conclusions

Our work reveals the importance of assessing the small-scale vertical and horizontal soil variability to accurately investigate soil processes in general and particularly spatial P distribution in temperate forest soils formed from siliceous parent material. For our sites, we found a gradient of increasing stage of podzolization (CON < MIT < LUE) as indicated by the distribution of pedogenic Al and Fe minerals in the soil profiles. Predominantly, spatial patterns of SOM and pedogenic Al and Fe oxyhydroxides contents determined the spatial patterns of organic P and different P fractions at the profile scale. We assume that different P distribution patterns and availabilities induce different plant and microbial strategies to sustain P nutrition. Our identification and explanation of how P accumulates in the studied soils (both in depth and horizontally) has implications on plant and microbial studies in temperate forest ecosystems with soils formed from

siliceous parent material. However, sampling more than one profile per site would have been beneficial for more robust explanations. Additionally, other methods, as e.g. P isotope approaches, would be needed to adequately translate our results into an unambiguous identification of the key pools responsible for ecosystem P nutrition. Our methods focused on the spatial imaging of P fractions derived from acidic forest soils; thus, as next steps, we suggest studying calcareous and agricultural soils, and additionally including advanced techniques of P speciation (e.g. NMR, XANES spectroscopy).

Acknowledgements

We thank Sigrid Hiesch and Gertraud Harrington for their indispensable assistance in the laboratory work and the anonymous reviewers for their constructive comments. This work was supported by the German Research Foundation (DFG), as part of the Priority Program SPP 1685, grant Pr 534/6-1.

Appendix A. Supplementary data

Supplementary data to this article can be found online at http://dx.doi.org/10.1016/j.geoderma.2017.04.026.

References

Achat, D.L., Bakker, M.R., Augusto, L., Saur, E., Dousseron, L., Morel, C., 2009. Evaluation of the phosphorus status of P-deficient podzols in temperate pine stands: combining isotopic dilution and extraction methods. Biogeochemistry 92 (3), 183–200. http://dx.doi.org/10.1007/s10533-008-9283-7.

Arai, Y., Sparks, D.L., 2007. Phosphate reaction dynamics in soils and soil components: a multiscale approach. In: Sparks, D.L. (Ed.), Advances in Agronomy. Academic Press, pp. 135–179.

Bhatti, J.S., Comerford, N.B., Johnston, C.T., 1998. Influence of oxalate and soil organic matter on sorption and desorption of phosphate onto a spodic horizon. Soil Sci. Soc. Am. J. 62 (4), 1089–1095. http://dx.doi.org/10.2136/sssaj1998.03615995006200040033x.

Blum, J.D., Klaue, A., Nezat, C.A., Driscoll, C.T., Johnson, C.E., Siccama, T.G., Eagar, C., Fahey, T.J., Likens, G.E., 2002. Mycorrhizal weathering of apatite as an important calcium source in base-poor forest ecosystems. Nature 417 (6890), 729–731. http://dx.doi.org/10.1038/nature00793.

Bol, R., Julich, D., Brödlin, D., Siemens, J., Kaiser, K., Dippold, M.A., Spielvogel, S., Zilla, T., Mewes, D., von Blanckenburg, F., Puhlmann, H., Holzmann, S., Weiler, M., Amelung, W., Lang, F., Kuzyakov, Y., Feger, K.-H., Gottselig, N., Klumpp, E., Missong, A., Winkelmann, C., Uhlig, D., Sohrt, J., von Wilpert, K., Wu, B., Hagedorn, F., 2016. Dissolved and colloidal phosphorus fluxes in forest ecosystems-an almost blind spot in ecosystem research. J. Plant Nutr. Soil Sci. 179 (4), 425–438. http://dx.doi.org/10.1002/jpln.201600079.

Borggaard, O.K., Raben-Lange, B., Gimsing, A.L., Strobel, B.W., 2005. Influence of humic substances on phosphate adsorption by aluminium and iron oxides. Geoderma 127 (3–4), 270–279. http://dx.doi.org/10.1016/j.geoderma.2004.12.011.

Cade-Menun, B.J., Liu, C.W., 2014. Solution phosphorus-31 nuclear magnetic resonance spectroscopy of soils from 2005 to 2013: a review of sample preparation and experimental parameters. Soil Sci. Soc. Am. J. 78 (1), 19–37. http://dx.doi.org/10.2136/sssaj2013.05.0187dgs.

Celi, L., Lamacchia, S., Marsan, F.A., Barberis, E., 1999. Interaction of inositol hexaphosphate on clays: adsorption and charging phenomena. Soil Sci. 164 (8), 574–585. http://dx.doi.org/10.1097/00010694-199908000-00005.

Condron, L.M., Turner, B.L., Cade-Menun, B.J., 2005. Chemistry and dynamics of soil organic phosphorus. In: Sims, J.T., Sharpley, A.N. (Eds.), Agronomy Monograph. American Society of Agronomy, Crop Science Society of America, and Soil Science Society of America, Madison, pp. 87–121.

Cressie, N.A.C., 2015. In: Cressie, N.A.C. (Ed.), Statistics for Spatial Data. John Wiley & Sons, Inc., Hoboken, NJ, USA, pp. 1–26.

Diggle, P.J., Ribeiro, P.J., 2002. Bayesian inference in Gaussian model-based geostatistics. Geogr. Environ. Model. 6 (2), 129–146. http://dx.doi.org/10.1080/1361593022000029467.

Elser, J.J., 2012. Phosphorus: a limiting nutrient for humanity? Curr. Opin. Biotechnol. 23 (6), 833–838. http://dx.doi.org/10.1016/j.copbio.2012.03.001.

Eriksson, A.K., Gustafsson, J.P., Hesterberg, D., 2015. Phosphorus speciation of clay fractions from long-term fertility experiments in Sweden. Geoderma 241, 68–74. http://dx.doi.org/10.1016/j.geoderma.2014.10.023.

Erkenberg, A., Prietzel, J., Rehfuess, K.-E., 1996. Schwefelausstattung ausgewählter europäischer Waldböden in Abhängigkeit vom atmogenen S-Eintrag. Z. Pflanzenernähr. Bodenkd. 159 (1), 101–109. http://dx.doi.org/10.1002/jpln.1996.3581590115.

Facelli, E., Facelli, J.M., 2002. Soil phosphorus heterogeneity and mycorrhizal symbiosis regulate plant intra-specific competition and size distribution. Oecologia 133 (1), 54–61. http://dx.doi.org/10.1007/s00442-002-1022-5.

Ferro Vázquez, C., Nóvoa Muñoz, J.C., Costa Casais, M., Klaminder, J., Martínez Cortizas, A., 2014. Metal and organic matter immobilization in temperate podzols: a high resolution study. Geoderma 217–218, 225–234. http://dx.doi.org/10.1016/j.geoderma.2013.10.006.

Gerke, J., Hermann, R., 1992. Adsorption of orthophosphate to humic-Fe-complexes and to amorphous Fe-oxide. Z. Pflanzenernähr. Bodenkd. 155 (3), 233–236. http://dx.doi.org/10.1002/jpln.19921550313.

Han, L., Sun, K., Jin, J., Xing, B., 2016. Some concepts of soil organic carbon characteristics and mineral interaction from a review of literature. Soil Biol. Biochem. 94, 107–121. http://dx.doi.org/10.1016/j.soilbio.2015.11.023.

Haygarth, P.M., Condron, L.M., Heathwaite, A.L., Turner, B.L., Harris, G.P., 2005. The phosphorus transfer continuum: linking source to impact with an interdisciplinary and multi-scaled approach. Sci. Total Environ. 344 (1–3), 5–14. http://dx.doi.org/10.1016/j.scitotenv.2005.02.001.

Hinsinger, P., 2001. Bioavailability of soil inorganic P in the rhizosphere as affected by root-induced chemical changes: a review. Plant Soil 237 (2), 173–195. http://dx.doi.org/10.1023/a:1013351617532.

Holmgren, G.G., 1967. A rapid citrate-dithionite extractable iron procedure. Soil Sci. Soc. Am. J. 31 (2), 210–211. http://dx.doi.org/10.2136/sssaj1967.03615995003100020020x.

Hornburg, V., Lüer, B., 1999. Vergleich zwischen Total- und königswasserextrahierbaren Elementgehalten in natürlichen Böden und Sedimenten. J. Plant Nutr. Soil Sci. 162 (2), 131–137. http://dx.doi.org/10.1002/(sici)1522-2624(199903)162:2<131::aid-jpln131>3.0.co;2-1.

Ilg, K., Wellbrock, N., Lux, W., 2009. Phosphorus supply and cycling at long-term forest monitoring sites in Germany. Eur. J. Forest Res. 128 (5), 483–492. http://dx.doi.org/10.1007/s10342-009-0297-z.

IUSS Working Group WRB, 2015. World Reference Base for Soil Resources 2014, Update 2015. International Soil Classification System for Naming Soils and Creating Legends for Soil Maps. FAO, Rome, pp. 106.

Jackson, R.B., Caldwell, M.M., 1993. Geostatistical patterns of soil heterogeneity around individual perennial plants. J. Ecol. 81 (4), 683–692. http://dx.doi.org/10.2307/2261666.

John, M.K., 1970. Colorimetric determination of phosphorus in soil and plant materials with ascorbic acid. Soil Sci. 109 (4), 214–220. http://dx.doi.org/10.1097/00010694-197004000-00002.

Jonard, M., Fürst, A., Verstraeten, A., Thimonier, A., Timmermann, V., Potočić, N., Waldner, P., Benham, S., Hansen, K., Merilä, P., Ponette, Q., de la Cruz, A.C., Roskams, P., Nicolas, M., Croisé, L., Ingerslev, M., Matteucci, G., Decinti, B., Bascietto, M., Rautio, P., 2015. Tree mineral nutrition is deteriorating in Europe. Glob. Chang. Biol. 21 (1), 418–430. http://dx.doi.org/10.1111/gcb.12657.

Kaiser, K., 2001. Dissolved organic phosphorus and sulphur as influenced by sorptive interactions with mineral subsoil horizons. Eur. J. Soil Sci. 52 (3), 489–493. http://dx.doi.org/10.1046/j.1365-2389.2001.00396.x.

Kruse, J., Abraham, M., Amelung, W., Baum, C., Bol, R., Kühn, O., Lewandowski, H., Niederberger, J., Oelmann, Y., Rüger, C., Santner, J., Siebers, M., Siebers, N., Spohn, M., Vestergren, J., Vogts, A., Leinweber, P., 2015. Innovative methods in soil phosphorus research: a review. J. Plant Nutr. Soil Sci. 178 (1), 43–88. http://dx.doi.org/10.1002/jpln.201400327.

Laliberté, E., Turner, B.L., Costes, T., Pearse, S.J., Wyrwoll, K.H., Zemunik, G., Lambers, H., 2012. Experimental assessment of nutrient limitation along a 2-million-year dune chronosequence in the south-western Australia biodiversity hotspot. J. Ecol. 100 (3), 631–642. http://dx.doi.org/10.1111/j.1365-2745.2012.01962.x.

Lang, F., Bauhus, J., Frossard, E., George, E., Kaiser, K., Kaupenjohann, M., Krüger, J., Matzner, E., Polle, A., Prietzel, J., Rennenberg, H., Wellbrock, N., 2016. Phosphorus in forest ecosystems: new insights from an ecosystem nutrition perspective. J. Plant Nutr. Soil Sci. 179 (2), 129–135. http://dx.doi.org/10.1002/jpln.201500541.

Lichter, J., 1998. Rates of weathering and chemical depletion in soils across a chronosequence of Lake Michigan sand dunes. Geoderma 85 (4), 255–282. http://dx.doi.org/10.1016/S0016-7061(98)00026-3.

Liptzin, D., Sanford, R.L., Seastedt, T.R., 2013. Spatial patterns of total and available N and P at alpine treeline. Plant Soil 365 (1–2), 127–140. http://dx.doi.org/10.1007/s11104-012-1379-0.

Lundström, U.S., van Breemen, N., Bain, D., 2000. The podzolization process. A review. Geoderma 94 (2–4), 91–107. http://dx.doi.org/10.1016/s0016-7061(99)00036-1.

Lützow, M.v., Kögel-Knabner, I., Ekschmitt, K., Matzner, E., Guggenberger, G., Marschner, B., Flessa, H., 2006. Stabilization of organic matter in temperate soils: mechanisms and their relevance under different soil conditions - a review. Eur. J. Soil Sci. 57 (4), 426–445. http://dx.doi.org/10.1111/j.1365-2389.2006.00809.x.

Mehra, O.P., Jackson, M.L., 1958. Iron oxide removal from soils and clays by a dithionite-citrate system buffered with sodium bicarbonate. Clay Clay Miner. 7 (1), 317–327. http://dx.doi.org/10.1346/ccmn.1958.0070122.

Missong, A., Bol, R., Willbold, S., Siemens, J., Klumpp, E., 2016. Phosphorus forms in forest soil colloids as revealed by liquid-state ^{31}P-NMR. J. Plant Nutr. Soil Sci. 179 (2), 159–167. http://dx.doi.org/10.1002/jpln.201500119.

Mohren, G.M.J., Vandenburg, J., Burger, F.W., 1986. Phosphorus deficiency induced by nitrogen input in Douglas fir in the Netherlands. Plant Soil 95 (2), 191–200. http://dx.doi.org/10.1007/Bf02375071.

Murphy, J., Riley, J.P., 1962. A modified single solution method for the determination of phosphate in natural waters. Anal. Chim. Acta 27, 31–36. http://dx.doi.org/10.1016/s0003-2670(00)88444-5.

Ohno, T., Amirbahman, A., 2010. Phosphorus availability in boreal forest soils: a geochemical and nutrient uptake modeling approach. Geoderma 155 (1–2), 46–54. http://dx.doi.org/10.1016/j.geoderma.2009.11.022.

Okin, G.S., Mahowald, N., Chadwick, O.A., Artaxo, P., 2004. Impact of desert dust on the biogeochemistry of phosphorus in terrestrial ecosystems. Glob. Biogeochem. Cycles

18 (2) GB2005. http://dx.doi.org/10.1029/2003GB002145.
Parfitt, R.L., 1989. Phosphate reactions with natural allophane, ferrihydrite and goethite. J. Soil Sci. 40 (2), 359–369. http://dx.doi.org/10.1111/j.1365-2389.1989.tb01280.x.
Pebesma, E.J., 2004. Multivariable geostatistics in S: the gstat package. Comput. Geosci. 30 (7), 683–691. http://dx.doi.org/10.1016/j.cargo.2004.03.012.
Prietzel, J., Klysubun, W., Werner, F., 2016. Speciation of phosphorus in temperate zone forest soils as assessed by combined wet-chemical fractionation and XANES spectroscopy. J. Plant Nutr. Soil Sci. 179 (2), 168–185. http://dx.doi.org/10.1002/jpln.201500472.
R Core Team, 2015. R: A Language and Environment for Statistical Computing. R Foundation for Statistical Computing, Vienna doi:.
Regelink, I.C., Koopmans, G.F., van der Salm, C., Weng, L., van Riemsdijk, W.H., 2013. Characterization of colloidal phosphorus species in drainage waters from a clay soil using asymmetric flow field-flow fractionation. J. Environ. Qual. 42 (2), 464–473. http://dx.doi.org/10.2134/jeq2012.0322.
Revelle, W., 2015. Psych: procedures for personality and psychological research. Northwestern University, Evanston, doi:.
Ribeiro Jr., P.J., Diggle, P.J., 2001. geoR: A package for geostatistical analysis. R-News 15–18.
Richardson, S.J., Peltzer, D.A., Allen, R.B., McGlone, M.S., Parfitt, R.L., 2004. Rapid development of phosphorus limitation in temperate rainforest along the Franz Josef soil chronosequence. Oecologia 139 (2), 267–276. http://dx.doi.org/10.1007/s00442-004-1501-y.
SanClements, M.D., Fernandez, I.J., Norton, S.A., 2010. Phosphorus in soils of temperate forests: linkages to acidity and aluminum. Soil Sci. Soc. Am. J. 74 (6), 2175–2186. http://dx.doi.org/10.2136/sssaj2009.0267.
Sauer, D., Sponagel, H., Sommer, M., Giani, L., Jahn, R., Stahr, K., 2007. Review article Podzol: soil of the year 2007 a review on its genesis, occurrence, and functions. J. Plant Nutr. Soil Sci. 170 (5), 581–597. http://dx.doi.org/10.1002/jpln.200700135.
Saunders, W.M.H., Williams, E.G., 1955. Observations on the determination of total organic phosphorus in soils. J. Soil Sci. 6 (2), 254–267. http://dx.doi.org/10.1111/j.1365-2389.1955.tb00849.x.
Schirkonyer, U., Bauer, C., Rothe, G.M., 2013. Ectomycorrhizal diversity at five different tree species in forests of the Taunus Mountains in Central Germany. Open Journal of Ecology 3 (1), 66–81. http://dx.doi.org/10.4236/oje.2013.31009.
Schwertmann, U., 1964. Differenzierung der Eisenoxide des Bodens durch Extraktion mit Ammoniumoxalat-Lösung. Z. Pflanzenernähr. Düng. Bodenk. 105 (3), 194–202. http://dx.doi.org/10.1002/jpln.3591050303.
Shang, C., Caldwell, D.E., Stewart, J.W.B., Tiessen, H., Huang, P.M., 1996. Bioavailability of organic and inorganic phosphates adsorbed on short-range ordered aluminum precipitate. Microb. Ecol. 31 (1), 29–39. http://dx.doi.org/10.1007/bf00175073.
Sherman, J., Fernandez, I.J., Norton, S.A., Ohno, T., Rustad, L.E., 2006. Soil aluminum, iron, and phosphorus dynamics in response to long-term experimental nitrogen and sulfur additions at the Bear Brook Watershed in Maine. USA. Environ. Monit. Assess. 121 (1–3), 421–429. http://dx.doi.org/10.1007/s10661-005-9140-2.
Sims, J.T., Pierzynski, G.M., 2005. Chemistry of Phosphorus in Soils. In: Tabatabai, M.A., Sparks, D.L. (Eds.), SSSA Book Series Soil Science Society of America, Madison, pp. 151–192.
Syers, J.K., Williams, J.D.H., Campbell, A.S., Walker, T.W., 1967. The significance of apatite inclusions in soil phosphorus studies. Soil Sci. Soc. Am. J. 31 (6), 752–756. http://dx.doi.org/10.2136/sssaj1967.03615995003100060016x.
Taylor, A.F.S., Martin, F., Read, D.J., 2000. In: Schulze, E.-D. (Ed.), Fungal diversity in ectomycorrhizal communities of Norway Spruce [*Picea abies* (L.) Karst.] and Beech (*Fagus sylvatica* L.) along North-South Transects in Europe. Springer Berlin Heidelberg, Berlin, Heidelberg, pp. 343–365.
Vincent, A.G., Turner, B.L., Tanner, E.V.J., 2010. Soil organic phosphorus dynamics following perturbation of litter cycling in a tropical moist forest. Eur. J. Soil Sci. 61 (1), 48–57. http://dx.doi.org/10.1111/j.1365-2389.2009.01200.x.
Vincent, A.G., Schleucher, J., Grobner, G., Vestergren, J., Persson, P., Jansson, M., Giesler, R., 2012. Changes in organic phosphorus composition in boreal forest humus soils: the role of iron and aluminium. Biogeochemistry 108 (1–3), 485–499. http://dx.doi.org/10.1007/s10533-011-9612-0.
Violante, A., Pigna, M., 2002. Competitive sorption of arsenate and phosphate on different clay minerals and soils. Soil Sci. Soc. Am. J. 66 (6), 1788–1796. http://dx.doi.org/10.2136/sssaj2002.1788.
Vitousek, P.M., Farrington, H., 1997. Nutrient limitation and soil development: experimental test of a biogeochemical theory. Biogeochemistry 37 (1), 63–75. http://dx.doi.org/10.1023/A:1005757218475.
Walker, T.W., Syers, J.K., 1976. The fate of phosphorus during pedogenesis. Geoderma 15 (1), 1–19. http://dx.doi.org/10.1016/0016-7061(76)90066-5.
Wang, R., Balkanski, Y., Boucher, O., Ciais, P., Peñuelas, J., Tao, S., 2014. Significant contribution of combustion-related emissions to the atmospheric phosphorus budget. Nat. Geosci. 8 (1), 48–54. http://dx.doi.org/10.1038/ngeo2324.
Webster, R., Oliver, M.A., 2008. In: Webster, R., Oliver, M.A. (Eds.), Reliability of the experimental variogram and nested sampling. John Wiley & Sons, Ltd., Chichester, UK, pp. 109–138.
Yan, Y.P., Liu, F., Li, W., Liu, F., Feng, X.H., Sparks, D.L., 2014. Sorption and desorption characteristics of organic phosphates of different structures on aluminium (oxyhydr) oxides. Eur. J. Soil Sci. 65 (2), 308–317. http://dx.doi.org/10.1111/ejss.12119.
Yang, N., Zavišić, A., Pena, R., Polle, A., 2016. Phenology, photosynthesis, and phosphorus in European beech (*Fagus sylvatica* L.) in two forest soils with contrasting P contents. J. Plant Nutr. Soil Sci. 179 (2), 151–158. http://dx.doi.org/10.1002/jpln.201500539.
Zavišić, A., Nassal, P., Yang, N., Heuck, C., Spohn, M., Marhan, S., Pena, R., Kandeler, E., Polle, A., 2016. Phosphorus availabilities in beech (*Fagus sylvatica* L.) forests impose habitat filtering on ectomycorrhizal communities and impact tree nutrition. Soil Biol. Biochemist 98, 127–137. http://dx.doi.org/10.1016/j.soilbio.2016.04.006.
Zhang, W., Faulkner, J.W., Giri, S.K., Geohring, L.D., Steenhuis, T.S., 2010. Effect of soil reduction on phosphorus sorption of an organic-rich silt loam. Soil Sci. Soc. Am. J. 74 (1), 240–249. http://dx.doi.org/10.2136/sssaj2009.0123.

Micro-scale heterogeneity of soil phosphorus depends on soil substrate and depth

by

Florian Werner, Carsten W. Mueller, Jürgen Thieme, Alessandra Gianoncelli, Camille Rivard, Carmen Höschen, and Jörg Prietzel

Submitted to **Nature Scientific Reports**

Accepted for publication 28th April 2017 by **Nature Scientific Reports**

Licence to publish

Manuscript id:	SREP-17-05108A
Proposed title:	Micro-scale heterogeneity of soil phosphorus depends on soil substrate and depth
The "Author(s)":	Florian Werner, Carsten W. Mueller, Jürgen Thieme, Alessandra Gianoncelli, Camille RIVARD, Carmen Höschen, Jörg Prietzel
The "Contribution":	All content of the article, with the Proposed title listed above, including but not limited to all text, supplementary information, tables, graphs and images.
The "Journal":	Scientific Reports
"NPG":	Nature Publishing Group, a division of Macmillan Publishers Ltd

Purpose

NPG will consider publishing the Contribution pursuant to the terms set forth herein, including granting readers rights to use the Contribution on an open access basis identified below.

Open access licence

Licence is preferred by many research funding bodies. We support use of this licence as it is recommended for maximum dissemination and use of open access materials.

Grant of rights

In consideration of NPG evaluating the Contribution for publication (and publishing the Contribution if NPG so decides) the Author(s) grant to NPG for the full term of copyright and any extensions thereto, except as set out in the Author rights below, the right and irrevocable licence:

a. to edit, adapt, publish, reproduce, distribute, display and store the Contribution in all forms, formats and media whether now known or hereafter developed (including without limitation in print, digital and electronic form) throughout the world;
b. to translate the Contribution into other languages, create adaptations, summaries or extracts of the Contribution or other derivative works based on the Contribution and exercise all of the rights set forth (a) above in the translations, adaptations, summaries, extracts and derivative works;
c. to licence others to do any or all of the above, including but not limited to the right to grant readers the right to use the Contribution under the Creative Commons licence listed above; and
d. to re-licence article metadata without restriction (including but not limited to author name, title, abstract, citation, references, keywords and any additional information, as determined by NPG).

Author rights

Ownership of the copyright in the Contribution remains with the Author(s).

However, the Author(s)' re-use rights in the Contribution are subject to the rights and restrictions set forth in this Section, and in the Pre-print services and Warranties a) Section. After the Author(s) have submitted the Contribution to NPG hereunder, the Author(s)' rights to re-use the Contribution shall be the same as those set forth in the Creative Commons licence listed above, with the following additional re-use rights:

a. to reproduce the Contribution in whole or in part in any printed volume (book or thesis) of which they are the Author(s); and
b. to reuse figures or tables created by the Author(s) and contained in the Contribution in oral presentations and other works created by them.

Pre-print services

NPG acknowledges that an earlier version of the Contribution may have been submitted to a pre-print service (in accordance with that service's standard licence terms).

Warranties

The Author(s) warrant and represent that:

a. the Author(s) are the sole Author(s) of and sole owners of the copyright in the Contribution and the Contribution is the original work of the Author(s) and not copied (in whole or part)

from another work. If however the Contribution includes materials from other sources, the Author(s) warrant they have obtained the necessary rights from the owners of the copyright in all such materials and hereby license to NPG the rights to use such materials in accordance with the Grant of rights Section above. Copies of all such grant of rights from third parties have been submitted.

b. all of the facts contained in the Contribution are true and accurate;
c. the signatory (the Author or the employer) who has signed this Agreement below has full right, power and authority to enter into this Agreement and grant the rights herein on behalf of all of the Authors;
d. nothing in the Contribution is obscene, defamatory, libelous, violates any right of privacy or publicity, infringes any intellectual property rights (including without limitation copyright, patent, database or trademark rights) or any other human, personal or other rights of any person or entity or is otherwise unlawful; and
e. nothing in the Contribution infringes any duty of confidentiality which any of the Author(s) may owe to anyone else or violates any contract, express or implied, of any of the Author(s), and all of the institutions in which work recorded in the Contribution was created or carried out, have authorized such publication.

Dispute resolution

The Author(s) authorise NPG to take such steps as it considers necessary at its own expense in the Author(s) name and on their behalf if NPG believes that a third party is infringing or is likely to infringe copyright in the Contribution including but not

limited to initiating legal proceedings.

The Author(s) grant NPG the perpetual right to edit, correct, or retract the Contribution if NPG considers (in its reasonable opinion) that such actions are required. The Author(s) hereby agree that they shall not object to NPG carrying out any such actions.

The Author(s) shall cooperate fully with NPG in relation to any legal action that might arise from the publication of the Contribution and the Author(s) shall give NPG access at reasonable times to any relevant accounts, documents and records within the power or control of the Author(s).

Reversion of rights

If the Contribution is rejected by NPG and not published, all rights under this licence shall revert to the Author(s).

Law & jurisdiction

This Agreement shall be governed by and construed in accordance with the laws of England and Wales. The parties irrevocably agree that the courts of England and Wales shall have exclusive jurisdiction to settle any dispute or claim that arises out of or in connection with this Agreement or its subject matter or formation.

Micro-scale heterogeneity of soil phosphorus depends on soil substrate and depth

Florian Werner[1,*], Carsten W. Mueller[1], Jürgen Thieme[2], Alessandra Gianoncelli[3], Camille Rivard[4], Carmen Höschen[1], and Jörg Prietzel[1]

[1]Technical University of Munich, Research Department Ecology and Ecosystem Management, Chair of Soil Science, Emil-Ramann-Straße 2, 85354 Freising, Germany
[2]National Synchrotron Light Source II, Brookhaven National Laboratory, 743 Brookhaven Avenue, Upton, NY 11973-5000, USA
[3]Elettra-Sincrotrone Trieste S.C.p.A., Area Science Park, Basovizza 34149, Trieste, Italy
[4]European Synchrotron Radiation Facility (ESRF), 38000 Grenoble, France
[*]corresponding author: florian.werner@wzw.tum.de

ABSTRACT

Soils comprise various heterogeneously distributed pools of lithogenic, free organic, occluded, adsorbed, and precipitated phosphorus (P) forms, which differ depending on soil forming factors. Small-scale heterogeneity of element distributions recently has received increased attention in soil science due to its influence on soil functions and soil fertility. We investigated the micro-scale distribution of total P and different P binding forms in aggregates taken from a high-P clay-rich soil and a low-P sandy soil by combining advanced spectrometric and spectroscopic techniques to introduce new insights on P accessibility and availability in soils. Here we show that soil substrate and soil depth determine micro-scale P heterogeneity in soil aggregates. In all investigated soil aggregates, P in P enrichment zones was predominantly co-located with aluminium and iron oxides and hydroxides, which are known to strongly adsorb P. Clay minerals were co-located with P only to a lesser extent. In the low-P topsoil aggregate, the majority of the P was bound organically. Aluminium and iron phosphate predominated in the quartz-rich low-P subsoil aggregate. Sorbed and mineral P phases determined P speciation in the high-P top- and subsoil, and apatite was only detected in the high-P subsoil aggregate. Our results indicate that micro-scale spatial and chemical heterogeneity of P influences P accessibility and bioavailability.

Introduction

Phosphorus (P) availability in soils is known to be governed by parent material, the stage of soil development, as well as weathering and erosion intensity[1]. In soils, P limitation often occurs due to unavailability of P[2]. The unavailability is a result of P leaching[1], strong chemical bonds with other elements such as calcium (Ca), iron (Fe), or aluminium (Al), e.g. as P minerals and as P bound to Al and Fe oxides and hydroxides (oxyhydroxides), as well as to organic matter through metal cations[3], and immobilization of P in organic residues and microbial biomass[4]. The primary P source in soils, lithogenic apatite, is mobilized during the first 20.000 years of pedogenesis[5], whereas the relative shares of organically- and soil mineral-bound P species increase with advancing soil development[6]. Micro-scale soil architecture has received increased attention in soil studies[7,8] to explain macroscopic soil properties and processes that have been examined for decades[9]. A robust assessment of the chemical and structural accessibility of P requires studying not only bulk P speciation in a soil or soil horizon, but also spatial and chemical P heterogeneity at the micro-scale. At the moment, only scant information[10] exists on spatial soil P micro-distribution patterns due to the lack of highly versatile, affordable analytical methods, instruments, and standardized data analysis[11]. Established chemical fractionation techniques of bulk soil[12], and also advanced techniques of P speciation, as e.g. solution ^{31}P nuclear magnetic resonance spectroscopy[13] are inappropriate, because they destroy the structure of soil aggregates.

Nanoscale Secondary Ion Mass spectrometry (NanoSIMS) enables high-resolution element distribution mapping while preserving the overall structural integrity, however eroding a sample surface at a nm scale[14]. Moreover, improvements of synchrotron-based X-Ray Fluorescence (µ-XRF) spectroscopy and mapping allow in-situ assessments of element distributions at the micro-scale[10]. In our study, both techniques were combined to overcome individual technique limitations, such as matrix effects for NanoSIMS[14] and the comparably large beam penetration depth for µ-XRF spectroscopy[15]. Additionally, direct P speciation of micro-environments can be obtained by synchrotron-based X-Ray Absorption Near Edge Structure (µ-XANES) spectroscopy[16,17]. Combining these techniques thus provides powerful data on soil P distribution and speciation at the micro-scale and allows a *direct* assessment of P accessibility in soil systems[18]. We hypothesise that in soil aggregates, chemical and structural P accessibility at the micro-scale is determined by the distribution of total P and different P species.

Here, we show that micro-scale spatial and chemical P heterogeneity is related to soil depth and soil substrate in four undisturbed aggregates of different horizons from two forest soils, which have developed from siliceous parent material with low and high-P content, respectively. Information is provided on the micro-scale P distribution as related to the distribution of major soil compounds, such as pedogenic soil minerals and soil organic matter (SOM), and on major P binding forms at 15 P micro-sites (three to four sites per sample) using, for the first time, a combination of spatially-resolving techniques, and an original data analysis procedure (details: see Methods section). Our research opens new perspectives on how P accessibility and thus availability in soils is influenced by the micro-scale spatial and chemical heterogeneity of soil P.

Results

Patterns of micro-scale soil P distribution

Raster imaging performed with NanoSIMS revealed that the micro-spatial P distribution was characterised by pronounced heterogeneity (Fig. 1, upper section). The relatively few P-rich areas (definition: see Methods section and Fig. S1) in the aggregates of the low-P soil showed larger distances from each other than the relatively abundant P-rich areas in the aggregates of the high-P soil. Phosphorus-rich areas were predominantly co-located with Al and Fe (mostly oxyhydroxides) and to a lesser extent with clay minerals (Fig. 1, lower section).

In the aggregates of the low-P soil, more P-rich areas were co-located with Al/Fe oxyhydroxides in the subsoil (59 – 85 %) than in the topsoil (44 – 62 %, Table 1), but topsoil Al/Fe oxyhydroxides were more frequently co-located with P than subsoil Al/Fe oxyhydroxides (Table S1). Additionally, SOM was strongly co-located with P in the low-P topsoil (16 – 31 %, Table 1).

In the high-P aggregate, Al and Fe oxyhydroxides were co-located with P-rich areas in high percentages in both top- (50 – 89 %) and subsoil (49 – 91 %, Table 1). Additionally, Al/Fe oxyhydroxides and clay minerals were frequently co-located with P in this soil, especially in the topsoil (Table S1).

Aggregate P speciation at the micro-scale

Spatially-resolved P speciation results using µ-XANES spectroscopy revealed that P micro-sites (definition: see Methods section, fitted spectra: see Fig. S2) in the low-P topsoil aggregate mostly comprised organic P (0 – 55 % of total P: free organic P, 9 – 38 % calcium (Ca)-bound organic P, Table 2). Moreover, we identified considerable amounts of orthophosphate adsorbed to Al oxyhydroxides (27 – 45 % of total P, Table 2) and of organic P adsorbed to Fe oxyhydroxides (0 – 43 %, Table 2). All soil compounds were to a larger extent co-located with P in the topsoil than in the subsoil (Table S1).

Scanning electron microscope (SEM) imaging revealed that the aggregates sampled in the low-P subsoil consisted of quartz grains which were encompassed with and agglutinated by a finer-grained matrix (Fig. S3). Phosphorus was incorporated in the fine matrix of mineral and SOM coatings (Fig. 1), and the retained P was predominantly inorganic (Tables 1 and 2). In the low-P subsoil aggregate, spatially-resolved P speciation conducted on P micro-sites showed that P was predominantly bound as $AlPO_4$ (8 – 100 % of total P) and $FePO_4$ (0 – 61 %, Table 2). In addition to Al/Fe phosphate-bound P, up to about a quarter of total P in the low-P subsoil aggregate was adsorbed to Al-saturated clay minerals and/or Fe oxyhydroxides (Tables 1 and 2).

As expected, P-rich micro-sites in the high-P topsoil aggregate were dominated by orthophosphate adsorbed to Al-saturated SOM (7 – 51 % of total P) and Al oxyhydroxides (0 – 26 %), as well as by $AlPO_4$ (0 – 45 %) and $FePO_4$ (9 – 34 %, Table 2). Fe oxyhydroxides influenced P binding marginally in the high-P topsoil aggregate (Table 2). Phosphorus bound in organic compounds was only a minor P species in this aggregate (0 – 13 %, Table 2). Unexpectedly, $MgHPO_4$ was detected in the high-P topsoil aggregate (0 – 28 %, Table 2). In contrast, apatite was detected solely, but consistently in the aggregate of the high-P subsoil (7 – 46 %, Table 2). Similar to topsoil percentages, we found 0 – 51 % of $AlPO_4$ and 0 – 28 % of $FePO_4$ (Table 2). Phosphorus adsorbed to Al-saturated clay minerals contributed only minor to P speciation in the high-P subsoil aggregate (0 – 14 %, Table 2).

Discussion

Micro-scale soil P distribution patterns are soil-dependent

The investigated aggregates showed striking differences with respect to the amount, distribution, and form of P-rich areas. At P-rich areas of the low-P topsoil aggregate, SOM was strongly co-located with P (Table 1), and co-localisation of P with Al/Fe oxyhydroxides and clay minerals increased when SOM was present (Table S1). In accordance, P was mainly bound organically in the bulk soil of the low-P topsoil (Table S2). These results show that in the sandy, quartz-rich low-P topsoil, the few Al and Fe oxyhydroxides and clay minerals, i.e. smectite and illite (Table S3) play a pivotal role in retaining P. The co-localisation of these compounds with SOM indicates that P-rich SOM is probably bound in complexes at the compound surfaces[19].

The aggregates of the high-P soil showed different P distribution patterns compared to the aggregates of the low-P soil. Here, Al and Fe oxyhydroxides were the dominant partners for co-localisation with P (Table 1). About half of the total P was bound organically in the bulk soil of both top- and subsoil (Table S2). Bulk soil studies have long pointed out that the large

surface areas of Al and Fe oxyhydroxides and Al-saturated high-activity clay minerals provide numerous sites to strongly bind inorganic and organic soil P, especially under acidic conditions[19], as present at this site (Table S2). The influence of clay minerals on P retention is exerted mostly by P sorption on cationic Al hydroxy polymer clusters on 2:1 clay mineral surfaces[20,21]. In both depths at the high-P site, illite and chlorite were the main phyllosilicates in the clay fraction (Table S3). Thus, apart from the presence and ion occupancy of P binding partners, the structural and chemical P accessibility in soil aggregates also depends on the heterogeneous distribution of P and different P species at the micro-scale. This implies that studies aiming at a robust mechanistic understanding of micro-scale P retention and P release as well as P accessibility and availability for plants and soil micro-organisms must account for the heterogeneous P distribution in soil aggregates.

Soil depth considerably influences P heterogeneity at advanced stage of pedogenesis

The soils on both sites were pronouncedly acidified (Table S2), but only the sandy low-P soil exhibited podzolization. Phosphorus distribution and micro-site P speciation differed strongly between the low-P top- and subsoil, whereas this was not the case for the high-P top- and subsoil. Our findings from the aggregates of the low-P soil indicate that soil depth is a major determinant of P speciation on the micro-scale, particularly at later stages of pedogenesis. In the low-P topsoil aggregate, P species were mainly organic (Table 2). Due to the high Ca ion content (Table S2), we suppose that the soil has been limed in the past, supporting the formation of Ca-P complexes[22] in the topsoil. Organically-bound P is subject to mineralisation[4] and thus generally accessible to plants and microbes. However, we suppose that the few Al and Fe oxyhydroxide-bound P resources are structurally inaccessible due to occlusion.

In the subsoil aggregate of the low-P aggregate, P was especially scarce (Table S2). The fine matrix of mineral and SOM coatings surrounding larger quartz grains (Fig. S3) contained mostly phosphate minerals (Tables 1 and 2). Even though there are doubts that Fe and Al phosphates, such as strengite or variscite can persist in soil environments with moderately acidic pH[23], crystalline $AlPO_4$ (berlinite) was found to be more resistant against dissolution at pH 6 – 7 than at pH 3[24]. In this context it must be emphasized that the XANES spectrum of amorphous $AlPO_4$ is identical with that of Al hydroxy phosphate, which is thermodynamically stable at moderately acidic pH values. In addition, the presence of Al hydroxy phosphate is more likely due to the large amount of secondary, primarily $Al(OH)_3$-, chlorite in the subsoil, but not in the topsoil clay fraction (Table S3). Even though Al and Fe are highly important for retaining P in sandy subsoil aggregates, the scarce P resources in these aggregates are presumably chemically, as well as structurally inaccessible to plants and microbes.

Soil substrate influence on P heterogeneity is stronger during early stages of pedogenesis

In aggregates of the high-P soil, P speciation and distribution patterns are governed by the clayey-silty soil substrate, which has originated from ongoing intense weathering of basalt rock fragments into Al and Fe oxyhydroxides and 2:1 clay minerals[25]. For example, the top- and subsoil percentages of $AlPO_4$, $FePO_4$, and of orthophosphate adsorbed to Al or Fe oxyhydroxides (Table 2) are similar, which is not the case for the pedogenetically older low-P soil. In contrast to our µ-XANES results on P micro-sites, no $AlPO_4$ had been identified for bulk soil samples at the high-P site (30 – 70 cm depth) in a recent XANES spectroscopy study[26]. Bulk soil XANES spectra are dominated by a diffuse background of low-P content[18] and therefore often fail to represent P micro-sites in the interior of soil aggregates. Thus, we surmise that even though considerable $AlPO_4$ (Al hydroxy phosphate) is bound at P micro-sites, this P form is below detection limit in bulk soil samples. Speciation results using µ-XANES spectroscopy of a transect from the agglutinating soil matrix to the interior of an Al-Fe concretion in the high-P subsoil (Fig. S4) also show that the proportion of $AlPO_4$ was increased especially in the matrix, whereas sorbed P species dominated at the concretion surface (Fig. S4).

Most noticeable, we expected higher percentages of clay mineral-bound P in the high-P aggregates. At a pH value of about 4, which was present in the high-P subsoil (Table S2), negatively charged surfaces of expandable clay minerals are mostly covered with Al hydroxy cations and thus have a P sorption efficiency similar to that of Al oxyhydroxides[21]. About two-thirds of the bulk soil mass was silt sized particles which were dominated by quartz and augite and no expandable clay minerals were detected (Table S3). In the high-P topsoil aggregate, SOM more pronouncedly influenced Al exchanger cations than clay minerals (Table 2). We assume that in the high-P topsoil, P remains accessible due to ongoing detachment of P after mineralisation of SOM. However, P also leaches as dissolved organic P and/or in colloids through the soil, as described for a similar German forest soil site[27]. In the subsoil, apatite weathering provides accessible P resources, even though other P species are structurally inaccessible. Thus, our results emphasize not only the importance of sorbed and mineral P phases at early stages of pedogenesis, but also the importance of investigating also micro-scale P heterogeneity when assessing P accessibility in soils.

Micro-scale P speciation patterns support micro-reactor concept

The "micro–chemical reactor concept" states that each soil micro-site represents an independent micro-reactor of unique chemical composition[8]. Even though individual reactors are interconnected with each other and adjacent compounds, each analysis is regarded as a separate perspective on a complex system. The presence of $AlPO_4$ and Al hydroxy phosphate in the high-P soil is an example where the chemical composition at P micro-sites enables understanding the characteristics of the

chemical transformations that must have occurred within these micro-sites. Another example is the existence of $MgHPO_4$ in our high-P topsoil sample (Table 2). This is surprising, as this compound is not stable in acidic solutions below pH 5. However, in contrast to the low-P soil, in the P-rich soil primary, i.e. $Mg(OH)_3$-chlorite made up 20 – 30 % of the total clay mineral content (Table S3). Thus, our XANES spectroscopy and XRD data suggest that, similar to clay-bound $Al(OH)_3$ in the P-poor soil, as reported above, clay-bound $Mg(OH)_3$, probably occluded in less acidic interior regions of soil aggregates, is a major P-bearing phase in the high-P soil. The same occlusion can be stated for orthophosphate adsorbed by Al oxyhydroxides in the high-P and low-P topsoil aggregate (Table 2). These results indicate that some biocycled P is retained at micro-sites in the topsoil aggregates of both sites by pedogenic Al oxyhydroxides due to occlusion, which furthermore supports the micro-reactor concept.

Conclusions

Micro-scale P distribution and speciation patterns were investigated in soil aggregates to increase our knowledge about P accessibility in soils. We demonstrated for the first time that Al/Fe oxyhydroxides and clay minerals are major binding partners of P in such aggregates. Our results showed that P species diversity and micro-scale distribution predominantly is dependent on soil substrate and soil depth. We showed that the analysis of P speciation at micro-sites is relevant for understanding the chemical changes in a soil micro-chemical reactor[8]. Four factors governing P availability are well-known: i) parent material, ii) stage of pedogenesis, iii) weathering intensity, and iv) erosion (as P input)[1]. Our study showed that the use of spatially-resolving tools is necessary to understand the governing factors of P availability, as related to the micro-scale spatial and chemical heterogeneity of soil P. The benefit of our study is not only based on effectively combining distribution and speciation analysis for soil aggregate studies, but also on opening these new perspectives on P availability in soils.

Methods

Soil material and sample preparation

Soil samples were obtained from two sites that were stocked with mature *Fagus sylvatica* forests of about 120 years of age, located in Germany, near Lüß (LU), Gauss-Krüger-coordinates: 3585473 E, 5857057 N, and Bad Brückenau (BB), Gauss-Krüger-coordinates: 3566195 E, 5579975 N. The sites are part of the International Co-operative Programme on Assessment and Monitoring of Air Pollution Effects on Forests (ICP Level II). They differed in soil and beech leaf P contents, and were end-members of a forest P availability gradient[28]. The soils were formed from siliceous parent material under temperate climate and were classified[29] as Hyperdystric Folic Cambisol (LU), and as Dystric Skeletic Cambisol (BB). The LU soil has formed from Pleistocene glacifluvial sands, the BB soil from basalt. A basic soil characterisation can be found in Table S2. In the main text, the sites LU and BB are named as low- and high-P sites, respectively.

Samples were taken from the mineral topsoil (directly below the organic layer) and the subsoil (30 cm depth) with a steel tube (⌀ 2 cm, sampling depth 3 cm). They were dried at 60° C for 48 hours and subsequently sieved (<2mm). For each site and depth, three dried, intact soil aggregates (size approximately 1 – 2 mm^3) were selected randomly from the dried bulk soils and embedded in an epoxy resin (Araldite 502 Kit, Electron Microscopy Sciences, Hatfield, PA, USA). The embedded aggregates were then cured at 60° C for 24 hours, and subsequently thin-sectioned, polished and coated with gold by physical vapor deposition[30]. One aggregate per site was randomly selected for scanning electron microscopy (Jeol JSM 5900LV, Eching, Germany) imaging to locate regions of interest for the subsequent imaging techniques.

Assessing element distributions using NanoSIMS

The NanoSIMS measurements were conducted with a Cameca NanoSIMS 50L instrument (Cameca, Gennevilliers Cedex, France) at Technical University of Munich, Germany. A Cs^+ source with a primary ion energy of 16 keV was used to produce secondary ions of the sample surface. The focused beam (lateral resolution about 100 nm) scanned over areas of $40 \cdot 40$ μm^2 while the mass signals of the secondary ions $^{12}C^-$, $^{16}O^-$, $^{12}C^{14}N^-$, $^{28}Si^-$, $^{27}Al^{16}O^-$, $^{31}P^{16}O_2^-$, and $^{56}Fe^{16}O^-$ (C, O, CN, Si, Al, P, Fe) were collected. In the latter three ions ionization is stronger than that of the individual Al, P, or Fe ions. The ion images were acquired using a 10 ms/pixel dwell time in an area of $512 \cdot 512$ $pixels^2$. On each aggregate 5 – 7 measurements were conducted.

Assessing element distributions using µ-XRF

We performed µ-XRF at the same sample locations as the NanoSIMS measurements. However, due to beam time limitation restrictions for measuring at the synchrotrons not all micro-regions analysed by NanoSIMS measurements could be evaluated with µ-XRF. Synchrotron-based µ-XRF measurements were conducted at the TwinMic Beamline of the ELETTRA synchrotron (storage ring energy 2.0 GeV) in Trieste, Italy, and at Beamline ID21 of the European Synchrotron Radiation Facility (ESRF, storage ring energy: 6.03 GeV) in Grenoble, France. The TwinMic Beamline was operated in low energy X-Ray Fluorescence

(LEXRF) mode and was equipped with a 600 lines per mm Au plane-grating monochromator. The fluorescence detector consisted of 8 silicon drift detectors (SDD)[31]. The samples were installed in a vertical plane, orthogonally to the incident photon beam. The data was acquired at 2.19 keV to optimize the P emission signal. The LEXRF dwell time varied between 1 and 7 s as a function of the samples, and the maps were acquired by raster scanning with a 1 µm step size and a minimum size of $40 \cdot 40$ pixels^2 ($= 40 \cdot 40$ µm^2).

The ID21 Beamline[32] of ESRF was equipped with a double crystal Si(111) monochromator (energy resolution: 0.4 eV). The samples were tilted by 28° with respect to the incident beam, and the fluorescence signal was collected by a SDD detector, placed at a 49° angle with respect to sample surface. Micro-XRF maps were obtained by raster scanning using a focused beam. After selection of the area of interest, maps were recorded at 2.165 keV to intensify P *K*-edge emission, with a dwell time of 150 ms and a step size of 0.5 µm. The elemental distributions were obtained by deconvoluting the µ-XRF spectra after incoming flux (and detector deadtime) correction, on maps of minimum size of $80 \cdot 80$ pixels^2 ($40 \cdot 40$ µm^2) with the PyMCA software[33].

Co-localisation analysis for determining distribution patterns

All XRF and NanoSIMS measurements were analysed with the statistical software *R*, Version 3.3.1[34]. First, we performed k-means cluster analysis[11] (Fig. S1) on every ion/element count rate of an ion/element to determine regions with similar element identity. The count rates of every pixel were assigned to one of five cluster centres, respectively. The three largest cluster centre values were combined to result images where each pixel is either assigned as "area rich in", or as a negligible count value (Fig. S1). For the NanoSIMS images, P, Fe, Al, CN and Si were selected. These latter four ions and their combinations were then assigned to soil compound classes: i) Fe/Al oxyhydroxides (Al, Fe, Fe+Al; also including Al and Fe oxyhydroxide surface precipitates), ii) Fe/Al oxyhydroxides + SOM (Al+CN, Fe+CN, Fe+Al+CN, Fe+CN+Si), iii) clay minerals (Al+Si, Fe+Al+Si), iv) clay minerals + SOM (Al+CN+Si, Fe+Al+CN+Si), v) quartz (Si), vi) SOM (CN, CN+Si), and vii) unspecified. The total number of pixels, respective total area, of these compounds and the compound-rich areas that were co-located with P were counted. Dividing the P-rich area that is co-located with a specific compound by the total P-rich area resulted in a proportional measure for P binding. Dividing the compound-rich area that is co-located with P by the total compound-rich area resulted in a proportional measure for compound P allocation. Both measures are displayed as percentage of total P/compound-rich area, respectively.

µ-XRF maps were processed alike, but the elements for co-localisation differed due to different instrument conditions. The ELETTRA instrument also allowed all stated P binding categories, however, CN was replaced by N only. The attribution to the seven categories persisted as stated. The ESRF instrument unfortunately did not provide information on N, but on the L_2-edge of Fe (719.9 eV). During compound classification, this element was treated similarly as the first Fe edge. The compound classes, to which element combinations were assigned to, were therefore limited to only those that did not include SOM (i, iii, v, and vii). This procedure and the heterogeneity of P and soil compounds resulted in different proportions of P and soil compounds depending on the instrument used.

Assessing P speciation using µ-XANES spectroscopy and spectra fitting

µ-XANES measurements were conducted at Beamline ID21 of ESRF to support the elemental raster images by direct P speciation results from linear combination fitting (LCF) with P reference spectra of all relevant P species. Phosphorus *K*-edge µ-XANES spectra were collected with a 0.2 eV step size, a dwell time of 0.1 s, and in an energy range from 2.13 to 2.20 keV. For each P micro-site (minute sites of increased P content), 10 to 40 spectra were recorded and merged. For LCF, we used 17 P standards, which represent P species in temperate forest soils, and whose *K*-edge XANES spectra had been acquired at beamline 8 of the Synchrotron Light Research Institute (SLRI) in Nakhon Ratchasima, Thailand[35]: 1) crystalline and 2) amorphous $Fe^{III}PO_4$ (its proportions combined, termed as $FePO_4$), 3) crystalline and 4) amorphous $AlPO_4$ (its proportions combined, termed as $AlPO_4$), 5) phytic acid sodium salt (IHP, termed as organic P), 6) apatite, 7) $MgHPO_4$, 8) orthophosphate and 9) IHP retained by boehmite (termed as orthophosphate and organic P adsorbed to Al oxyhydroxides), 10) orthophosphate and 11) IHP retained by ferrihydrite (termed as orthophosphate and organic P adsorbed to Fe oxyhydroxides), 12) orthophosphate and 13) IHP retained by Al-saturated montmorillonite (termed as orthophosphate and organic P adsorbed to clay minerals), 14) orthophosphate and 15) IHP retained by Al-saturated soil organic matter (termed as orthophosphate and organic P adsorbed to SOM), P retained by 16) precipitated Ca_3-IHP (termed as Ca-bound organic P), 17) IHP adsorbed to $CaCO_3$[21]. Spectra were calibrated in energy by comparing apatite spectra taken at SLRI and ESRF, a correction value of $\delta E = -1.15$ eV was applied.

µ-XANES spectra were base-line corrected and edge-step normalized following a standard protocol published recently[36] using the statistical software *R*, Version 3.3.1[34]. The reference spectra were base-line corrected from -36 to -15 eV and normalized from +37 to +57 eV with respect to the edge-step of the respective spectra. As for the samples, the first base-line correction parameter was allowed to vary from -28 to -18 eV (step: 1 eV) and the second from -16 to -8 eV (step: 0.5 eV) with respect to the edge-step. The first normalization parameter was allowed to vary between +29 and +39 eV (step: 0.5 eV) and the second between +42 and +48 eV (step: 1 eV) with respect to the edge-step. The actual LCF was performed from -14 to 46 eV

with respect to the edge-step of a sample spectrum. Phosphorus speciation shares below 5 % of total P were excluded and LCF was repeated without the respective standards. Only fits with R-factors smaller than 0.005 were included because fits with R-factors greater than this value were obviously unreliable. Results from LCF (Fig. S2) only show those P reference spectra proportions that were detected as more than 5% of total P at least once.

References

1. Bol, R. *et al.* Dissolved and colloidal phosphorus fluxes in forest ecosystems-an almost blind spot in ecosystem research. *J. Plant Nutr. Soil Sci.* **179**, 425–438 (2016). DOI 10.1002/jpln.201600079.
2. Elser, J. J. Phosphorus: a limiting nutrient for humanity? *Curr. Opin. Biotechnol.* **23**, 833–838 (2012). DOI 10.1016/j.copbio.2012.03.001.
3. Hesterberg, D. Chapter 11 - Macroscale Chemical Properties and X-Ray Absorption Spectroscopy of Soil Phosphorus. In Balwant, S. & Markus, G. (eds.) *Developments in Soil Science*, vol. Volume 34, 313–356 (Elsevier, 2010).
4. Turner, B. L., Condron, L. M., Richardson, S. J., Peltzer, D. A. & Allison, V. J. Soil organic phosphorus transformations during pedogenesis. *Ecosystems* **10**, 1166–1181 (2007). DOI 10.1007/s10021-007-9086-z.
5. Walker, T. W. & Syers, J. K. The fate of phosphorus during pedogenesis. *Geoderma* **15**, 1–19 (1976). DOI 10.1016/0016-7061(76)90066-5.
6. Turner, B. L. *et al.* Soil microbial biomass and the fate of phosphorus during long-term ecosystem development. *Plant Soil* **367**, 225–234 (2013). DOI 10.1007/s11104-012-1493-z.
7. Totsche, K. U. *et al.* Biogeochemical interfaces in soil: The interdisciplinary challenge for soil science. *J. Plant Nutr. Soil Sci.* **173**, 88–99 (2010). DOI 10.1002/jpln.200900105.
8. Hesterberg, D., Duff, M. C., Dixon, J. B. & Vepraskas, M. J. X-ray microspectroscopy and chemical reactions in soil microsites. *J. Environ. Qual.* **40**, 667–678 (2011). DOI 10.2134/jeq2010.0140.
9. Baveye, P. C. & Laba, M. Moving away from the geostatistical lamppost: Why, where, and how does the spatial heterogeneity of soils matter? *Ecol. Model.* **298**, 24–38 (2015). DOI 10.1016/j.ecolmodel.2014.03.018.
10. Majumdar, S. *et al.* Applications of synchrotron μ-XRF to study the distribution of biologically important elements in different environmental matrices: A review. *Anal. Chim. Acta* **755**, 1–16 (2012). DOI 10.1016/j.aca.2012.09.050.
11. Bertrand, I., Grignon, N., Hinsinger, P., Souche, G. & Jaillard, B. The use of secondary ion mass spectrometry coupled with image analysis to identify and locate chemical elements in soil minerals: The example of phosphorus. *Scanning* **23**, 279–291 (2001). DOI 10.1002/sca.4950230409.
12. Hedley, M. J., Stewart, J. W. B. & Chauhan, B. S. Changes in Inorganic and Organic Soil-Phosphorus Fractions Induced by Cultivation Practices and by Laboratory Incubations. *Soil Science Society of America Journal* **46**, 970–976 (1982). DOI 10.2136/sssaj1982.03615995004600050017x.
13. Cade-Menun, B. J. & Liu, C. W. Solution phosphorus-31 nuclear magnetic resonance spectroscopy of soils from 2005 to 2013: A review of sample preparation and experimental parameters. *Soil Sci. Soc. Am. J.* **78**, 19–37 (2014). DOI 10.2136/sssaj2013.05.0187dgs.
14. Mueller, C. W. *et al.* Advances in the analysis of biogeochemical interfaces: NanoSIMS to investigate soil microenvironments. In Sparks, D. L. (ed.) *Adv. Agron.*, vol. 121, 1–46 (Academic Press, Burlington, 2013).
15. Eriksson, A. K., Hesterberg, D., Klysubun, W. & Gustafsson, J. P. Phosphorus dynamics in Swedish agricultural soils as influenced by fertilization and mineralogical properties: Insights gained from batch experiments and XANES spectroscopy. *Sci. Total Environ.* **566-567**, 1410–1419 (2016). DOI 10.1016/j.scitotenv.2016.05.225.
16. Lombi, E. & Susini, J. Synchrotron-based techniques for plant and soil science: opportunities, challenges and future perspectives. *Plant Soil* **320**, 1–35 (2009). DOI 10.1007/s11104-008-9876-x.
17. Kruse, J. *et al.* Innovative methods in soil phosphorus research: A review. *J. Plant Nutr. Soil Sci.* **178**, 43–88 (2015). DOI 10.1002/jpln.201400327.
18. Rivard, C., Lanson, B. & Cotte, M. Phosphorus speciation and micro-scale spatial distribution in North-American temperate agricultural soils from micro X-ray fluorescence and X-ray absorption near-edge spectroscopy. *Plant Soil* **401**, 7–22 (2015). DOI 10.1007/s11104-015-2494-5.
19. Violante, A. & Pigna, M. Competitive sorption of arsenate and phosphate on different clay minerals and soils. *Soil Sci. Soc. Am. J.* **66**, 1788–1796 (2002). DOI 10.2136/sssaj2002.1788.

20. Kasama, T., Watanabe, Y., Yamada, H. & Murakami, T. Sorption of phosphates on al-pillared smectites and mica at acidic to neutral pH. *Applied Clay Science* **25**, 167–177 (2004). DOI 10.1016/j.clay.2003.09.005.

21. Prietzel, J. *et al.* Reference spectra of important adsorbed organic and inorganic phosphate binding forms for soil P speciation using synchrotron-based K-edge XANES spectroscopy. *J. Synchrotron Radiat.* **23**, 532–544 (2016). DOI 10.1107/S1600577515023085.

22. Celi, L., Lamacchia, S. & Barberis, E. Interaction of inositol phosphate with calcite. *Nutr. Cycl. Agroecosys.* **57**, 271–277 (2000). DOI 10.1023/a:1009805501082.

23. Bache, B. W. Aluminum and iron phosphate studies relating to soils. *J. Soil Sci.* **14**, 113–123 (1963). DOI 10.1111/j.1365-2389.1963.tb00936.x.

24. Prietzel, J. Mobilization of X-ray amorphous and crystalline aluminum and iron phosphates by common soil extraction procedures. *J. Plant Nutr. Soil Sci.* (2016). DOI 10.1002/jpln.201600374.

25. Eggleton, R. A., Foudoulis, C. & Varkevisser, D. Weathering of basalt: Changes in rock chemistry and mineralogy. *Clays Clay Miner.* **35**, 161–169 (1987). DOI 10.1346/Ccmn.1987.0350301.

26. Prietzel, J., Klysubun, W. & Werner, F. Speciation of phosphorus in temperate zone forest soils as assessed by combined wet-chemical fractionation and XANES spectroscopy. *J. Plant Nutr. Soil Sci.* **179**, 168–185 (2016). DOI 10.1002/jpln.201500472.

27. Missong, A., Bol, R., Willbold, S., Siemens, J. & Klumpp, E. Phosphorus forms in forest soil colloids as revealed by liquid-state ^{31}P-NMR. *J. Plant Nutr. Soil Sci.* **179**, 159–167 (2016). DOI 10.1002/jpln.201500119.

28. Zavišić, A. *et al.* Phosphorus availabilities in beech (*Fagus sylvatica* L.) forests impose habitat filtering on ectomycorrhizal communities and impact tree nutrition. *Soil Biol. Biochem.* **98**, 127–137 (2016). DOI 10.1016/j.soilbio.2016.04.006.

29. WRB, I. W. G. World Reference Base for Soil Resources 2014, update 2015. International soil classification system for naming soils and creating legends for soil maps. World Soil Resources Reports 106, FAO (2015).

30. Herrmann, A. M. *et al.* A novel method for the study of the biophysical interface in soils using nano-scale secondary ion mass spectrometry. *Rapid Commun. Mass Spectrom.* **21**, 29–34 (2007). DOI 10.1002/rcm.2811.

31. Gianoncelli, A., Kourousias, G., Merolle, L., Altissimo, M. & Bianco, A. Current status of the TwinMic beamline at elettra: a soft x-ray transmission and emission microscopy station. *J. Synchrotron Radiat.* **23**, 1526–1537 (2016). DOI 10.1107/s1600577516014405.

32. Salomé, M. *et al.* The ID21 Scanning X-ray Microscope at ESRF. *J. Phys.: Conf. Ser.* **425**, 182004 (2013). DOI 10.1088/1742-6596/425/18/182004.

33. Solé, V. A., Papillon, E., Cotte, M., Walter, P. & Susini, J. A multiplatform code for the analysis of energy-dispersive X-ray fluorescence spectra. *Spectrochim. Acta B* **62**, 63–68 (2007). DOI 10.1016/j.sab.2006.12.002.

34. R Core Team. R: A language and environment for statistical computing (2015).

35. Klysubun, W., Sombunchoo, P., Deenan, W. & Kongmark, C. Performance and status of beamline BL8 at SLRI for X-ray absorption spectroscopy. *J. Synchrotron Radiat.* **19**, 930–936 (2012). DOI 10.1107/S0909049512040381.

36. Werner, F. & Prietzel, J. Standard protocol and quality assessment of soil phosphorus speciation by P *K*-edge XANES spectroscopy. *Environ. Sci. Technol.* **49**, 10521–10528 (2015). DOI 10.1021/acs.est.5b03096.

Acknowledgements

This work was funded by the German Research Foundation (DFG), as part of the Priority Program SPP 1685 (grant Pr 534/6-1). Synchrotron analyses were conducted on the ID21 beamline at the European Synchrotron Radiation Facility (Grenoble, France) on in-house research beamtime. We thank Johann Lugmeier for his help with the NanoSIMS measurements, Matteo Altissimo from ELETTRA, and Marine Cotte and Murielle Salome from ESRF for their help in µ-XRF and µ-XANES spectroscopy. We thank Werner Häusler for XRD analysis.

Author contributions statement

F.W. prepared the samples, conducted SEM measurements, conducted NanoSIMS, as well as the µ-XRF and µ-XANES spectroscopy data acquisition, developed approaches for data analysis, processed the data, and wrote the manuscript. C.W.M. prepared the samples, conducted SEM measurements, and commented on the manuscript. J.T. conducted µ-XRF and µ-XANES spectroscopy data acquisition at ELETTRA and ESRF and commented on the manuscript. A.G. conducted µ-XRF

data acquisition at ELETTRA and commented on the manuscript, C.R. conducted μ-XRF and μ-XANES spectroscopy data acquisition at ESRF and commented on the manuscript, C.H. conducted NanoSIMS analyses and commented on the manuscript, J.P. planned the study, conducted μ-XRF and μ-XANES spectroscopy data acquisition at ELETTRA and ESRF, and provided input to the manuscript.

Competing financial interests

The authors declare that they have no competing financial interests.

Data availability

The Supplementary Tables and Figures are provided on the *Nature Scientic Reports* website at doi:nat/scirep.doi. Raw NanoSIMS and μ-XRF mapping data (including cluster center assignment), as well as raw μ-XANES spectra are available on the public data repository website of *PANGAEA* at doi:10.1594/PANGAEA.874444. The *R* code for linear combination fitting of P *K*-edge XANES spectra has been published at the *Comprehensive R Archive Network* under the package name *LCF*.

Table 1. Phosphorus (P)-rich areas that are co-located with aluminium and iron (Al/Fe) oxyhydroxides, clay minerals, quartz, and soil organic matter (SOM). Nanoscale Secondary Ion Mass Spectrometry (NanoSIMS) and synchrotron-based X-Ray Fluorescence (μ-XRF) mapping (at the synchrotrons ELETTRA, Italy, and ESRF, France) were used. In three aggregates, μ-XRF imaging included two NanoSIMS measurements (displayed as subscript 1 and 2).

		P-rich areas that are co-located with				
		Al/Fe oxy-hydroxides[a]	clay minerals[a]	quartz	SOM	unspec-ified
		(% of total P-rich area)				
low-P topsoil	ELETTRA	49 (41)	2 (2)	–	31	18
	ESRF	62	14	1	–	24
	$NanoSIMS_1$	61 (48)	16 (16)	1	19	3
	$NanoSIMS_2$	44 (37)	21 (18)	7	16	12
low-P subsoil	ELETTRA	85 (37)	8 (6)	1	3	4
	ESRF	59	25	5	–	11
	NanoSIMS	70 (7)	30 (10)	–	–	–
high-P topsoil	ELETTRA	89 (43)	2 (2)	–	3	6
	ESRF	64	30	3	–	2
	$NanoSIMS_1$	50 (45)	41 (35)	1	5	4
	$NanoSIMS_2$	81 (22)	17 (3)	–	–	1
high-P subsoil	ELETTRA	89 (17)	3 (3)	–	1	8
	ESRF	91	4	2	–	3
	$NanoSIMS_1$	59 (37)	34 (24)	1	3	4
	$NanoSIMS_2$	49 (25)	48 (31)	1	1	2

[a]Brackets: share of compound that is also co-located with SOM

Table 2. Results from linear combination fitting of synchrotron-based X-Ray Absorption Near Edge Structure (XANES) spectra by various phosphorus (P) reference standards (details: see Methods section). Fifteen P micro-sites (P1 to P15) were investigated on soil aggregates. Quality of the fit given by R-factor; accuracy of the fitting 5 – 10 %[36].

								organic P adsorbed to	orthophosphate adsorbed to				
		Organic P	Ca-bound organic P	Apatite	$MgHPO_4$	$AlPO_4$[a]	$FePO_4$[a]	Fe oxyhydroxides	Fe oxyhydroxides	Al oxyhydroxides	Al-saturated clays	Al-saturated SOM	R-factor
		(% of total P)											
low-P topsoil	P1	–	36	–	–	–	–	21	–	43	–	–	0.0047
	P2	16	9	–	–	–	–	43	–	32	–	–	0.0029
	P3	9	38	–	–	–	–	8	–	45	–	–	0.0034
	P4	55	17	–	–	–	–	–	–	27	–	–	0.0040
low-P subsoil	P5	–	–	–	–	8	61	14	–	–	17	–	0.0032
	P6	–	–	–	–	32	48	20	–	–	–	–	0.0026
	P7	–	–	–	–	100	–	–	–	–	–	–	0.0037
high-P topsoil	P8	–	–	–	–	37	16	5	8	26	–	7	0.0012
	P9	13	–	–	16	–	34	–	–	12	–	24	0.0019
	P10	9	–	–	28	–	13	–	–	–	–	51	0.0028
	P11	–	–	–	19	45	9	–	–	13	–	14	0.0037
high-P subsoil	P12	–	–	35	–	51	8	–	–	6	–	–	0.0014
	P13	–	–	46	–	46	–	–	–	9	–	–	0.0025
	P14	–	10	17	–	–	28	6	–	40	–	–	0.0045
	P15	–	–	7	–	35	–	–	11	33	14	–	0.0014

[a]Includes orthophosphate bound to Al and Fe oxyhydroxides by surface precipitation, respectively

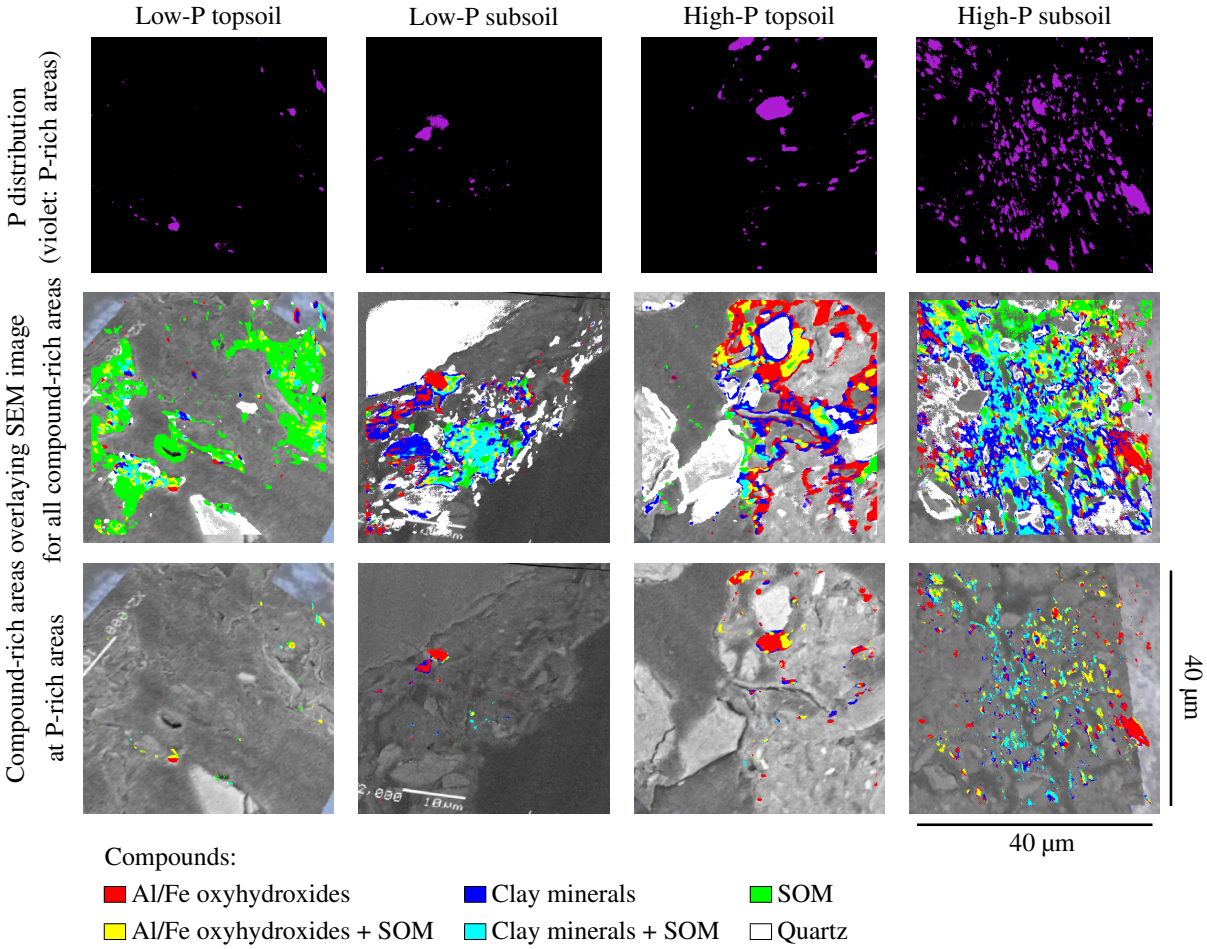

Figure 1. Clustered Nanoscale Secondary Ion Mass spectrometry (NanoSIMS) images of topsoil and subsoil micro-sites in aggregates of two forest soils. Top: Distribution maps of phosphorus (P)-rich areas after clustering (definition: see Methods section). Middle: All compound-rich areas overlaying scanning electron microscope (SEM) images. Bottom: Only those compound-rich areas that co-locate with P at the P-rich areas, overlaying SEM images.

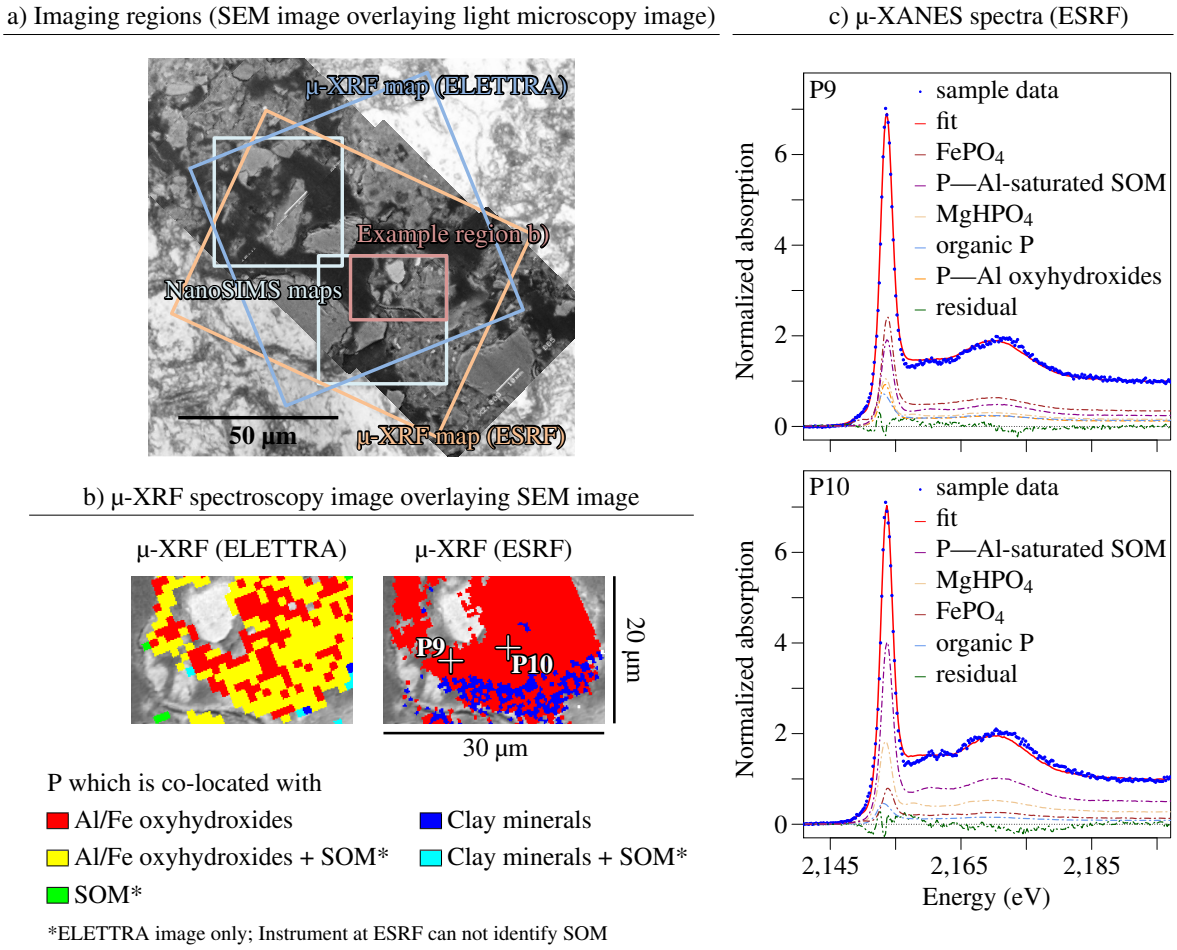

Figure 2. Example of micro-scale X-Ray Fluorescence (μ-XRF) and X-Ray Absorption Near Edge Structure (μ-XANES) spectroscopy. a) Scanning electron microscope (SEM) (back scattered electron) images overlaying light microscope image of the soil aggregate from the high-Phosphorus (P) topsoil, raster imaging regions of Nanoscale Secondary Ion Mass spectrometry (NanoSIMS) and μ-XRF mapping, indicated as rectangles, b) exemplary detail of μ-XRF mapping results obtained at ELETTRA and ESRF from P-rich areas, c) two μ-XANES spectra from selected P micro-sites (P9 and P10, ESRF) with the linear combination fit, and calculated shares of P species.

Danksagung

Ohne die Unterstützung folgender Menschen hätte ich im besten Fall die Promotion gar nicht erst angefangen, im schlechstesten hätte ich aufgegeben. Vielen herzlichen Dank an:

- Jörg Prietzel für die Möglichkeit für und die großartige Förderung und unermüdliche Unterstützung bei der Durchführung meiner Promotion
- Sandra Spielvogel für ihr Engagement, die fachliche Förderung und persönlich als Mentorin
- Ingrid Kögel-Knabner für die Begutachtung der Dissertation und ihre beständige Arbeit für den Lehrstuhl für Bodenkunde, sowie Anja Rammig für den Vorsitz der Prüfungskommission
- meinen Co-Autoren für die vielen spannenden Diskussionen und interdisziplinären Beiträge, ohne die meine Publikationen eine weniger herausragende Wirkung entfaltet hätten
- Sigrid Hiesch, Gertraud Harrington und Christine Pfab für die Unterstützung bei der Probenaufbereitung und der verschiedenen Laboranalysen
- Carsten W. Müller, Carmen Höschen und Johann Lugmeier für die Hilfe bei der Sekundärionen-Massenspektrometrie
- Wantana Klysubun, Jürgen Thieme, Alessandra Gianoncelli und Camille Rivard für die Unterstützung bei der Röntgenabsorptionspektroskopie
- Peter Schad für die Möglichkeit, an seinen tollen Bodenkundeexkursionen teilnehmen zu dürfen
- den Teilnehmern des Schwerpunktprogramms 1685 für die vielen interessanten und lehrreichen Treffen
- die TUM Graduate School und das Graduiertenzentrum Weihenstephan für das promotionsbegleitende Fortbildungsangebot

- der Deutschen Forschungsgemeinschaft (DFG) für die Finanzierung des Projektes Pr 534/6-1
- allen ehemaligen und aktuellen Angehörigen des Lehrstuhls für Bodenkunde, die mit meinen Antworten auf ihre Fragen und ihren Antworten auf meine Fragen auch wesentlich zu meiner wissenschaftlichen Entwicklung beigetragen haben, insbesondere meinen Doktorandenkollegen Maike, Gerrit, Lydia, Steffi und Lydia, meiner Lieblingsbürokollegin
- Dominik, Caro, Cordula, Markus, Daniel, Lilli, Sebastian, Nils, Vroni und Flo für die großartige Zeit in Freising
- meinen Eltern und meiner langjährigen Freundin Clau